Reducing Environmental Impacts of the Petroleum Refining Operations: Studies Related to Water Treatment and Carbon Dioxide Emissions Management

by

Farooq Ahmed Al-Sheikh

A thesis
presented to the University of Waterloo
in fulfillment of the
thesis requirement for the degree of
Doctor of Philosophy
in
Chemical Engineering

Waterloo, Ontario, Canada, 2018

AUTHOR'S DECLARATION

I hereby declare that I am the sole author of this thesis. This is a true copy of the thesis, including any required final revisions, as accepted by my examiners.

I understand that my thesis may be made electronically available to the public.

Examining Committee Membership

The following served on the Examining Committee for this thesis. The decision of the Examining Committee is by majority vote.

External Examiner:	Jiangning Wu Professor
Supervisor:	Ali Elkamel Professor
Supervisor:	William A. Anderson Professor
Internal Member:	Eric Croiset Professor
Internal Member:	Aiping Yu Professor
Internal-external Member:	Safa Fatih Erenay Professor

Abstract

Petroleum refining is one of the most important chemical processing industries, converting crude oil into many usable and useful products, but it can cause adverse environmental impacts. Two environmental issues were addressed: i) reducing ammonia concentrations in wastewater and ii) reducing selected carbon dioxide emissions using carbon capture technology. Ammonia removal during waste water treatment is important because of its potential toxic effects in aqueous environments. Although biological treatment is generally favourable, its application in cold climates is ineffective due to slow kinetics. An adsorption process is one viable alternative process that can be used to reduce ammonia concentrations, and accordingly 10 commercial ion exchange resins and 6 zeolites were tested to assess their effectiveness for the removal of ammonia from real polluted water samples (3.8 to 8 mg/L NH_3−N) containing other cations. In subsequent tests, the performance of six selected adsorbents was further characterized using Langmuir, and Freundlich isotherm and pseudo-1st, and pseudo-2nd order kinetic models. The results showed that the Dowex resin was best characterized by the Langmuir isotherm while LEWATIT resin, AZLB-Na and NV-Na zeolites were by the Freundlich one. Also, each adsorbent was best characterized by pseudo-2nd order kinetics. Adsorbent equilibrium capacities in the range of 0.2 to 0.4 mg/g were determined for ammonia concentrations of approximately 1 mg/L. Because of its high selectivity towards ammonia, a LEWATIT S 108 H resin was tested to assess its effectiveness in the batch and continuous adsorption of ammonia from the real wastewater. Batch adsorption tests were conducted using different masses of LEWATIT for 22.7 mg/L (NH_3−N) wastewater and the equilibrium data so obtained were characterized using Langmuir and Freundlich isotherms to obtain model

constants. Continuous adsorption tests were then carried out in two different sized fixed-bed-glass columns to obtain breakthrough curves. Also, ammonia desorption from LEWATIT was achieved using (5:100 w/v) HCl with an efficiency of approximately 50%. The Bohart-Adams and Thomas models were used to fit the experimental breakthrough curves for finding model parameters. The results show that the LEWATIT performance can be well-characterized by both the Bohart-Adams and Thomas models in the fixed-bed column. For comparison, a column was loaded with the AZLB-Na zeolite to generate a breakthrough curve, and the desorption process was achieved using sodium hydroxide. Bohart-Adams and Thomas models were employed to find model parameters that would describe the breakthrough curve of the adsorption process. These were then compared with experimental results, showing good agreement.

With respect to carbon dioxide emissions, the Fluid Catalytic Cracking (FCC) unit was the focus because it causes the bulk of the CO_2 emissions in a refinery (around 30%). Simplified mathematical models were derived using static and dynamic heat balances of both the reactor and regenerator. The main purpose of studying dynamic responses was to find the most influencing flow rates and their lower/upper limits to ensure that reactors/regenerator temperatures work within normal operating conditions, which are used as side constraints in the optimization technique. In the regenerator where combustion takes place, two systems were examined: post-combustion and oxy-combustion since percentages of the CO_2 content differ. In an oxy-combustion system, the CO_2 captured will not only be sequestered but also will be used as a side stream to the FCC unit since the operation will be continuous.

Acknowledgements

First, I would like to acknowledge Iraq, my home forever where I was born, grew up and will die, for giving me the opportunity to complete my PhD in Canada by funding my scholarship through the Ministry of Higher Education and Scientific Research and the University of Technology, Baghdad, Iraq.

Second, I extend my deep thanks to Canada and the University of Waterloo for their warm welcome. It was winter when I first arrived in Canada. With snow covering everything around me**,** Canada looked like a bride in her white dress.

Third, I warmly acknowledge my supervisors, Professor Ali Elkamel and Professor William A. Anderson, for their scientific advice, support and help during my PhD years.

Fourth, I would like to acknowledge the staff of the Iraqi cultural office in United States of America, especially Professor Dr. Asaad Omran and the staff of the Iraqi cultural office in Canada, especially Professor Dr. Sabah Wajid Ali for their continual assistance.

Fifth, I warmly acknowledge, Professor Mark Pritzker and Dr. Carol Moralejo for their scientific help during my PhD years.

Finally, I am grateful to the administrative and technical staff in the Department of Chemical Engineering, especially Judy Caron, Linda Sherwood, and Dennis Herman, for their continual help.

Dedication

To

my brothers, and sisters,

and the memory of my mother and father

Table of Contents

List of Figures

List of Tables

List of Symbols

C_b	NH_3−N concentration in wastewater at breakthrough (mg/L)
C_e	NH_3−N concentration in wastewater at equilibrium (mg/L)
$C_{el,o}$	NH_3−N concentration in elution solution at initial (mg/L)
$C_{el,t}$	NH_3−N concentration in elution solution at time *t* (mg/L)
C_o	Inlet NH_3−N concentration in wastewater (mg/L)
Cp_{air}	Specific heat of air (kJ/kg.^{o}C)
Cp_{feed}	Specific heat of fresh feed (kJ/kg.^{o}C)
Cp_{freshcat}	Specific heat of fresh catalyst (kJ/kg.^{o}C)
$Cp_{\mathrm{fluegases}}$	Specific heat of flue gases (kJ/kg.^{o}C)
Cp_{oxy}	Specific heat of mixture oxygen and carbon dioxide (kJ/kg.^{o}C)
$Cp_{products}$	Specific heat of products (kJ/kg.^{o}C)
Cp_{regcat}	Specific heat of regenerated catalyst (kJ/kg.^{o}C)
Cp_{spdcat}	Specific heat of spent catalyst (kJ/kg.^{o}C)
Cp_{stream}	Specific heat of steam (kJ/kg.^{o}C)
C_s	NH_3−N concentration in wastewater at saturation (mg/L)
C_t	NH_3−N concentration in wastewater at time *t* (mg/L)
H_{LB}	Enthalpy of rich-CO_2 MEA exiting at the bottom of an absorber (kJ/kg)

H_{LT}	Enthalpy of lean-CO_2 MEA entering at the top of an absorber (kJ/kg)
H_{VB}	Enthalpy of flue gas entering at the bottom of an absorber (kJ/kg)
H_{VT}	Enthalpy of stripped-CO_2 gases exiting at the top of an absorber (kJ/kg)
m_{air}	Mass flow rate of air (kg/min)
m_{feed}	Mass flow rate of feed (kg/min)
m_{freshcat}	Mass flow rate of fresh catalyst (kg/min)
$m_{\mathrm{fluegases}}$	Mass flow rate of flue gases (kg/min)
m_{oxy}	Mass flow rate of oxygen (kg/min)
$m_{products}$	Mass flow rate of products (kg/min)
m_{regcat}	Mass flow rate of regenerated catalyst (kg/min)
m_{spdcat}	Mass flow rate of spent catalyst (kg/min)
k_p	Steady state gain (dimensionless)
k_d'	Apparent desorption rate constant (1/min)
k_f	Freundlich constant related to the adsorption capacity ((mg/g).(L/mg)$^{1/n}$)
k_L	Langmuir equilibrium constant of the free energy of adsorption (L/mg)
$k_L a$	Volumetric mass transfer coefficient (1/min)
k_{Th}	Rate constant in Thomas model (L/mg.min)
L_B	Mass flow rate of rich-CO_2 MEA exiting at the absorber bottom (kg/min)
L_T	Mass flow rate of lean-CO_2 MEA entering at the absorber top (kg/min)

m	Mass of adsorbent (g)
m_{ads}	Adsorbed NH_3 mass (mg)
m_d	Desorbed NH_3 mass (mg)
m_{total}	Total NH_3 mass (mg)
M_{coke}	Mass of coke (kg)
$M_{\mathrm{fluegases}}$	Mass of flue gases (kg)
M_{products}	Mass of reactor products (kg)
M_{spdcat}	Mass of spent catalyst (kg)
M_{regcat}	Mass of regenerated catalyst (kg)
n	Freundlich constant of the desorption intensity (dimensionless)
N	Number of samples collected during continuous adsorption (dimensionless)
N_o	Saturation concentration in Bohart-Adams model (mg/L)
Q	Volumetric flow rate of wastewater (L/min)
q_e	Adsorption capacity at equilibrium (mg/g)
q_b	Adsorption capacity at breakthrough (mg/g)
q_{max}	Maximum adsorption capacity (mg/g)
q_s	Adsorption capacity at saturation (mg/g)
R_L	Separation factor of Langmuir isotherm (dimensionless)
t	Time (min)

t_b	Time to achieve breakthrough (min)
t_{el}	Time at which elution is terminated (min)
t_p	Time to achieve maximum NH_3-N concentration during desorption (min)
t_s	Time to achieve saturation (min)
T	Temperature (K)
T_{air}	Air temperature (°C)
T_{feed}	Feed temperature (°C)
$T_{\mathrm{fluegases}}$	Flue gases temperature (°C)
T_{freshcat}	Fresh catalyst temperature (°C)
T_{oxy}	Oxygen temperature (°C)
T_{products}	Products temperature (°C)
T_{rec}	Reactor temperature (°C)
T_{ref}	Reference temperature (°C)
T_{reg}	Regenerator temperature (°C)
T_{spdcat}	Spent catalyst temperature (°C)
T_{steam}	Steam temperature (°C)
υ	Linear velocity of wastewater (cm/min)
V	Volume of adsorbate (mL or L)

V_B	Mass flow rate of flue gas entering at the absorber bottom (kJ/kg)
V_T	Mass flow rate of stripped-CO_2 gases exiting at the absorber top (kJ/kg)
W	Catalyst weight (kg)
Z	Bed depth (cm)
ρ	Density of wastewater (mg/cm^3)
ε	Porosity of column (dimensionless)
ΔH_{rxn}	Heat of reaction (kJ/min)
$\Delta H_{\mathrm{combxn}}$	Heat of combustion (kJ/min)
λ_{ij}	Elements of relative gain array (dimensionless)

Chapter 1:
Introduction

1.1 Background

In the petroleum refining industry, more than 2500 useful refined products are converted from crude oil including products from atmospheric and vacuum distillation columns such as liquefied petroleum gas, gasoline, kerosene, aviation fuel, diesel fuel, fuel oils, lubricating oils, and products for the petrochemical industry. In the refinery, processes start with transporting crude oil form storage until shipping the refined products including all petroleum treatments and refining operations. Figure 1.1 shows the general petroleum refining processes that are used by many refineries around the world. The importance of those processes can vary among refineries depending on many factors such as the refinery size and feedstock nature, etc. Because of refining activities, refineries have emissions and containments sources which have negative effects on air and water. Therefore, it is mandatory that any refinery must have wastewater treatment units and air pollution control (Addington *et al.*, 2011).

Due to consuming massive amounts of the water for refining operations such as distillation and hydro-treating, wastewaters amount produced form those operations are equal to 0.4-1.6 of the refined petroleum (Colvin, *et al.*, 1991; Yan *et al.*, 2014). Therefore, all refineries must have wastewater plants for either discharging wastewaters to the environment safely under acceptable limits or reuse in the refinery. Effluents from the various wastewater refining were collected from different processing units and then treated in the treatment plants using appropriate methods. Because of the various refinery pollutants, selecting the appropriate methods and design of the wastewater treatment plants are very complicated since the

pollutants vary from dissolved solids, oil, phenols, sulfides, and toxic chemicals such as ammonia (Addington *et al.*, 2011).

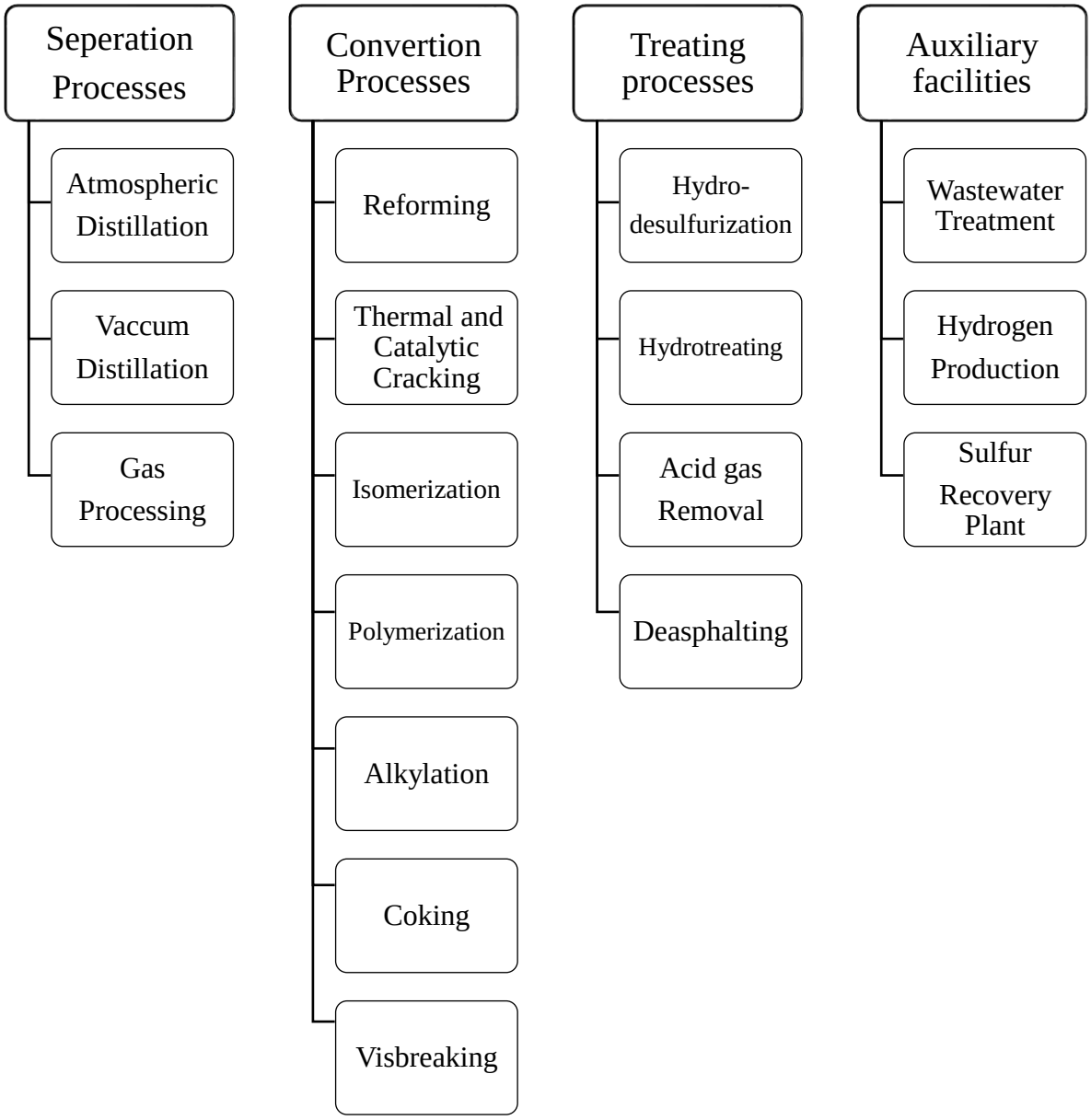

Figure 1.1: Processes of the general petroleum refining.

For example, Figure 1.2 shows ammonia percentages in each refinery process. Ammonia percentages are 44%, 26% and 10% for distillation, fluidized catalytic cracking and catalytic reforming respectively as well as 4% for each alkylation and crude desalting, 3% for each visbreaking, and hydrocracking unit and 2% for each coking, isomerization and hydrotreating unit (DOE, 2003). Refinery configuration plays a key role in a petroleum wastewater quality. Generally, a range of ammonia concentration in petroleum wastewater is 3.28-51.65 mg/L (NH_3−N) (Tyagi *et al.*, 1993).

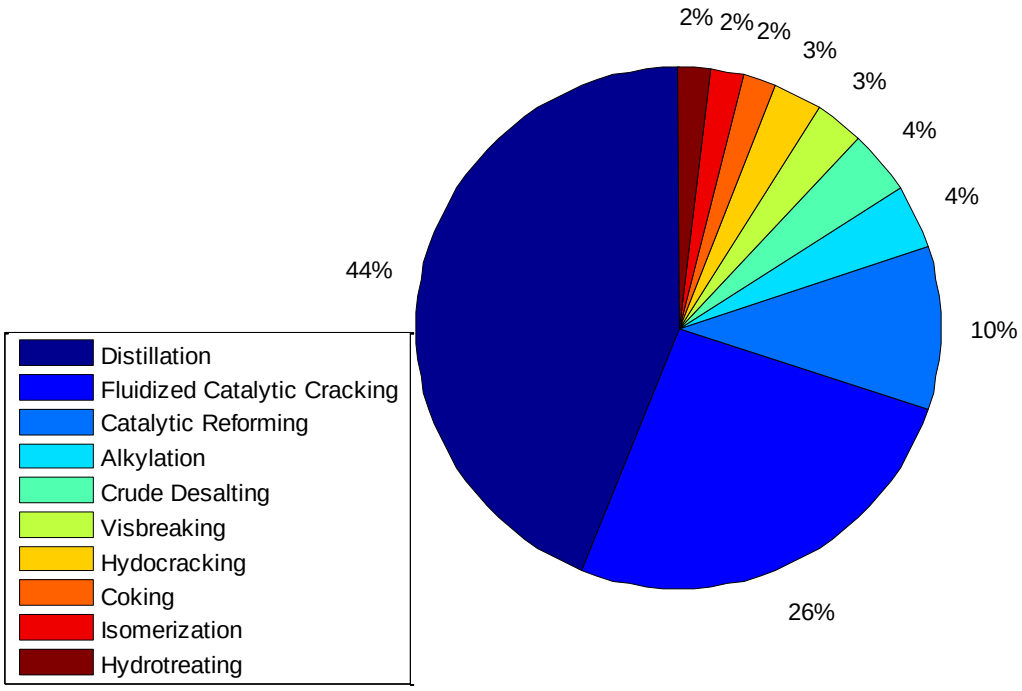

Figure 1.2: Ammonia percentages in the petroleum refining wastewaters produced by each unit.

Also, petroleum refining operations represent one of the major sources of carbon dioxide (CO_2) emissions with 4% of the global CO_2 emissions which are equal to one billion tons of CO_2 per year. Therefore, CO_2 emissions management are imperative to reduce their effects on

atmosphere. In addition, refineries are considered as a good option for carbon capture and storage (CCS) due to the large amount of carbon dioxide, especially in the FCC unit which represents approximately 30 – 40% of the total carbon emissions respectively (Stockle and Bullen, 2008; de Mello *et al*., 2009, 2013; van Straelen *et al*., 2010; Miracca *et al*., 2013).

1.2 Research Outline

The objectives of this work can be summarized as follows:

1. Screening tests of 16 adsorbents in ammonia removal from wastewaters of the refineries and industries sites.
2. Advanced tests of best two resins and two zeolites with applying isotherms and kinetics of the batch process.
3. Studying a continuous adsorption and desorption of the one resin and one zeolite using two different-size columns.
4. Implement carbon capture techniques in the petroleum refinery, especially in the FCC unit, that were considered as rich CO_2 sources with study the dynamics of the two processes.
5. Compare the two combustion schemes for the FCC unit by applying optimization techniques for each scheme.
6. Study relative gain array of two combustion schemes for the FCC unit.

A typical FCC unit will be taken as case studies in the simulation work using MATLAB software for deriving dynamic models and finding results of the optimization techniques.

1.3 Thesis Structure

This thesis consists of six chapters and two appendices organized as follows: chapter two delivers a batch adsorption process using various adsorbents to find the most efficient ones. Chapters three and four present a continuous adsorption process in which one resin and one zeolite were tested experimentally through analyzing their breakthrough curves to find out model's parameters and design theoretically. Also, chapter four investigates a use of the photoreactor as a second process to remove the ammonia from wastewaters in a batch process. Chapter five starts by a brief literature review that is related to models and optimization techniques in petroleum refining and CO_2 capture. Methods and techniques such as state space analysis, and relative gain array and optimization techniques are presented. The chapter includes then simulation results of the FCC unit. Chapter six provides recommendations and future works. Finally, Appendix A gives more details in terms of photos, figures and tables about the adsorption process while Appendix B provides simulation data of the FCC unit.

Chapter 2:
Batch Adsorption Process

2.1 Introduction

Wastewater from industrial activities contains heavy metals, organic substances, and suspended liquid and solids at hazardous levels. This is harmful to environmental life and has many potential health risks to people (Alwan *et al.*, 2010; Alwan & Mehdi, 2010). Ammonia in wastewater, for instance, can be toxic to species in the aquatic environment at concentrations over about 2 mg/L, depending on pH, temperature and other factors. Also, ammonia in wastewaters can be classified into two forms: unionized ammonia (NH_3) and an ionized ammonium (NH_4^+) but unionized ammonia is more toxic than ionized one (Batley, & Simpson, 2009; EPA 2013). In many locations, the ammonia can be biologically converted to nitrate, but in colder climates the biological oxidation process is too slow to be used as an effective treatment option for much of the year (Jermakka *et al.*, 2015). Therefore, in these situations other treatment options must be considered and employed, such as air-stripping, breakpoint chlorination, or capture methods based on adsorption (Gupta *et al.,* 2015; Jermakka *et al.,* 2015). Adsorption processes have some attractive features in these situations compared to air-stripping and chlorination, being relatively simple to operate and not requiring oxidizing chemicals (Widiastuti *et al.*, 2011; Huang *et al.*, 2017). One approach to ammonia adsorption for other wastewaters has been based on zeolite minerals (Leyva-Ramos *et al.*, 2010; Wang and Peng, 2010). Zeolites are hydrated aluminosilicate minerals with a porous structure that can accommodate a wide variety of cations such as Na^+, K^+, Ca^{2+} and Mg^{2+} and that can readily be exchanged for other cations in a solution (Wang and Peng, 2010). Zeolites from a variety

of sources have been shown to be capable of adsorbing ammonia (in the NH_4^+ form) from a range of different waters and wastewaters (Cooney *et al.*, 1999; Hedström, 2001; Wang *et al.*, 2007; Vassileva and Voikova, 2009; Huang *et al.*, 2010; Widiastuti *et al.*, 2011; Zhang *et al.*, 2011; Huo *et al.*, 2012). Adsorption of cations such as ammonium can also be achieved using ion exchange resins, which are polymer-based rather than natural or inorganic materials like zeolites (Abrams and Millar, 1997). Although ion exchange resins tend to be more expensive (Huang *et al.*, 2017), there may be advantages in terms of capacity and selectivity (Widiastuti *et al.*, 2011; Gupta *et al.*, 2015). The adsorption of ammonia in water by ion exchange resins has been studied but to a much lesser extent than zeolites (Huang *et al.*, 2017). For example, Jorgensen and Weatherley (2003, 2006) examined the removal of ammonia using Clinoptilolite, Dowex 50w-x8, and Purolite MN500 resins from wastewaters containing organics for finding a synergistic effect and Malovanyy *et al.* (2014) used Purolite C104 for ammonia removal from municipal wastewater. However there seems to be a lack of studies on the potential application of ion exchange resins to industrial wastewaters, which are typically low in organics content but contain a variety of inorganic ions (Jermakka, 2015). In this thesis, we expand on these studies by: i) using a diverse range of types of adsorbents (10 resins & 6 zeolites) for removing ammonia at lower concentrations (3.8 – 22.7 mg/L) from real wastewater samples to characterize their capacities and determine the most effective ones, and ii) selecting the most promising adsorbents for more detailed study of their behavior in a batch adsorption process, including quantification of the absorbents using isotherms and kinetic models. Since activated carbon cannot be easily regenerated and regeneration is an important component of our industrial partner requirements; therefore it was not considered in this thesis.

2.2 Types of Wastewaters

Two types of wastewater were used in an ammonia adsorption: first was synthetic wastewater in which 0.8 L of DI water was mixed with 3 mL of 11.692 g/L NH_4Cl stock solution in a one-liter plastic container to ensure that initial ammonia concentrations (NH_3–N), approximately 10.4 mg/L, were as similar as possible for the adsorbents. pH was measured before and after mixing and adjusted to approximately 7.0 by adding dropwise of 0.01 M sodium peroxide (NaOH). Unused bulk solutions were maintained in cold storage at 4 ^oC to prevent ammonia degradation due to bacteria activity and then used in the laboratory at 22.5 ^oC for adsorption experiments. Second was the 40-L real wastewater, delivered from a Canadian company located in the north, stored in a cold room and used as same as synthetic wastewater. Depending on the provided data from industry, Table 2.1 shows the full composition of the wastewaters.

Table 2.1: A full composition analysis of the real wastewater used.

Element	Ag	Al	As	Cd	Cr	Hg
Concentration (ppb)*	0.051	180.4	19.23	0.686	14.24	<0.005
Element	Mn	Mo	Pb	Se	Tl	Zn
Concentration (ppb)	181.7	24.91	1.598	8.224	0.009	53.53
Element	B	Ba	Be	Bi	Br	Ca
Concentration (mg/L)	0.139	0.076	<0.001	<0.014	3.52	272.2
Element	Cl	Co	Cu	F	Fe	K
Concentration (mg/L)	451.1	0.012	0.038	<0.20	0.361	69.57
Element	Li	Mg	Na	Ni	P	S
Concentration (mg/L)	0.019	14.75	146.7	0.648	0.018	163.4
Element	Sb	Si	Sn	SS	Te	Ti
Concentration (mg/L)	<0.003	4.941	<0.005	6.8	<0.028	<0.005
Element	V	Zr				
Concentration (mg/L)	<0.004	<0.003				
Component	NH_3	NO_2	NO_3	PO_4	SO_4	pH = 8.3
Concentration (mg/L)	22.6	12.1667	132.2	<2.00	499.5	

* ppb: part per billion.

2.3 Adsorbents

A variety of ion exchange resins and zeolites were assessed for their ability to remove ammonia from the wastewater as follows in Figure A.1, Table 2.2 and Table A.1 which provided from manufacturers' guide: resins are polymeric beads made of polystyrene cross-linked with divinylbenzene and have fast kinetics and high ammonia removal efficiency (Malovanyy *et al.*, 2014; Sica *et al.*, 2014). The resins that used in this research were sulfonic acid functional group into two forms as follows: the Na^+ form cationic exchange resins Diaion PK216, Diaion PK228, SK1B, Tulsion T-42 Na, and Tulsion T-52 Na BC are all strong acid cation exchange resins. The H^+ form cationic exchange resins are Dowex 50Wx8 50-100 Mesh, Lanxess LEWATIT MonoPlus S108H, Purolite Hypersol-Macronet MN500, Purolite C100H are strong-acid cation-exchange resins. One weak-acid cation-exchange resin, Purolite C104 Plus, was tested. Zeolites are crystalline miso-porous aluminium silicates (Vocciante *et al.*, 2018) and could be classified into many types such as Clinoptilolite (Ca and Na forms), Chabazite and Mordenite (Weatherley & Miladinovic, 2004; Langwaldt, 2008). The zeolites employed were NM-Ca (Cliniptilolite, Ca form), NV-Na (Cliniptilolite, Na form), AZLB-Na (Chabazite, Na form), NV-Na *TM Ammonia Specific (Cliniptilolite, Na form) and AZLB-Ca (Chabazite, Ca form). All the zeolites were washed, filtered and oven-dried before use. The type and modification of the resins/zeolites, pH, and temperature are essential factors that effect on their capacity for removal ammonia from wastewater (Jha & Hayashi, 2009; Leyva-Ramos *et al.*, 2010; Lin *et al.*, 2013). For strong acid resins, the selectivity of Na^+ form is more than that of H^+ one as follows: $Fe^{3+} > Al^{3+} > Pb^{2+} > Sr^{2+} > Ca^{2+} > Co^{2+} > Ni^{2+} > Cu^{2+} > Zn^{2+} > Mg^{2+} > Mn^{2+} > Ag^+ > Cs^+ > Cd^{2+} > K^+ \approx NH_4 > Na^+ > H^+ > Li^+ > Hg^{2+}$ (Alchin, 1998).

For chabazite zeolites, $Ti^{+} > K^{+} > Ag^{+} > Rb^{+} > NH_4^{+} > Pb^{2+} > Na^{+} = Ba^{2+} > Sr^{2+} > Ca^{2+} > Li^{+}$ (Langwaldt, 2008) or $K^{+} > NH_4^{+} > > Na^{+} > Mg^{2+}$ (Lahav & Green,1998).

For clinoptilolite zeolites, $Cs^{+} > Rb^{+} > K^{+} > NH_4^{+} > Ba^{2+} > Sr^{2+} > Ca^{2+} > Fe^{3+} > Al^{3+} > Mg^{2+} > Li^{+}$ (Ames, 1960).

Table 2.2: Some physical and chemical specifications of the selected adsorbents.

Adsorbent	Capacity	Surface Area m^2/g	Particle size mm	Density g/mL	Operating pH	Temperature ^oC
Dowex 50Wx8	1.7 Meq/L	-	0.1-0.2	0.80	0 − 14	100
Purolite MN500	0.8 eq/L	-	0.3-1.2	1.19	0 − 14	120
Purolite C104Plus	3.8 eq/L	-	0.3-1.6	1.18	0 − 14	120
Purolite C100H	2.0 eq/L	-	0.3-1.6	1.20	0 − 14	140
Zeolite NM-Ca	0.8-1.2 Meq/g	15	-	1.60	3 − 10	650
Zeolite NV-Na	1.85 Meq/g	40	-	1.60	3 − 10	650
Zeolite AZLB-Na	2.5 Meq/g	520	-	1.73	3 − 12	650
Zeolite NV-Na *TM	1.85 Meq/g	40	-	1.60	3 − 10	650
Zeolite AZLB-Ca	2.5 Meq/g	460	-	1.73	3 − 12	650
DIAION PK228	2.1 Meq/g	-	0.74	1.32	0 − 14	120
DIAION SK1B	2.0 Meq/g	-	0.75	1.28	0 − 14	120
DIAION PK216	1.75 Meq/g	-	0.72	1.26	0 − 14	120
Tulsion T-42	2.0 eq/L	-	0.3-1.2	0.87	0 − 14	140
Tulsion T-52	1.90 eq/L	-	0.3-1.2	0.86	0 − 14	120
LEWATIT	2.2 eq/L	-	0.62	1.26	0 − 14	120
KMI Zeolite	1.6-20 meg/g	40	-	1.89	3 − 10	700

*Meq: milliequivalents.

2.4 Adsorbent Analysis

For the adsorption experiments on synthetic/real wastewater, analysis was conducted using a UV-visible spectrophotometer (HP8452A diode array), pH meter (JENCO Electronics LTD, Model 1671) as shown in Figure A.2, and high-range Hach kits for ammonia (Ammonia HR

TNT, Hach Company/Hach Lange GmbH, USA). The pH meter was used to measure the pH of the wastewater before and after addition of the adsorbents. The Hach kits were used to colorimetrically determine the ammonia concentration as nitrogen (NH_3–N) using the manufacturer's procedure published for the kits as follows: A 0.1-mL sample containing ammonia was combined in the test vials with a hypochlorite solution to form mono-chloramine and then a salicylate reagent was added to form 5-aminosalicylate, which is yellow, and then a sodium nitroprusside agent to form a blue-coloured complex. The blue colour is masked by the yellow coloured 5-aminosalicylate, which is in excess, and the resulting colour is green. After 20 min, the absorbance is ready to be measured by a spectrophotometer at 655 nm wavelength and quantified using a pre-set instrument program method (343 N, Ammonia HR TNT). The accuracy of using Hach kits under these conditions is about ±5%.

2.5 Experimental Work

Two sets of batch adsorption experiments were conducted: screening and advanced tests.

2.5.1 Screening Tests

For initial screening tests of ammonia adsorption performance, simple vial tests of the ion exchange adsorbents were performed using the following procedure: 35 mL of the real wastewater were added into 40 mL amber vials. A 0.1 mL sample of the solution was collected and analyzed for NH_3–N before any adsorbent was added. Then 1.0 gram of each adsorbent was added to the real wastewater in each of the vials and the contents were left to stand for 7 hours while being shaken multiple times by hand before a final sample was collected and

analyzed NH_3–N. The percentage of NH_3 removal was calculated for each adsorbent as follows:

$$\% NH_3 = \frac{C_0 - C_t}{C_0} \times 100 \quad (2.1)$$

where C_o and C_t are concentrations (NH_3–N) (mg/L) at the initial and time t, respectively. The results in mg NH_3/g adsorbent were compiled to determine the most efficient adsorbent before proceeding onto more detailed studies of the selected adsorbents. Also, pH for each adsorbent was recorded before and after the screening test.

2.5.2 Advanced Tests

Based on the preliminary results of the ammonia adsorption from initial testing for the 16 adsorbents, more detailed timed studies were conducted on the best 6 selected adsorbents to compare their efficiencies at equilibrium. For these more detailed tests, each of the 6 adsorbents was tested in deionized (DI) water with the sample water tests. To ensure that the starting concentrations for the adsorbents were as similar as possible. For preparation of DI water spiked with NH_4Cl (synthetic wastewater), the procedure was as follows: 800 mL of DI water was collected in a one-liter plastic container and pH was measured. Then 3 mL of an 11.692 g/L stock solution of NH_4Cl solution was added, the solution was mixed, and the pH measured. The pH was adjusted to approximately 7.0 by dropwise addition of 0.01 M NaOH. A 0.1 mL sample was collected for analysis of NH_3–N using the Hach kit. Unused solutions were kept in cold storage and brought to room temperature (22.5°C) for each use. For the adsorption process, the procedure was as follows: an empty 125 mL plastic container was weighed, 120 mL of the synthetic wastewater was added, and the container was weighed again with the

difference recorded as the volume of water. Last, the adsorbent (1.5 g) was added to the 120 mL of the synthetic wastewater, the container was capped, and the mixture was vigorously shaken by hand initially and then several times throughout the experiment. Water samples were collected, and the corresponding pH measured immediately (usually within 5 seconds of addition of the adsorbent) and then after 5, 10, 20, 30, 60, 120, and 180 min of exposure to the adsorbent. One mL from the solution was removed using a syringe and then filtered through a 0.45 µm syringe filter into a test tube. A 0.1 mL aliquot was collected from the test tube and tested for NH_3−N content using the Hach kit. The percentage of NH_3 removal was calculated for each adsorbent using Equation 2.1. The same procedure above was used for the tests involving real wastewater in which 3 g of the selected adsorbents contacted the real wastewater having an initial concentration of 22.7 mg/L NH_3−N.

2.6 Isotherms

The adsorption equilibrium was assessed using Langmuir and Freundlich isotherms, which have been used in different adsorption processes by many researchers (Widiastuti *et al.,* 2011; Huo *et al.,* 2012; Sadaf & Bhatti, 2014; Wang *et al.,* 2014; Largitte & Pasquier, 2016), at different adsorbent masses (1, 2 and 3 g) and initial ammonia concentrations in the real wastewater (3.8, 8 and 22.7 mg/L). The solution temperature was maintained at the lab room temperature (22.5°C). The adsorption capacity of ammonia at equilibrium can be defined as follows:

$$q_e = \frac{(C_o - C_e)V}{m} \quad (2.2)$$

where C_e is the ammonia concentration (mg/L) (as nitrogen, i.e., NH_3–N) of wastewaters at equilibrium, m is the mass of the adsorbent (g), and V is the volume of the adsorbate (L). The most common isotherms were used to describe an isotherm of the ammonia adsorption using adsorbents (resins/zeolites). Those models are as follow: the Langmuir isotherm is (Langmuir, 1918):

$$q_e = \frac{q_{max} k_L C_e}{1 + k_L C_e} \tag{2.3}$$

can be re-written in the following linearized form

$$\frac{C_e}{q_e} = \frac{1}{q_{max} k_L} + \left(\frac{1}{q_{max}}\right) C_e \tag{2.4}$$

where q_{max} is the experimental maximum adsorption capacity at time (mg/g) and k_L is the Langmuir constant of the free energy of adsorption (L/mg). If adsorption follows Langmuir behavior, a plot of C_e/q_e versus C_e should be linear with a slope $1/q_{max}$ and intercept $1/q_{max} k_L$ from which q_{max} and k_L can be determined.

The essential characteristics of the Langmuir isotherm can be explained in terms of the dimensionless equilibrium parameter in Equation 2.5:

$$R_L = \frac{1}{1 + K_L C_o} \tag{2.5}$$

where R_L is the separation factor of the Langmuir isotherm (dimensionless).

The R_L value denotes the adsorption type as follows: irreversible (R_L = 0), linear (R_L = 1), favorable (0 < R_L < 1) and unfavorable (R_L > 1) (Weber & Chakravorti, 1974).

The Freundlich isotherm is given by the relationship below (Freundlich, 1906):

$$q_e = k_f C_e^{1/n} \tag{2.6}$$

or the linearized version is:

$$ln\ q_e = ln\ k_f + \frac{1}{n} ln\ C_e \tag{2.7}$$

where k_f is the Freundlich constant of the adsorption capacity ((mg/g).(L/mg)$^{1/n}$), n is the Freundlich constant of the adsorption intensity (dimensionless). A plot of $ln\ q_e$ vs. $ln\ C_e$ should yield a straight line with intercept $ln\ k_f$ and slope $1/n$.

2.7 Kinetics

The adsorption kinetics for two batch experiments were characterized for both pseudo-1st and pseudo-2nd order behavior: the first was conducted at an initial concentration of 10.4 mg/L and 1.5 g adsorbent in 120 mL synthetic wastewater, while the second was at an initial concentration of 22.7 mg/L and 3 g adsorbent in 120 mL real wastewater. The solution temperature was maintained at the lab room temperature (22.5°C). The adsorption capacity q_t (mg/g) of ammonia at time t can be calculated as follows:

$$q_t = \frac{(C_0 - C_t)\,V}{m} \tag{2.8}$$

where C_o and C_t are the ammonia concentrations (mg/L) (as nitrogen, i.e., NH_3–N) of wastewaters at $t = 0$ and some later time t, respectively, m is the mass of the adsorbent (g) and V is the volume of the adsorbate (L). The pseudo-1st and pseudo-2nd order kinetic

equations are useful for characterizing the rate of ammonia adsorption onto the adsorbents (resins or zeolites) as follows:

A pseudo-first-order kinetic equation was derived by (Lagergren, 1898), i.e.,

$$\frac{dq_t}{dt} = -k_1(q_e - q_t) \tag{2.9}$$

Integration of Equation 2.9 and substitution of the initial condition $q_t = 0$ at $t = 0$ yields:

$$q_t = q_e(1 - exp(-k_1 t)) \tag{2.10}$$

which can be re-arranged in linearized form to be

$$ln(q_e - q_t) = ln(q_{eth}) - k_1 t \tag{2.11}$$

where k_1 is the rate constant of the pseudo-1st-order kinetic model (min^{-1}), q_e is the experimental adsorption capacity (mg/g) at equilibrium, q_{eth} is the theoretical adsorption capacity (mg/g) and t is time (min). If pseudo-1st-order behavior is followed, a plot of $ln(q_e - q_t)$ vs. t should yield a straight line with slope $-k_1$ and intercept $ln\, q_{eth}$.

A pseudo-2nd order kinetic equation (Ho & McKay, 1999) is as follows:

$$\frac{dq_t}{dt} = -k_2(q_e - q_t)^2 \tag{2.12}$$

can be integrated using an initial condition $q_e = 0$ at $t = 0$ to yield:

$$q_t = \frac{k_2 q_{eth}^2 t}{1 + k_2 q_{eth} t} \tag{2.13}$$

which can be re-written in linearized form as:

$$\frac{t}{q_t} = \frac{1}{k_2 q_{eth}^2} + \left(\frac{1}{q_{eth}}\right) t \quad (2.14)$$

where k_2 is the rate constant of the pseudo-2nd-order kinetic model (g/mg.min). If the system obeys pseudo-2nd order kinetics, a plot of t/q_t vs. t should yield a straight line with slope $1/k_2 q_{eth}^2$ and intercept $1/q_{eth}$ from which q_{eth} and k_2 can be determined.

2.8 Regression

Root-mean-square error (RMSE) was used as a minimization criterion to fit the data obtained from experiments to those obtained from isotherms and kinetics models for each absorbent. A definition of the RMSE is as follows:

$$RMSE = \sqrt[2]{\frac{1}{N-2}\sum_{i=1}^{N}\left(q_{exp,i} - q_{eth,i}\right)^2} \quad (2.15)$$

where N is the number of the experiment samples and $q_{exp,i}$, and $q_{eth,i}$ are the experimental and model values at each sample i.

2.9 Results and Discussion

2.9.1 Screening Tests

For the purposes of narrowing down the field of potential ammonia absorbents, sixteen candidates (10 ion exchange resins and 6 zeolites) were tested with the real wastewater, as shown in Table 2.3. Screening tests were done using adsorbents of the first group in 8 mg/L

(NH_3−N) real wastewater. Then after one month, the same procedure was done using adsorbents of the second group in 3.8 mg/L (NH_3−N) real wastewater. The initial ammonia concentration declined due to biodegradation (bacteria activity) in the wastewater sample, so the decision was made to select the best resin and zeolite from the first group (Dowex and AZLB-Na) and the second one (LEWATIT and NV-Na) with the addition of two more resins (DIAION PK216 and SK1B) suggested by an industrial sponsor. The results from the first group of the adsorbents indicated that Dowex and NV-Na were the most effective resins and zeolites, respectively, at removing the ammonia from the real water (63%, and 23% adsorption within 5 sec respectively and 95%, and 65% adsorption within 7 hours respectively). Furthermore, the first group of adsorbents were re-tested at a lower temperature by placing the materials in a refrigerator prior and during use. Also, the results indicated that the effect of temperature was not significantly detrimental to ammonia adsorption in this wastewater. According to the capacities and percentage of ammonia removal of each adsorbent, these preliminary results were sufficient to select a few of the best adsorbents to conduct more extensive tests, namely the ion exchange resins Dowex 50Wx8 and Puralite C100H, and AZLB-Na as an example of the best zeolite material. Also, Purolite C104Plus showed low ammonia removal efficiency (Malovanyy *et al.*, 2014). The results from using a second group of the adsorbents indicated that LEWATIT and AZLB-Na appeared to be the most effective resins and zeolites respectively (15%, and 34% adsorption within 5 sec respectively and 65%, and 65% adsorption within 7 hours respectively).

Table 2.3: Ammonia absorption capacities of the adsorbents in two different real wastewater samples (35 mL), showing percentages of ammonia removal and pH using 1 g of each adsorbent, with ammonia concentrations given as NH_3–N.

Adsorbent	(mg NH_3/g) at 5 sec	(mg NH_3/g) at 7 hr	(%) removal at 5 sec	(%) removal at 7 hr	pH at 7 hr
First group: Initial NH_3–N (mg/L) = 8 mg/L - Initial pH = 5.16 at 22.5 ºC					
Dowex 50Wx8	0.175	0.266	62.5	95.0	1.84
Purolite MN500	0.059	0.175	21.2	62.5	1.91
Purolite C104Plus	0.003	*	1.20	*	2.80
Purolite C100H	0.059	0.252	21.2	90.0	1.83
Zeolite NM-Ca	0.031	0.105	11.2	37.5	5.21
Zeolite NV-Na	0.066	0.168	23.7	60.0	6.71
Second group: Initial NH_3–N (mg/L) = 3.8 mg/L - Initial pH = 5.12 at 22.5 ºC					
Zeolite AZLB-Na	0.045	0.087	34.20	65.78	6.32
Zeolite NV-Na *TM	0.017	0.021	13.15	15.78	10.26
Zeolite AZLB-Ca	0.031	0.066	23.68	50.00	7.40
DIAION PK228	0.028	0.070	21.05	52.63	5.67
DIAION SK1B	0.035	0.070	26.31	52.63	4.70
DIAION PK216	0.038	0.059	28.94	44.73	4.35
Tulsion T-42 Na N-B1-TX	0.038	0.056	28.94	42.10	5.25
Tulsion T-52 Na BCN-B1-TX	0.014	0.098	10.50	73.68	3.87
LEWATIT monoPlus S 108 H	0.021	0.087	15.70	65.78	4.18
KMI Zeolite	0.031	0.042	23.68	31.75	6.94
First group: Initial NH_3–N (mg/L) = 8 mg/L - Initial pH = 5.2 at 7.7 ºC					
Dowex 50Wx8	0.227	0.269	81.25	96.25	1.99
Purolite MN500	0.154	0.203	55.00	72.50	2.11
Purolite C104Plus	0.143	0.042	51.25	15.00	2.85
Purolite C100H	0.143	0.241	51.25	86.25	2.05
Zeolite NM-Ca	0.112	0.161	40.00	57.50	6.06
Zeolite NV-Na	0.122	0.171	43.75	61.25	6.71

*Concentration of ammonia as N in the Purolite C104Plus test sample increased after 7 hr.

2.9.2 Advanced Tests

A more detailed study of the six selected adsorbents (Dowex, LEWATIT, AZLB-Na zeolite, NV-NA, DIAION PK216 and DIAION SK1B) was conducted over a three-hour period with samples collected as same as in the illustrated procedure. As shown in Figures 2.1-2.3, the starting concentration was also plotted as mg/g to keep the plots on a reasonable scale for comparison although no adsorbent was present for the time zero sample. Dowex 50Wx8 50-100 and LEWATIT Monoplus S 108 H resins exhibited the fastest responses by removing 99.4 and 96.2% of the ammonia from synthetic wastewater, respectively, within 5 minutes. By 10 minutes, 100% of the ammonia has been removed by both the Dowex and LEWATIT resins. By contrast, AZLB-Na zeolite, NV-NA zeolite, DIAION PK216 and DIAION SK1B removed only 88.7, 63.0, 56.1, and 55.1 % ammonia, respectively, within the same 5-minute period. NV-NA zeolite and PK216 required ~180 minutes for 100 % adsorption, while AZLB-Na zeolite and SK1B only attained only 98.1 and 97.5 % adsorption, respectively, by 180 minutes. Ammonia removal of the AZLB-Na and NV-NA zeolites decrease with contact time even though those have the fast removal at initial because of decreasing concentration gradient and adsorption sites (Karadag, *et al.*, 2008; Huang *et al.*, 2017). The effect of the ion-exchange resins on the solution pH was markedly different from that of the zeolite.

After being in contact with Dowex and LEWATIT for 10 and 5 minutes, respectively, the pH of the test solutions decreased from an initial value of 7.0 to 2.95 and 3.17, respectively. The pH increased from 7.0 to final stable values of 8.26 in the case of AZLB-Na and 7.96 for NV-Na by the end of 60 minutes, whereas it decreased to 6.06 for the SK1B. PK216 reached pH stability at 120 minutes decreasing from 7.00 to a final pH of 6.04. The reason is related to

compositions of the both resins and zeolites since H^+ is released by the ion exchange reaction, whereas adsorption by zeolite does not. These same experiments were conducted using the real water at initial ammonia concentration 22.7 mg/L NH_3–N using 3 g of each adsorbents.

As shown in Figures 2.4-2.6, the same procedure of the advanced tests was used to adsorb ammonia from real wastewater at 22.7 mg/L using 1.5 g of the NV-Na and DIAION PK216. Comparing with the results in Figures 2.1 & 2.2, the results showed that 1.5 g of the mentioned adsorbents was not sufficient to adsorb all ammonia present by the end of 180 minutes due to its concentration in the real water. Also, presence of the cations (Ca^{2+}, Cd^{2+}, K^+, Na^+, Mg^{2+}, and Zn^{2+}) and components (NO_3^-, PO_4^{3-}, and SO_4^{2-}) in real wastewater reduce ammonia removal percentage of the adsorbents (Wang *et al.*, 2006; Marañón *et al.*, 2006) while those mentioned substances are not exist in synthetic wastewater.

As can be observed in Figures 2.7-2.9, the Dowex 50WX8 50-100 and LEWATIT S 108 H Monoplus resins once again most readily adsorbed ammonia with 94.9 and 89.4 % removal within 5 minutes compared to 85.3, 84.9, 83.6, and 78.0 for DIAION SK1B, AZLB-Na zeolite, DIAION PK216 and NV-NA zeolite, respectively. None of the resins or zeolites adsorbed 100% of the ammonia by 180 minutes presumably due to an insufficient amount present although competition due to adsorption of other species in the wastewater could also contribute. The maximum adsorption levels of 94.9, 95.9, 96.0, 95.0, 91.3, and 90.9% were reached within 5, 30, 120, 180, 30 and 120 min for Dowex, LEWATIT, AZLB-Na, NV-Na, PK216, and SK1B, respectively. After contact with Dowex for 5 minutes and LEWATIT for 20 minutes, the pH of the solutions decreased from an initial value of 7.68 to 1.97 and 1.99, respectively. The pH increased from an initial value of 7.85 to a stable value of 8.03 by 30

minutes in the case of AZLB-Na and to 7.98 by 120 minutes in the case of NV-Na. The pH after contact with PK216 and SK1B was still increasing by the end of the 180-minute experiment and had reached 7.21 and 7.15, respectively, after initially decreasing to lows of 6.6 and 6.69 after 5 minutes from a starting pH of 7.68. The results demonstrate that the ammonia adsorption capacity was most efficient in the case of the Dowex and LEWATIT resins, least efficient for the two DIAION resins and intermediate for the zeolites. In all cases, the adsorbents reached equilibrium with the real wastewater before all ammonia was absorbed unlike the situation with the spiked DI water. In addition to inadequate adsorbent mass, other species in the real water could have adsorbed more easily to the DIAION resins.

2.9.3 Kinetics and Isotherms

Based on the results of the advanced tests, the kinetics and isotherms for adsorption of ammonia onto the various adsorbents in both synthetic and real wastewater were quantitatively analyzed. Figure 2.10 showed the plots according to the Langmuir and Freundlich isotherms different adsorbent masses (1, 2 and 3 g) and initial ammonia concentrations in the real wastewater (3.8, 8 and 22.7 mg/L). The isotherm constants calculated from the slopes and intercepts according to Equations 2.4 & 2.7 are listed in Table 2.4. The R_L values for ammonia adsorption using the four different adsorbents in this study all fell in the range of 0 – 1 and n values are larger than 1.0, therefore; the process was a favorable adsorption using all selected adsorbents. Also, the results showed that the Dowex resin was best characterized by the Langmuir isotherm which is the same result of Jorgensen and Weatherley (2003) while LEWATIT, AZLB-Na and NV-Na zeolite were by Freundlich one. Figures 2.11 & 2.12 show plots according to the pseudo-1st and 2nd-order kinetics using 1.5 and 3 g of the adsorbent in

synthetic and real wastewater, respectively. The kinetic parameters obtained from the slopes and intercepts based on Equations 2.11 & 2.14 are presented in Table 2.5. A comparison of the fits for the two different rate laws clearly shows that adsorption of ammonia onto all adsorbents in both solutions follows pseudo-2nd order very well and much better than it does pseudo-1st order, as quantified by the RMSE values. Those results were agreed by other researchers using zeolites and resins in ammonia adsorption (Bashir *et al.*, 2010; Widiastuti *et al.*, 2011; Zhang *et al.*, 2011; Huo *et al.*, 2012; Guaya *et al.*, 2015).

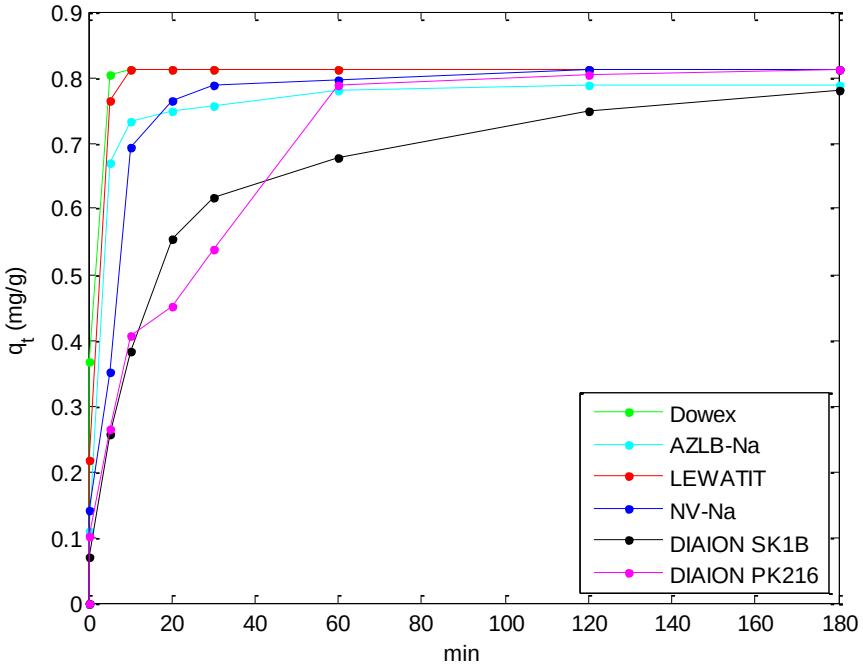

Figure 2.1: Adsorption capacities in synthetic wastewater using 1.5 g of each adsorbent.

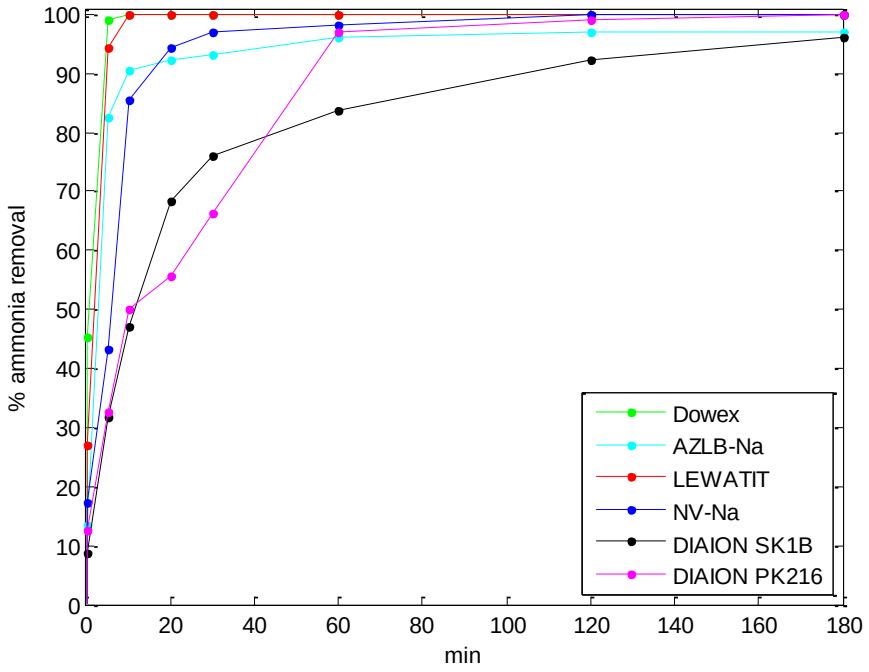

Figure 2.2: Percentage of the ammonia removal from synthetic wastewater using 1.5 g of each adsorbent..

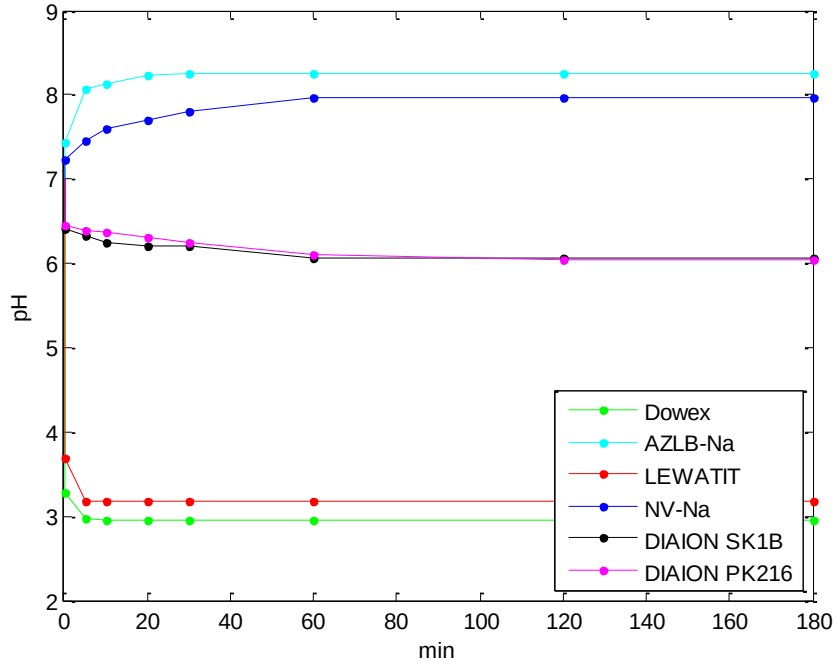

Figure 2.3: pH of synthetic wastewater using 1.5 g of each adsorbent.

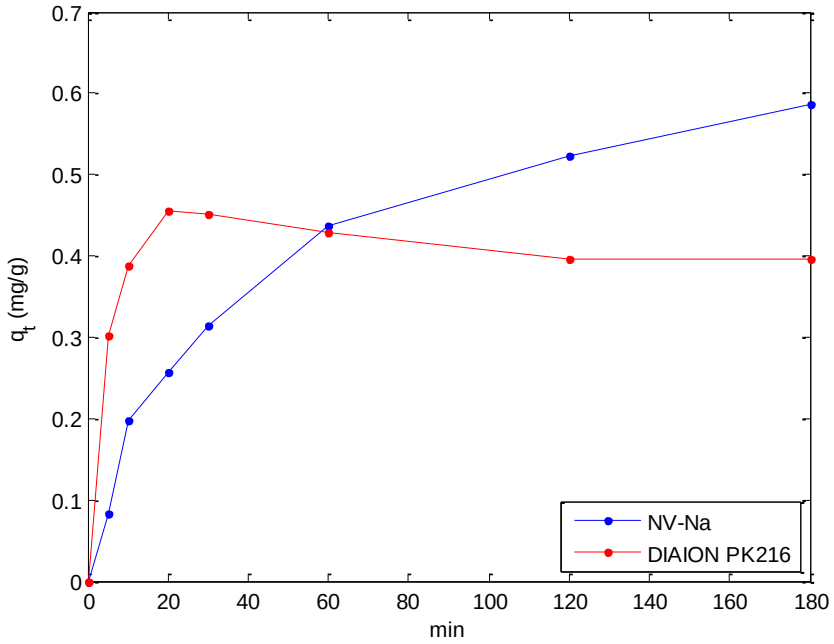

Figure 2.4: Adsorption capacities in real wastewater using 1.5 g of NV-Na and DIAION PK216.

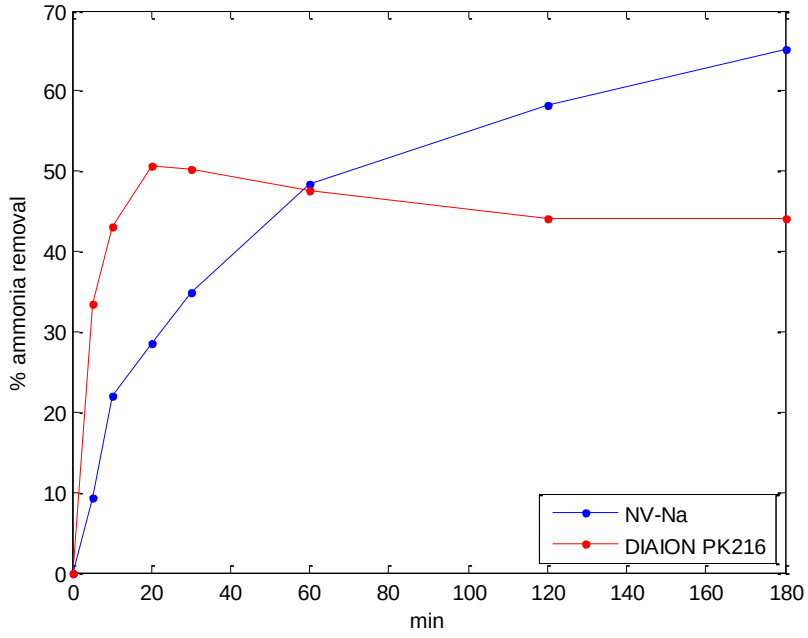

Figure 2.5: Percentage of the ammonia removal from synthetic wastewater using 1.5 g of each NV-Na & DIAION PK216.

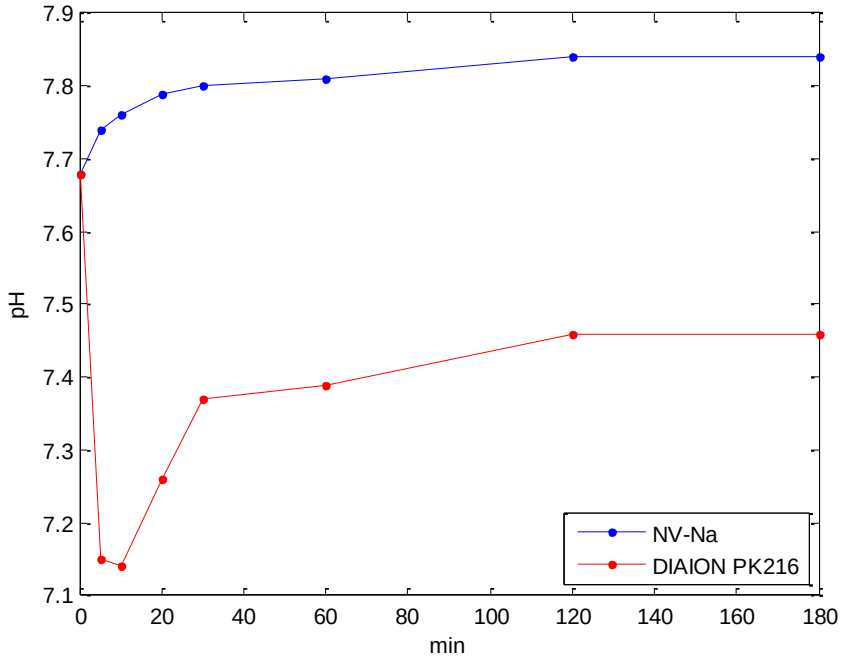

Figure 2.6: pH of real wastewater using 1.5 g of each NV-Na & DIAION PK216.

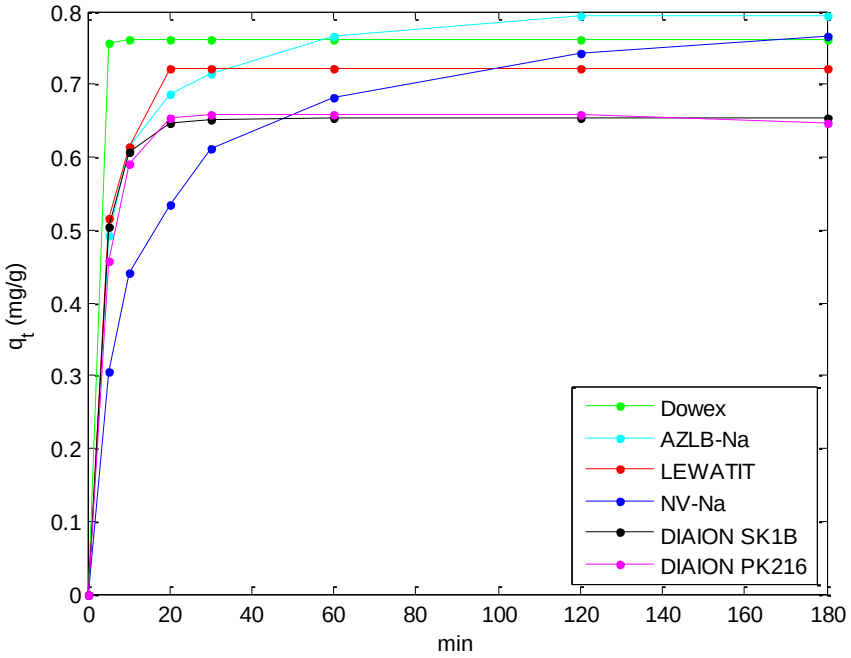

Figure 2.7: Adsorption capacities in real wastewater using 3 g of each adsorbent.

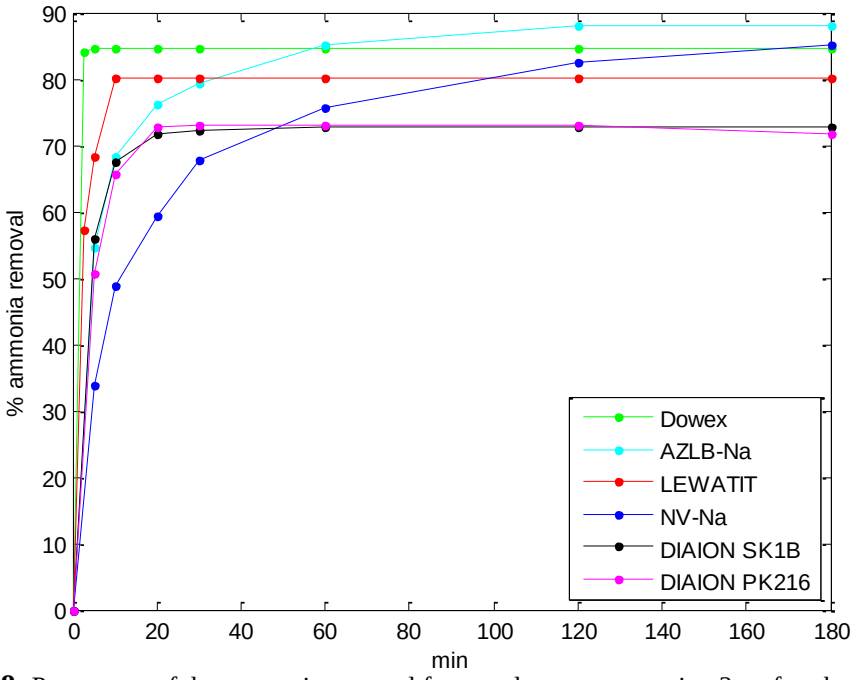

Figure 2.8: Percentage of the ammonia removal from real wastewater using 3 g of each adsorbent.

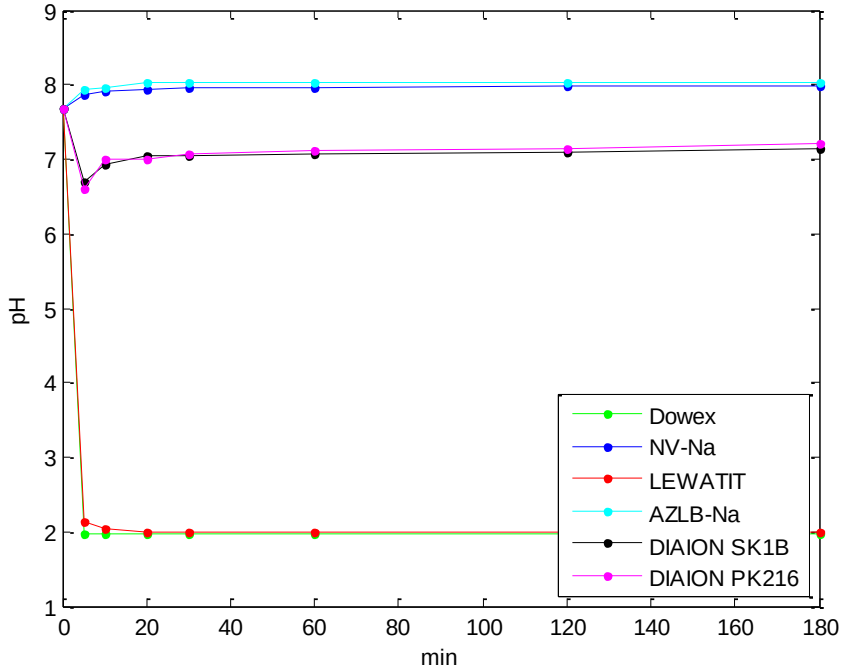

Figure 2.9: pH of real wastewater using 3 g of each adsorbent.

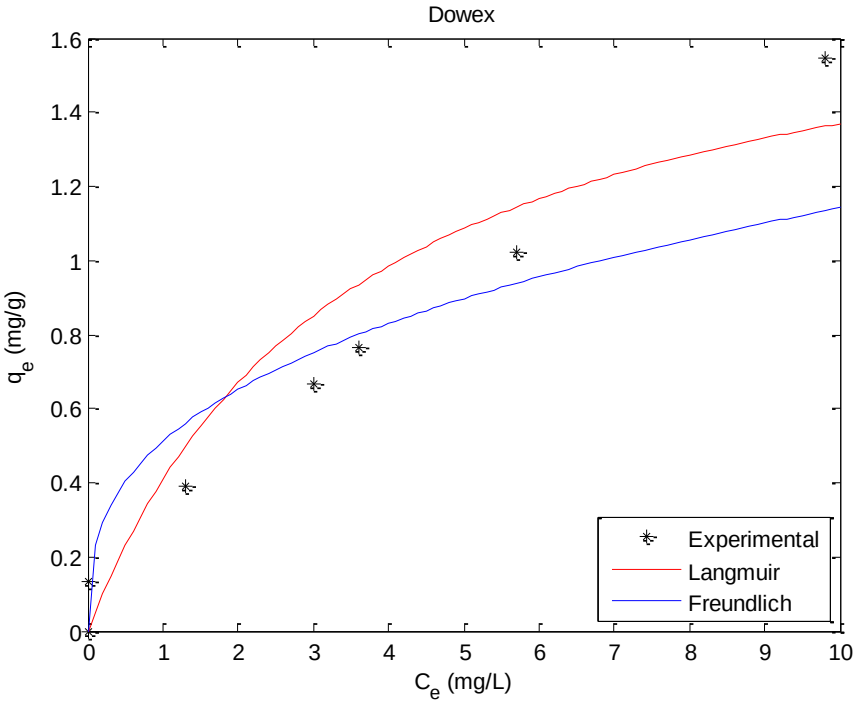
Dowex
1.6
1.4
1.2
1
0.8
0.6
0.4
0.2
0
0
1
2
3
4
5
6
7
8
9
10
q_e (mg/g)
C_e (mg/L)
Experimental
Langmuir
Freundlich

(a)

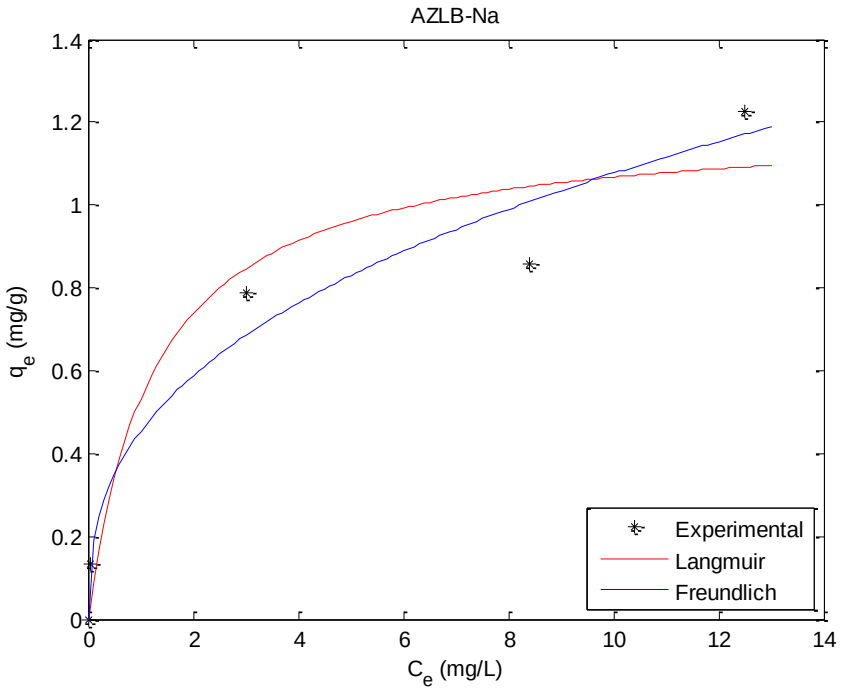
AZLB-Na
1.4
1.2
1
0.8
0.6
0.4
0.2
0
0
2
4
6
8
10
12
14
q_e (mg/g)
C_e (mg/L)
Experimental
Langmuir
Freundlich

(b)

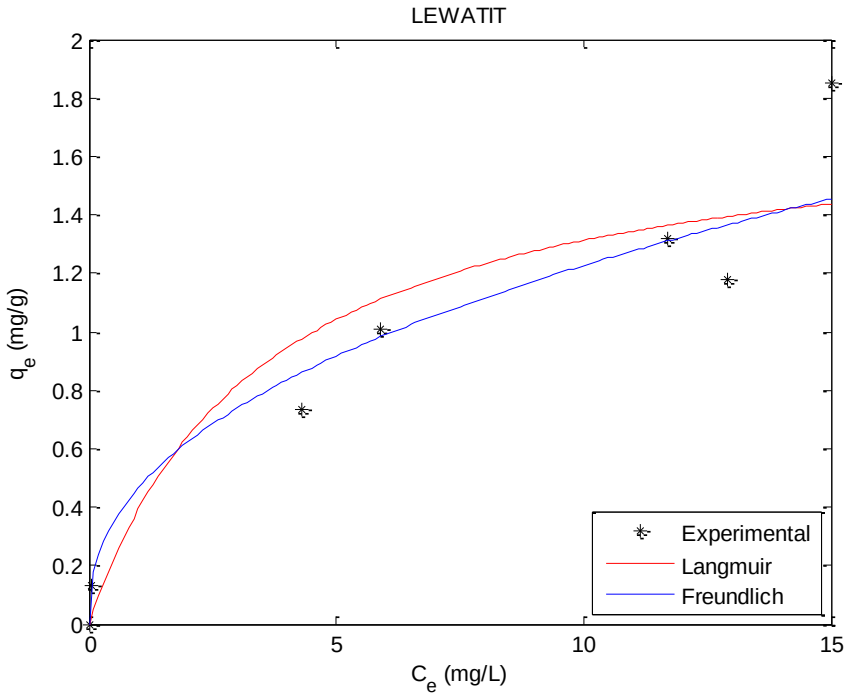

(c)

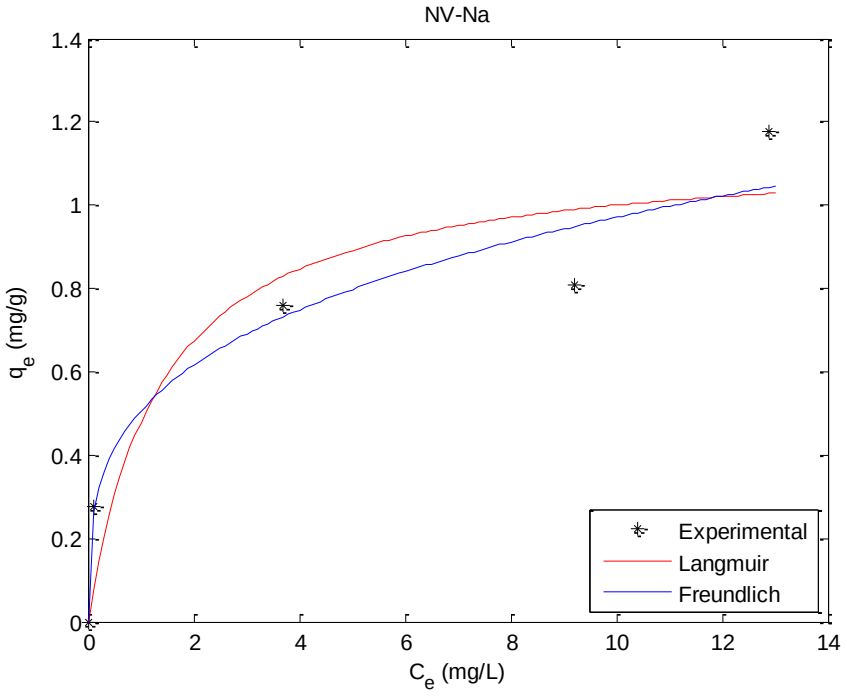

(d)

Figure 2.10: Langmuir & Freundlich isotherms for the selected adsorbents in real wastewater.

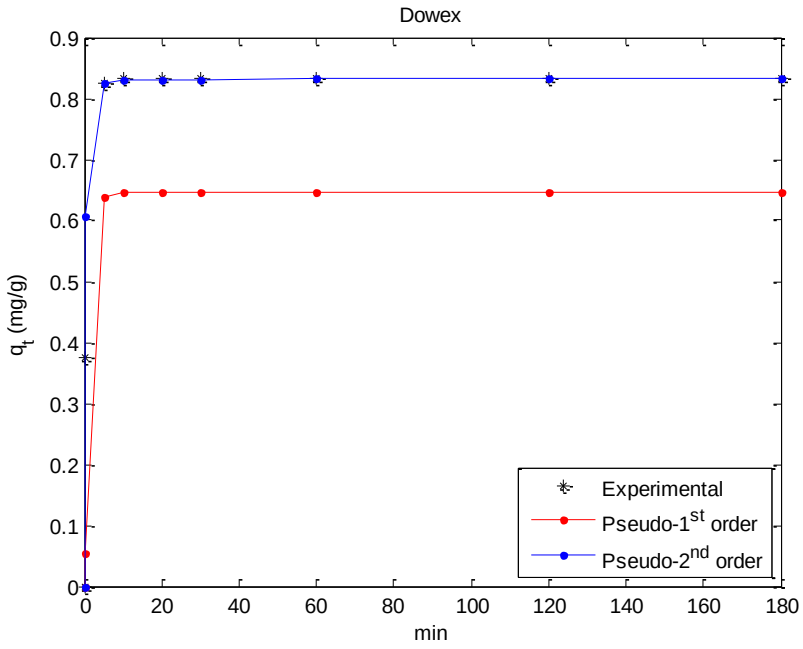
Dowex
0.9
0.8
0.7
0.6
0.5
0.4
0.3
0.2
0.1
0
q_t (mg/g)
0
20
40
60
80
100
120
140
160
180
min
Experimental
Pseudo-1st order
Pseudo-2nd order

(a)

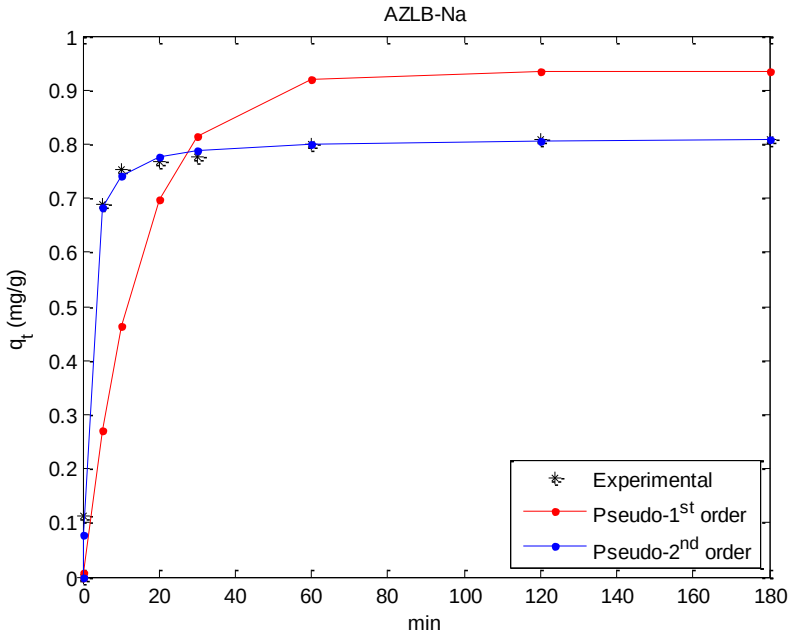
AZLB-Na
1
0.9
0.8
0.7
0.6
0.5
0.4
0.3
0.2
0.1
0
q_t (mg/g)
0
20
40
60
80
100
120
140
160
180
min
Experimental
Pseudo-1st order
Pseudo-2nd order

(b)

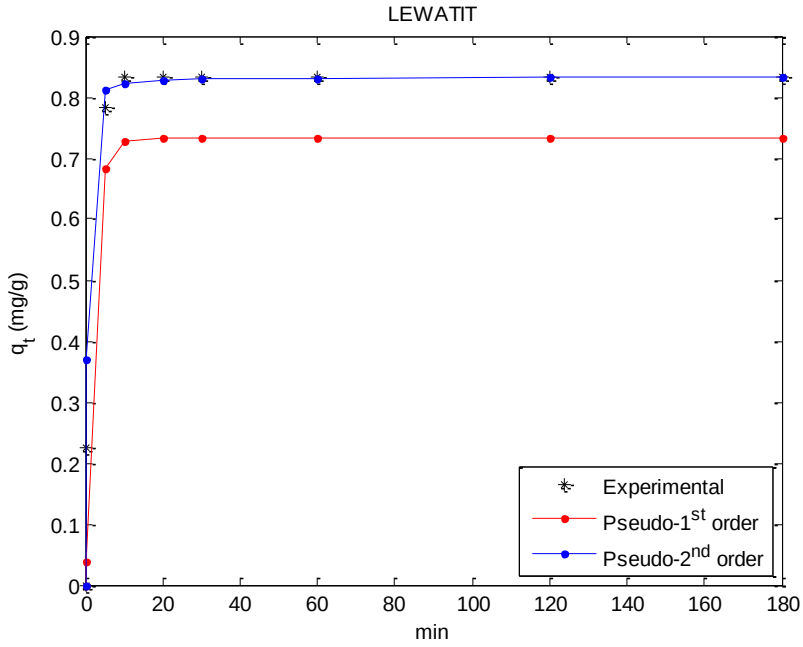

(c)

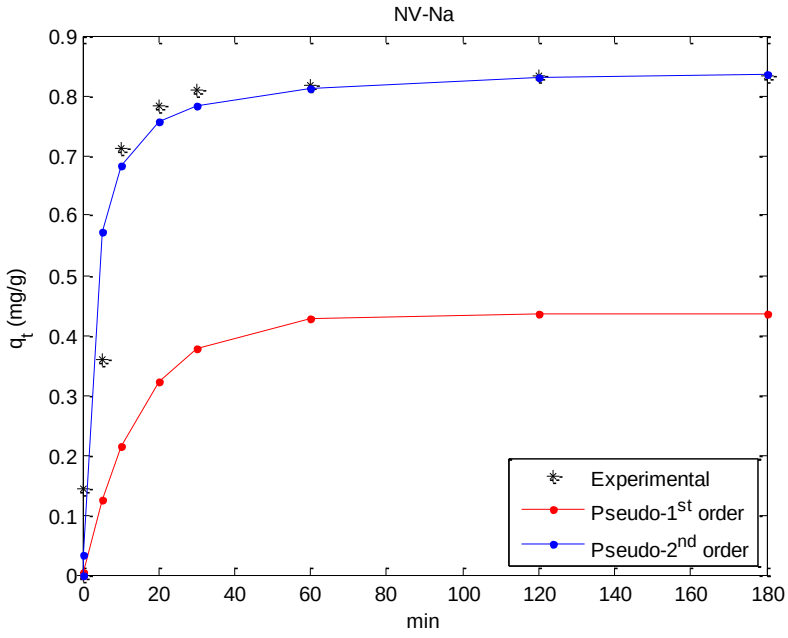

(d)

Figure 2.11: Pseudo-1st and pseudo-2nd order kinetics of synthetic wastewater using 1.5 g of each adsorbent.

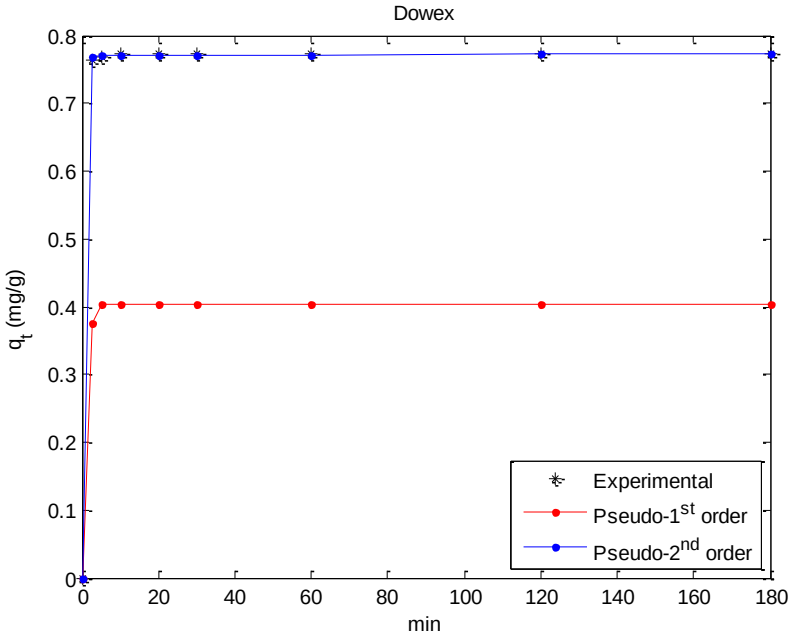
Dowex
0.8
0.7
0.6
0.5
0.4
0.3
0.2
0.1
0
q_t (mg/g)
0
20
40
60
80
100
120
140
160
180
min
Experimental
Pseudo-1st order
Pseudo-2nd order

(a)

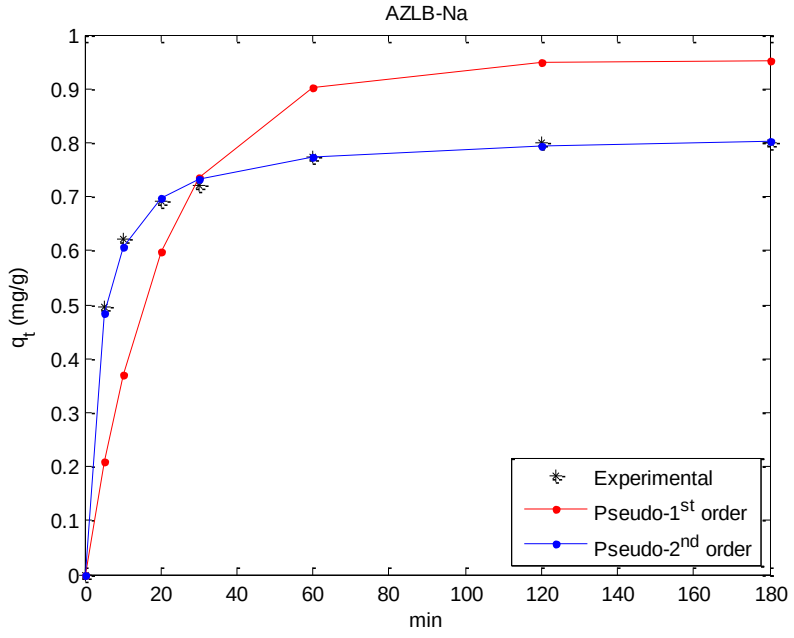
AZLB-Na
1
0.9
0.8
0.7
0.6
0.5
0.4
0.3
0.2
0.1
0
q_t (mg/g)
0
20
40
60
80
100
120
140
160
180
min
Experimental
Pseudo-1st order
Pseudo-2nd order

(b)

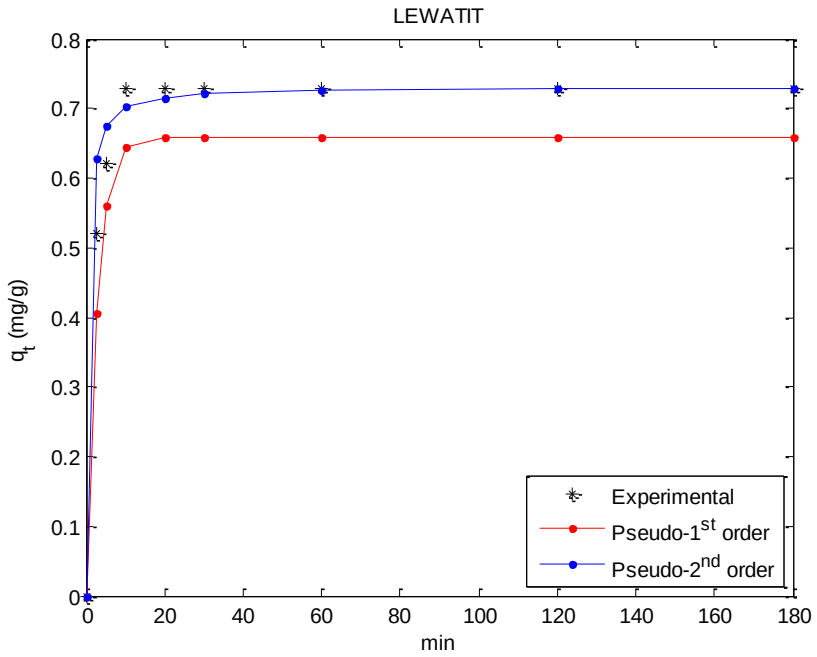

(c)

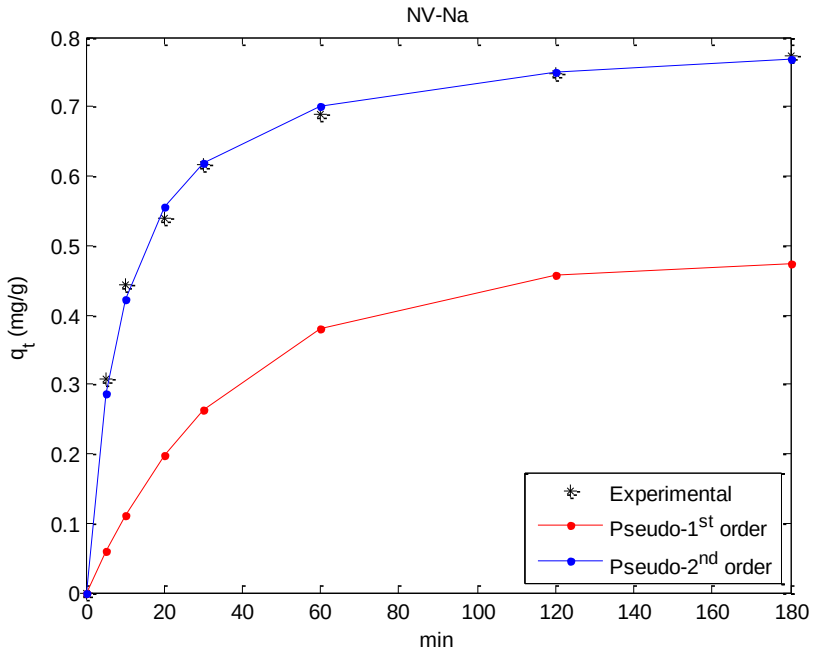

(d)

Figure 2.12: Pseudo-1st and pseudo-2nd order kinetics of real wastewater using 3 g of each adsorbent.

Table 2.4: Constants of the Langmuir and Freundlich isotherms of the selected adsorbents.

Adsorbent	Langmuir				Freundlich		
	q_{max} mg/g	k_L L/mg	RMSE mg/g	R_L	n	k_f ((mg/g).(L/mg)$^{1/n}$)	RMSE mg/g
Dowex	1.815	0.283	0.217	0.134	2.873	0.512	0.306
AZLB-Na	1.201	0.794	0.180	0.052	2.657	0.452	0.134
LEWATIT	1.774	0.284	0.272	0.134	2.378	0.465	0.227
NV-Na	1.137	0.726	0.218	0.056	3.530	0.505	0.137

Table 2.5: Constants of the pseudo-1st- and pseudo-2nd order kinetic equations of synthetic /real wastewater for selected adsorbents.

Adsorbent	q_e mg/g	Pseudo-first order equation			Pseudo-second order equation		
		q_{eth} mg/g	k_1 1/min	RMSE mg/g	q_{eth} mg/g	k_2 g/mg.min	RMSE mg/g
Synthetic wastewater using 1.5 g of the adsorbent at initial concentration 10.4 mg/L NH_3–N.							
Dowex	0.832	0.645	0.879	0.214	0.832	32.32	0.133
AZLB-Na	0.808	0.933	0.068	0.202	0.812	1.299	0.014
LEWATIT	0.832	0.731	0.545	0.221	0.832	9.585	0.086
NV-Na	0.832	0.435	0.068	0.352	0.845	0.495	0.092
Real wastewater using 3 g of the adsorbent at initial concentration 22.7 mg/L NH_3–N.							
Dowex	0.772	0.404	1.052	0.308	0.772	114.49	0.003
AZLB-Na	0.800	0.049	0.951	0.166	0.817	0.355	0.008
LEWATIT	0.728	0.659	0.381	0.147	0.730	3.365	0.070
NV-Na	0.772	0.477	0.026	0.291	0.807	0.135	0.014

2.10 Conclusions

The following conclusions can be drawn about the use of these adsorbents to remove ammonia from synthetic/real wastewaters:

1. The ion exchange resin adsorbents had a range of adsorption efficiencies but at least two of acidic resins, Dowex and Purolite C100H were very effective under the wastewater conditions, at 95 and 90% adsorption efficiency, respectively.
2. The adsorption kinetics were very fast for the acidic resins (approximately 10 minutes) and relatively slower (120 to 180 min) for the neutral or basic zeolites.
3. According to the RMSE values of the isotherms and kinetics, the adsorption process of Dowex follows the Langmuir isotherm, based on monolayer adsorption. However the AZLB-Na, LEWATIT and NV-Na followed the Freundlich isotherm, based on multilayer adsorption. Regarding the kinetics, all selected adsorbents could be characterized using the pseudo-2nd order kinetic equation.
4. For target concentrations of 1 mg/L ammonia or less, the studied adsorbents have an equilibrium capacity on the order of approximately 0.2 to 0.4 mg/g.

Chapter 3:
Continuous Adsorption Using LEWATIT

3.1 Introduction

Wastewater from industrial discharges contains heavy metals, organic substances, and suspended liquid and solids at unacceptable levels causing many environmental and potential -health risks to the public life (Alwan *et al.,* 2010; Alwan & Mehdi, 2010). The increasing ammonia level in wastewater (see Table 3.1) resulting from industrial activities has become a critical issue due to harmful effects such as the higher toxicity of the aquatic environment and more extensive corrosion of soil especially ammonia is a main source of the nitrate and nitrate (Batley, & Simpson, 2009; EPA 2013). Ion exchange and adsorption have become two options for the treatment of this type of wastewater (Foo & Hameed, 2009; Bashir *et al.*, 2010). Such an approach has many advantages such as high treatment loading and removal efficiency, fast kinetics and low cost (Widiastuti *et al.*, 2011; Gupta *et al.*, 2015; Huang *et al.*, 2017). Many other techniques have been used in the past for ammonia removal, e.g., air stripping, biodegradation, catalytic oxidation, cationic ion-exchange and membrane separation. For this, we have chosen batch and continuous (in a fixed-bed column) adsorption using a LEWATIT resin to remove ammonia from real water because it is easy to maintain and operate, inexpensive relative to air stripping and appropriate for a cold environment unlike biodegradation. Breakthrough studies of different adsorption processes have been conducted by many researchers, e.g., nickel adsorption using bentonite clay (Vieira *et al.,* 2009), biosorption of cadmium and copper using wheat straw (Muhamad *et al.,* 2010), salicylic acid and carbamazepine removal from aqueous solution using synthetic zeolites (Cabrera-Lafaurie

et al., 2014), cadmium, copper, lead and zinc from synthetic wastewater using a biosorbent combining of maple leaves, mandarin peel, and tea waste (Abdolali *et al.*, 2017), amoxicillin from water using activated carbon (de Franco *et al.*, 2017) and levulinic acid from aqueous solution (Lin *et al.*, 2017) using SY-01 resin. In this research, we investigated the novel use of a LEWATIT resin to remove 22.7 mg/L NH_3–N from real water. In particular, the Langmuir and Freundlich models were fit to equilibrium data obtained from batch experiments to obtain parameters used to predict breakthrough curve and compare with the predictions of a fixed-bed column obtained using the Bohart & Adams and Thomas models.

3.2 Real Wastewater and LEWATIT Resin

A real of 40-L wastewater was delivered from a Canadian company located in the north, stored in a cold room at 4 ^{o}C to prevent ammonia degradation due to bacteria activity and then used in the laboratory at 22.5 ^{o}C for adsorption experiments. Depending on the provided data from industry, Table 3.1 shows the full composition of the wastewaters. As in Table 3.2, LEWATIT Lanxess Monoplus S108 H used in this study is strongly acidic resin based on a styrene-divinylbenzene copolymer matrix and originally in the H^+ form (Huang *et al.*, 2014). Commercially, it consists of an organic polymer cross-linked backbone with different functional groups such as sulfonic acids, quaternary amino groups, carboxylic acid groups, or primary, secondary, and tertiary amino groups. Also, it can be modified to exchange cations or anions in water based on the application (Malovanyy *et al.*, 2014; Sica *et al.*, 2014).

Table 3.1: A full composition analysis of the real wastewater used.

Element	Ag	Al	As	Cd	Cr	Hg
Concentration (ppb)*	0.051	180.4	19.23	0.686	14.24	<0.005
Element	Mn	Mo	Pb	Se	Tl	Zn
Concentration (ppb)	181.7	24.91	1.598	8.224	0.009	53.53
Element	B	Ba	Be	Bi	Br	Ca
Concentration (mg/L)	0.139	0.076	<0.001	<0.014	3.52	272.2
Element	Cl	Co	Cu	F	Fe	K
Concentration (mg/L)	451.1	0.012	0.038	<0.20	0.361	69.57
Element	Li	Mg	Na	Ni	P	S
Concentration (mg/L)	0.019	14.75	146.7	0.648	0.018	163.4
Element	Sb	Si	Sn	SS	Te	Ti
Concentration (mg/L)	<0.003	4.941	<0.005	6.8	<0.028	<0.005
Element	V	Zr				
Concentration (mg/L)	<0.004	<0.003				
Component	NH_3	NO_2	NO_3	PO_4	SO_4	pH = 8.3
Concentration (mg/L)	22.6	12.1667	132.2	<2.00	499.5	

* ppb: part per billion.

Table 3.2: Some physical and chemical properties of the LEWATIT.

Mean bead size	0.6 ± 0.05 mm	Operating pH	0 − 14
Density	1.26 g/mL	Operating Temperature	Max. 120 ^oC
Total capacity	2.2 eq/L	Regenerant	HCl, H_2SO_4, NaCl

3.3 Adsorption Analysis

For the adsorption experiments on real wastewater, analysis was conducted using high-range Hach kits for ammonia (Ammonia HR TNT, Hach Company/Hach Lange GmbH, USA) to mix with ammonia samples using the manufacturer's procedure provided for the kits, a pH meter (JENCO Electronics LTD, Model 1671) to measure the pH of the wastewater before and after

adding LEWATIT, and an UV-vis spectrophotometer (HP8452A diode array) to determine the ammonia concentration as nitrogen (NH_3–N). The manufacturer's procedure is as follows: A 0.1- mL sample containing ammonia was combined in the test vials with a hypochlorite solution to form mono-chloramine and then a salicylate reagent was added to form 5-aminosalicylate, which is yellow, and then a sodium nitroprusside agent to form a blue-coloured complex. The blue colour is masked by the yellow coloured 5-aminosalicylate, which is in excess, and the resulting colour is green. After 20 min, the absorbance is ready to be measured by a spectrophotometer at 655 nm wavelength and quantified using a pre-set instrument program method (343 N, Ammonia HR TNT).

3.4 Isotherms

The adsorption equilibrium was assessed using Langmuir and Freundlich isotherms, which have been applied previously by numerous researchers. A series of experiments was conducted using different adsorbent masses (0.5, 1, 2, 3, 6 and 9 g) in 0.12 L wastewater at an initial ammonia concentration of 22.7 mg/L NH_3–N. The adsorption capacity of ammonia at equilibrium can be defined as follows:

$$q_e = \frac{(C_o - C_e)\,V}{m} \tag{3.1}$$

where C_o and C_e are the NH_3–N concentrations at $t = 0$ and equilibrium, respectively, m is the mass of the adsorbent (g) and V is volume of the adsorbate (L). The equation for the Langmuir isotherm is (Langmuir, 1918):

$$q_e = \frac{q_{max} k_L C_e}{1 + k_L C_e} \quad (3.2)$$

where q_{max} is the maximum adsorption capacity (mg/g) and k_L is the Langmuir equilibrium constant of the free energy of adsorption (L/mg). If adsorption follows Langmuir behavior, the essential characteristics of the Langmuir isotherm can be explained in terms of the dimensionless equilibrium parameter R_L:

$$R_L = \frac{1}{1 + K_L C_o} \quad (3.3)$$

The dimensionless separation factor R_L value denotes the adsorption type as follow: irreversible (R_L = 0), linear (R_L = 1), favorable (0 < R_L < 1) and unfavorable (R_L > 1) (Weber & Chakravorti, 1974).

The Freundlich isotherm is given by the relationship as follows (Freundlich, 1906):

$$q_e = k_f C_e^{1/n} \quad (3.4)$$

where k_f is the Freundlich constant for adsorption ((mg/g).(L/mg)$^{1/n}$) and n is the dimensionless Freundlich constant.

3.5 Relationship Between Isotherms and Breakthrough Curve

Based on constants obtained from Langmuir and Freundlich isotherms, breakthrough curves can be predicted using the following expressions derived by Chern and Chien (2002):

Langmuir: $$t = t_{0.5} + \frac{\rho q_{max}}{\varepsilon k_L a C_o}\left[\ln 2(C_t/C_o) + \frac{1}{1 + k_L C_o} \ln \frac{1}{2(1 - (C_t/C_o))}\right] \quad (3.5)$$

Freundlich: $t = t_{0.5} + \frac{\rho k_f C_o^{n-1}}{\varepsilon k_L a}\left[\int_{0.5}^{1} \frac{1}{(C_t/C_o)-(C_t/C_o)^{1/n}} d(C_t/C_o)\right]$ for $C_t/C_o \geq 0.5$ (3.6)

$$t = t_{0.5} + \frac{\rho k_f C_o^{n-1}}{\varepsilon k_L a}\left[\int_{0.5}^{0} \frac{1}{(C_t/C_o)-(C_t/C_o)^{1/n}} d(C_t/C_o)\right] \text{ for } C_t/C_o \leq 0.5 \quad (3.7)$$

where C_t is the NH_3–N concentration (mg/L) in wastewater at time t, $k_L a$ is the volumetric mass transfer coefficient (1/min), $t_{0.5}$ is the time when $C_t/C_o = 0.5$, ρ is the density of the wastewater (mg/cm^3) and ε is the porosity of the column.

By finding a volumetric mass transfer coefficient as Equation 3.8 (Chern & Chien, 2002; Kananpanah *et al.*, 2009), it will be easy to predict a breakthrough curve in a fixed-bed column using Equation 3.5 for Langmuir isotherm and Equations 3.6 (when C_t/C_o is between 0-0.5) & 3.7 (when C_t/C_o is between 0.5-1) for Freundlich isotherm with ascending and descending intervals of C_t/C_o respectively.

$$\left(\frac{d(C_t/C_o)}{dt}\right)_{0.5} = \frac{\varepsilon k_L a}{\rho k_f C_o^{n-1}}\left((C_t/C_o) - (C_t/C_o)^{1/n}\right) \quad (3.8)$$

3.6 Fixed-Bed Column

Two different-sized columns were used for the continuous adsorption experiments. The small column shown in Figure A.3 (right) was made from a piece of glass tubing (10-mm inner diameter × 330-mm length) sealed at one end with a piece of 5 μm Whatman filter. A series of experiments was conducted by passing wastewater through this column loaded with different masses of LEWATIT resin (3, 6, and 9 g) until ammonia breakthrough curve was observed. Once the appropriate amount of LEWATIT was added into the column, the height of the fixed-bed was measured. Real wastewater was then introduced into the top of the column and a timer

was immediately started. Samples of the wastewater in the discharge from the column were collected and the NH_3−N concentration measured using a Hach kit. This procedure was repeated before and after observing the breakthrough curve. The total volumes of wastewater passed through the column were 0.3, 0.6 and 0.96 L for a 3, 6, 9-g LEWATIT resin respectively. The large column (Ace chromatography column) was made of a 25-mm inner diameter × 600-mm long piece of glass tubing with taped threaded glass ends and threaded teflon endcaps, as shown in Figure A.3 (left). Appropriate plastic tubing (1/4'' and 1/8" ID) was connected to an adjustable-headed peristaltic pump (Stunner pumps) with duct tape to pass wastewater into the column at operating range of 0.0057-0.1051 L/min as shown in Figure A.4. The column contained a mass of 131.4 g LEWATIT to get to a sufficient height in the column, while the wastewater was delivered at rate of 0.0385 L/min through the column until ammonia breakthrough curve was observed. The experiments in the large column were conducted as follows: the desirable LEWATIT mass was weighed and then added into the column with measuring the bed depth to be used in the Bohart-Adams model. A peristaltic pump was connected to the column top with the appropriate tubing as mentioned above and the speed was adjusted to be ~ 0.0385 L/min. DI water was first passed into the column to remove any LEWATIT attached to the column wall, ensure the whole mass filled the column and the height of the water to be 2 cm above the LEWATIT resin before introducing wastewater. The bottom valve was adjusted so that the column discharged solution at the same rate as it was introduced into the top of the column. A 1-L beaker was located under the bottom valve to collect the samples until breakthrough was reached.

3.7 Breakthrough Curve Analysis

3.7.1 Models

The Bohart-Adams and Thomas models were used to describe the behavior of continuous ammonia adsorption in a fixed-bed column using LEWATIT for comparison with our experimental data (Bohart and Adams, 1920; Thomas, 1944). According to the Bohart-Adams model, the NH_3–N concentration in the discharge from the column is given by the following expression:

$$\frac{C_t}{C_o} = \frac{1}{1+exp\left(\frac{-k_{BA}N_oZ}{v}+k_{BA}C_ot\right)} \tag{3.9}$$

$$ln\left(\frac{C_o}{C_t}-1\right) = \frac{-k_{BA}N_oZ}{v} + k_{BA}C_ot \tag{3.10}$$

where k_{AB} is the Bohart-Adams rate constant (L/mg-min), N_o is the saturation concentration (mg/L), v is the linear velocity of wastewater (cm/min) and Z is the bed depth (cm). Based on Equation 3.10, a plot of $ln\left(\frac{C_o}{C_t}-1\right)$ versus t should be linear and k_{BA} and N_o can be determined by applying $slope/C_o$ and $intercept\ v/k_{AB}\,Z$, respectively. The corresponding relations based on the Thomas models are:

$$\frac{C_t}{C_o} = \frac{1}{1+exp\left(\frac{k_{Th}q_{max}m}{Q}-k_{Th}C_ot\right)} \tag{3.11}$$

$$ln\left(\frac{C_o}{C_t}-1\right) = \frac{k_{Th}q_{max}m}{Q} - k_{Th}C_ot \tag{3.12}$$

where k_{Th} is the Thomas rate constant (L/mg.min), q_{max} is the maximum concentration (mg/g) and Q is the volumetric flow rate of wastewater (L/min). Based on Equation 3.12, this model also predicts that a plot of $ln\left(\frac{C_o}{C_t}-1\right)$ versus t should be linear and that the model parameters

k_{Th} and q_{max} can be determined from $^{slope}/_{C_o}$ and $^{intercept\ Q}/_{k_{Th}\ m}$, respectively.

3.7.2 Experimental Design

To study the effect of operating variables (mass of LEWATIT, bed depth and flowrate) on the discharge concentration and breakthrough curves, the following equations were used (Bertagnolli *et al.*, 2011; Sotelo *et al.*, 2013; de Franco *et al.*, 2017):

$$q_b = \frac{C_o Q}{m} \int_0^{t_b} \left(1 - \frac{C_b}{C_o}\right)\, dt \tag{3.13}$$

$$q_s = \frac{C_o Q}{m} \int_0^{t_s} \left(1 - \frac{C_s}{C_o}\right)\, dt \tag{3.14}$$

where C_b and C_s are the NH_3–N concentrations in wastewater (mg/L) at breakthrough ($0.05C_o$) and saturation ($0.95C_o$), respectively, q_b and q_s are the adsorption capacities at breakthrough and saturation (mg/g), respectively, and t_b and t_s are the times (min) required for breakthrough and saturation, respectively, to be reached. The fractional bed utilization FBU is the ratio between the ammonia capacity at breakthrough to the ammonia capacity at saturation, i.e.,

$$FBU = \frac{q_b}{q_s} \tag{3.15}$$

The adsorption efficiency AE % is the ratio between the mass m_{ads} of adsorbed ammonia to the inlet mass m_{total} of ammonia fed to the column expressed as a percentage (Goshadrou & Moheb, 2011):

$$AE\% = \frac{m_{ads}}{m_{total}} \times 100 \tag{3.16}$$

m_{ads} and m_{total} are calculated from Equations 3.17 & 3.18 as follows:

$$m_{ads} = QC_o \int_0^{t_s} \left(1 - \frac{C_s}{C_o}\right) dt \quad (3.17)$$

$$m_{total} = QC_o t_s \quad (3.18)$$

The mass transfer zone MTZ can be calculated as follows (Vieira *et al.,* 2009, Bertagnolli *et al.,* 2011):

$$MTZ = (1 - \frac{q_b}{q_s})Z \quad (3.19)$$

In adsorption columns tests, data obtained from the laboratory can be used to determine service times for scaling up to the pilot plant. Many mathematical models have been developed but the following one obtained from the linearized Bohart and Adams model has been widely used (Hutchins, 1973) and is applied in this study to calculate the service time t:

$$t = \frac{N_o}{C_o v} Z - \frac{1}{C_o k_{BA}} \ln\left(\frac{C_o}{C_b} - 1\right) \quad (3.20)$$

$$t = aZ - b \quad (3.21)$$

$$a = \frac{N_o}{C_o v} \quad (3.22)$$

$$b = \frac{1}{C_o k_{BA}} \ln\left(\frac{C_o}{C_b} - 1\right) \quad (3.23)$$

where a and b are the slope and intercept of the linearized Bohart-Adam model, respectively.

Using the bed depth service time (BDST) technique, three laboratory adsorption column tests are enough to design an adsorption column on an industrial scale by determining the Bohart-Adams model constants and the initial concentration of the adsorbate. In this technique, three different bed depths at minimum should be used to obtain three service times

(breakthrough/saturation times) experimentally at an inlet adsorbate concentration C_{lab}. Then, a plot of service time versus bed depth can be made and the parameters a_{lab} and b_{lab} determined from the slope and intercept, respectively, as per Equation 3.24. The corresponding parameters a_{plant} and b_{plant} for the industrial scale column operating with an inlet adsorbate concentration C_{plant} can then be obtained using the relationships given in Equations 3.25 & 3.26 (Maji *et al.*, 2007).

$$t = a_{lab}Z - b_{lab} \tag{3.24}$$

$$a_{plant} = a_{lab}\frac{C_{lab}}{C_{plant}} \tag{3.25}$$

$$b_{plant} = b_{lab}\left(\frac{C_{lab}}{C_{plant}}\right)\frac{\ln(C_{plant}/C_s - 1)}{\ln(C_{lab}/C_b - 1)} \tag{3.26}$$

3.8 Desorption Process

The efficiency of the desorption process depends on many factors such as concentration and flow rate of hydrochloric acid (HCl) and direction of the flow into a column (co-current or counter-current). Obviously, the LEWATIT resin must be regenerated after completion of the adsorption step. The following regeneration procedure was used. All wastewater was drained from the resin column before the regenerant HCl solution (5:100 w:v) was introduced. This solution was passed through the column at an 8-pump setting (~ 0.0829 L/min) (superficial velocity ≈ 34.0 cm/min) in the co-current flow direction as was the wastewater. Co-current operation was used since it was expected to lead to more effective regeneration of the LEWATIT resin based on the recommendation of the resin manufacturers. The mass m_d

desorbed by (5:100 w:v) HCl can be calculated from the area under the elution curve of the NH_3–N concentration C_{el} in the eluent versus time as follows (Sotelo *et al.*, 2013):

$$m_d = Q \int_{t_p}^{t_{el}} C_{el} dt \tag{3.27}$$

where Q is the volumetric flow rate, C_{el} is the ammonia NH_3–N concentration in elution solution, t_{el} is the time for termination of the elution step and t_p is the time to achieve maximum NH_3–N concentration in elution solution.

The elution efficiency DE % is the ratio between m_d and m_{ads} expressed as a percentage:

$$DE\% = \frac{m_d}{m_{ads}} \times 100 \tag{3.28}$$

Finally, the concentration factor CF is the ratio between the maximum NH_3–N concentration C_p during the desorption step to the NH_3–N concentration in the inlet to the adsorption step (Volesky *et al.*, 2003; Sotelo *et al.*, 2013):

$$CF = \frac{C_p}{C_o} \tag{3.29}$$

For the desorption process, apparent desorption rate coefficient can be calculated as follows:

$$\frac{d(C_{el,t}/C_{el,o})}{dt} = -k'_d C_{el,t} \tag{3.30}$$

By integration Equation 3.30 since $C_{el,t}/C_{el,o} = 1$ at $t = 0$, the first order rate model is expressed as (Sparks & Jardine, 1981):

$$\ln\left(C_{el,t}/C_{el,o}\right) = -k'_d\, t \tag{3.31}$$

where $C_{el,o}$ and $C_{el,t}$ are the NH_3–N concentration in the elution solution at initial and time (mg/L) respectively and k'_d is the apparent desorption rate constant (1/min). In plotting $\ln(C_{el,t}/C_{el,o})$ vs. t, $k'_d = -slope$.

3.9 Regression

The models were fit to the experimental data by minimizing the root-mean-square error (RMSE) between the measured $(C_t/C_o)_{exp,i}$ and computed $(C_t/C_o)_{mod,i}$ values for each absorbent and the coefficient of determination (R^2)(Barrett, 1974), i.e.,

$$RMSE = \sqrt[2]{\frac{1}{N-2}\sum_{i=1}^{N}\left((C_t/C_o)_{exp,i} - (C_t/C_o)_{mod,i}\right)^2} \quad (3.32)$$

$$R^2 = 1 - \frac{\sum_{i=1}^{N}(C_t/C_o)_{exp,i} - \overline{(C_t/C_o)_{mod,i}}}{\sum_{i=1}^{N}(C_t/C_o)_{exp,i} - (C_t/C_o)_{mod,i}} \quad (3.33)$$

where N is the number of samples collected and $\overline{(C_t/C_o)_{mod,i}}$ is the mean of the computed values.

3.10 Results and Discussion

3.10.1 Isotherms

Isotherms were determined from adsorption experiments of ammonia onto the wastewater using LEWATIT. Figure 3.1 shows plots of q_e versus C_e obtained using 0.5, 1, 2, 3, 6 and 9 g LEWATIT in 0.12 L wastewater. For comparison, the computed isotherms according to the Langmuir and Freundlich models are also included. The fitted isotherm parameters obtained

for each model are listed in Table 3.3 using standard non-linear-regression Levenberg-Marquardt technique (Levenberg, 1944; Marquardt, 1963). The results shown in Figure 3.1 reveal very close agreement of the fitted models with each other and with the experimental values. Examination of the Langmuir and Freundlich parameters shows the adsorption to fall in the favorable category based on the R_L value being less than 1.0 and the n value being larger than 1.0. The R_L value for ammonia adsorption using LEWATIT in this study falls in the range of 0 – 1.

3.10.2 Fixed-Bed Column

As shown in Figure 3.2 and Table 3.4, important aims of the small-column tests were to determine if breakthrough could be reached in a reasonable amount of time and how that might differ depending on the mass of LEWATIT adsorbent. The flow rate during the breakthrough experiments using the small column was observed to remain approximately stable at a calculated value of 0.0054 L/min (superficial velocity ≈ 6.8 cm/min) for all the LEWATIT masses (3, 6, and 9 g) used in this part of the study. the results of these continuous LEWATIT adsorption experiments demonstrated that breakthrough progressed rapidly. The bulk sample volume collected over the experiment increased from 0.345 to 0.53 to 0.96 to 1.54 to 2.1 L as the experiment progressed to speed up the breakthrough. According to the breakthrough results obtained in the large column containing 131.4 g LEWATIT, breakthrough and saturation occurred after approximately 247 and 334 min, respectively. The Bohart-Adams and Thomas model parameters were calculated using the intercepts and slope from Figure 3.2 and applying Equations 3.10 & 3.12. It can be observed in Table 3.4 that the rate constants according to both models agree with each other. Table 3.5 represents design values using parameters obtained

from Thomas and Bohart-Adams models. It can be observed that increasing the bed height is reverse to the volumetric mass transfer coefficient and proportional to the length of the mass transfer zone at constant the flowrate (Sotelo *et al.,* 2012).

Figure 3.3 shows a plot of the breakthrough time t_b (when discharge NH_3–N concentration reaches 0.05 C_o) and saturation time t_s (when discharge NH_3–N concentration reaches 0.95 C_o) versus the bed depth Z obtained from the experiments ($where\ 5 \leq Z \leq 15$) in the small column. The best-fit linear relationships are as follows:

$$t_b = 8.5Z - 37.8 \tag{3.34}$$

$$t_s = 10.9Z + 13.7 \tag{3.35}$$

With these values of a_{lab} and b_{lab} in Equations 3.22 & 3.23, the corresponding values of a_{plant} and b_{plant} can be calculated using Equations 3.25 & 3.26 for any flowrate and inlet ammonia concentrations to scale up to an industrial-scale operation (Sotelo *et al.,* 2012).

3.10.3 Desorption Process

Elusion efficiency effects by many factors; percentage, and flowrate of the regenerate, contact time, surface area, type of the flow (co-current or counter current), and type of the regenerate (basic, acid or salt). A LEWATIT desorption is usually recommended using (4-6 wt%) HCl according to the manufacturer's procedure of the LEWATIT and because of high selectivity for hydrogen ions (Malovanyy *et al.,* 2013). Comparing to the other work, Malovanyy *et al.,* 2013 also used HCl to regenerate strong- and weak acidic cation resins. As shown in Figures 4 & 5, at approximately 0.0835 L/min flow rate (superficial velocity ≈16.9 cm/min) of (5:100 w/v) HCl was passed to regenerate LEWATIT in the large column and the mass desorbed was

calculated using Equation 30. This analysis showed the peak NH_3–N concentration C_p and CF were found to be 596.4 mg/L and 26.27 respectively while the desorption efficiency was 50.4 %. k_d' was 0.249 ± 0.123 1/min using linear fitting with $R^2 = 0.83$.

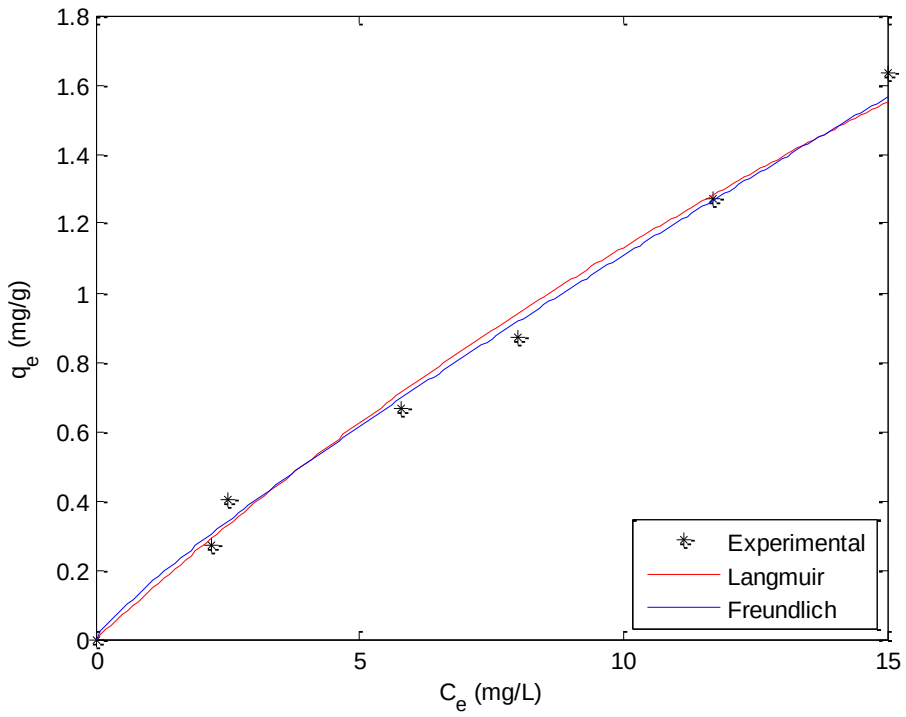

Figure 3.1: Comparison of the experimental isotherm with those fitted according to the Langmuir and Freundlich isotherms for adsorption of ammonia on 0.5, 1, 2, 3, 6 and 9 g LEWATIT in 0.12 L wastewater.

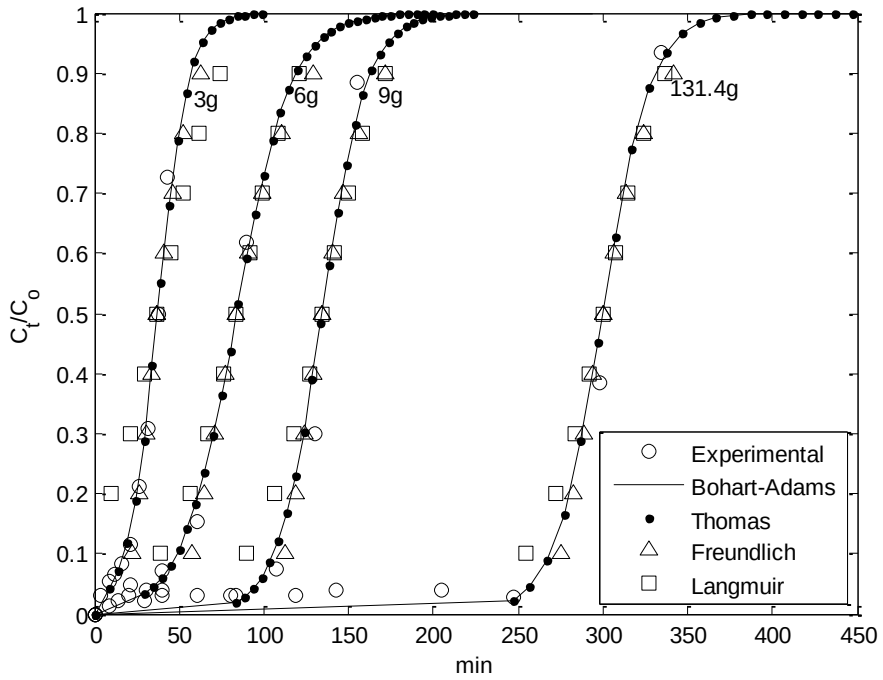

Figure 3.2: Breakthrough curves using both small and large columns.

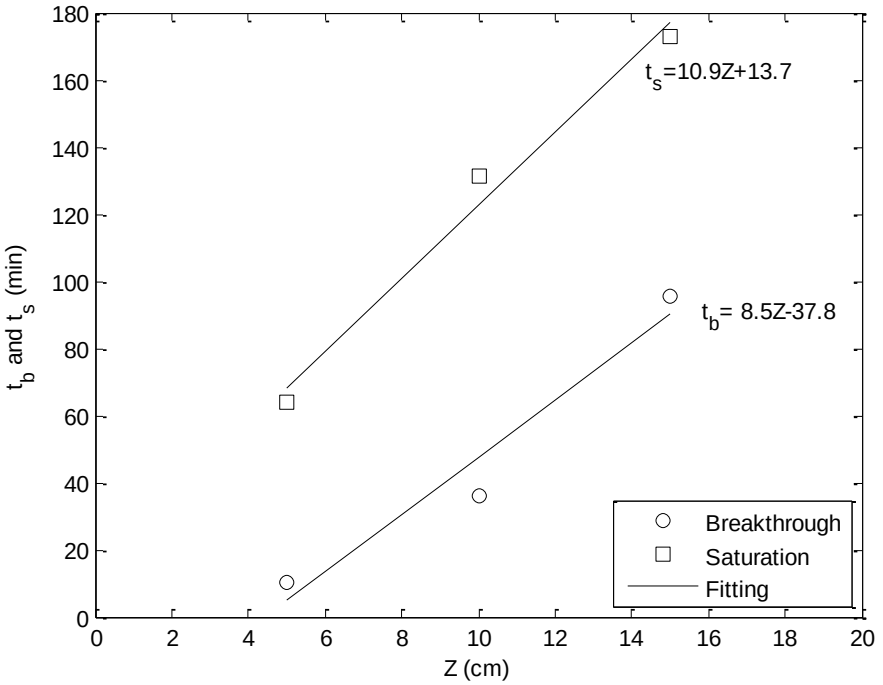

Figure 3.3: Bed depth versus breakthrough and saturation times using a small column.

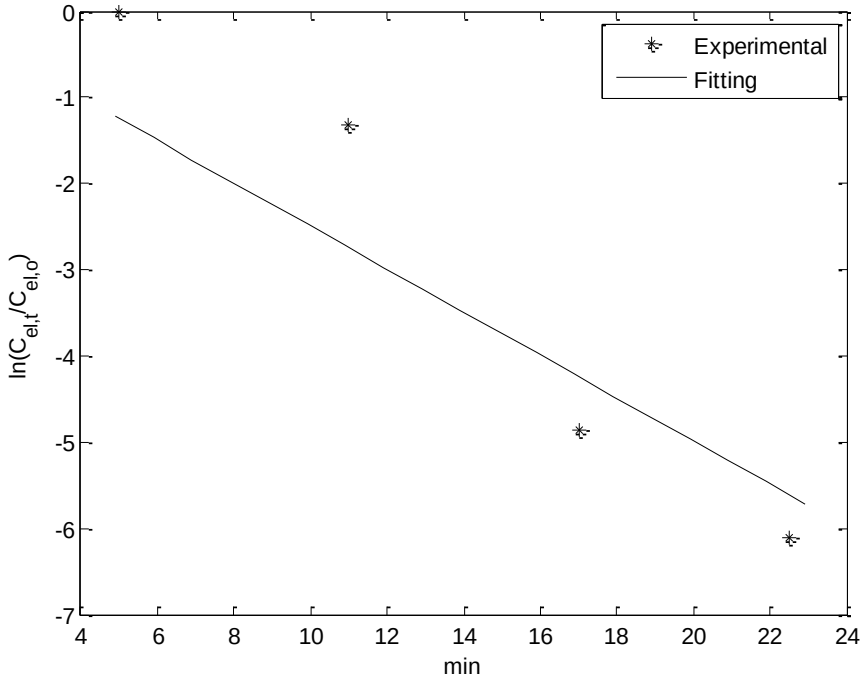

Figure 3.4: Plot of the apparent desorption rate coefficient.

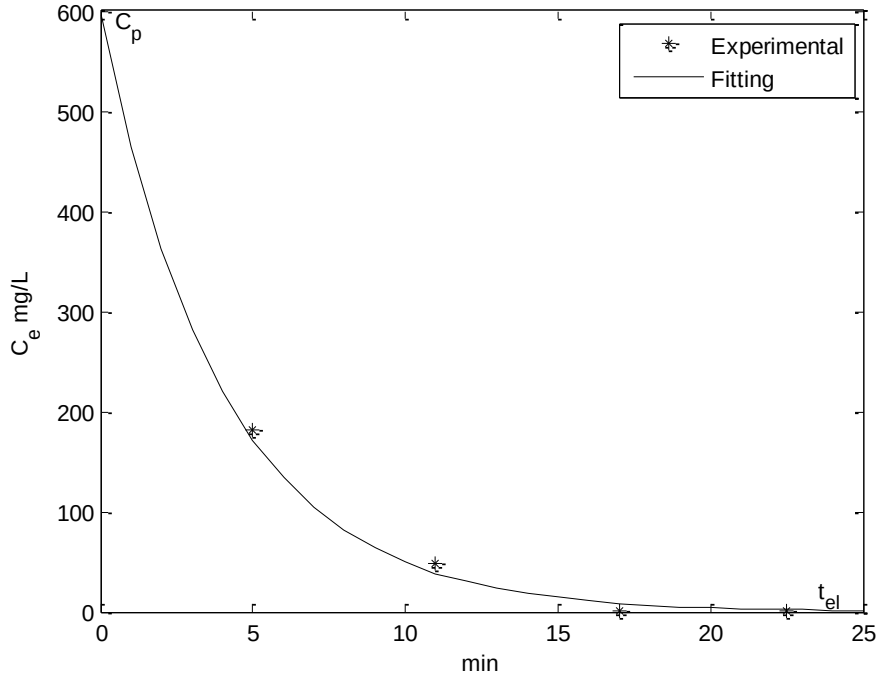

Figure 3.5: Elution plot of LEWATIT.

Table 3.3: Fitted constants obtained for the Langmuir and Freundlich isotherms.

Langmuir		Freundlich	
q_{max}, mg/g	12.69	k_f, ((mg/g).(L/mg)$^{1/n}$)	0.14
k_L, L/mg	0.009	n	1.11
RMSE	0.059	RMSE	0.051
R^2	0.983	R^2	0.987
For Langmuir isotherm, $R_L = 0.82$			

Table 3.4: Fitted constants with 95% confidence ranges obtained for the Thomas and Bohart-Adams models.

Column type	Bohart-Adams			Thomas		
	k_{BA} L/mg.min	N_o mg/L	RMSE	k_{Th} L/mg.min	q_{max} mg/g	RMSE
3 g-Small	0.0049 ± 0.001	874.8 ± 0.21	0.188	0.0049 ± 0.001	1145.2 ± 0.12	0.188
6 g-Small	0.0027 ± 0.005	683.3 ± 1.11	0.229	0.0027 ± 0.005	894.5 ± 2.4	0.229
9 g-Small	0.0034 ± 0.002	526.2 ± 0.45	0.435	0.0034 ± 0.002	688.8 ± 1.2	0.435
131.4 g-Large	0.0031 ± 0.003	316.5 ± 0.59	0.410	0.0031 ± 0.003	348.8 ± 20.9	0.410

Table 3.5: Design parameters obtained for the Thomas and Bohart-Adams models.

Q L/min	W g	Z cm	$k_L a$ 1/min	t_b min	t_s min	q_b mg/g	q_s mg/g	FBU	AE %	MTZ cm
0.0054	3	5	0.137	10.4	63.8	0.391	1.545	0.20	40	3.9
0.0054	6	10	0.076	36.3	131.4	0.601	1.514	0.28	43	7.1
0.0054	9	15	0.093	95.7	172.8	0.686	1.379	0.33	41	10.0
0.0385	131.4	29.5	0.082	257.9	341.8	0.351	0.702	0.33	69	19.6

3.11 Conclusions

Based on the experimental- and theoretical results obtained in this chapter, the following conclusions can be made:

1. The batch process using LEWATIT behaves as Freundlich isotherm more than Langmuir one based on the RMSE and R^2 values.
2. Bohart-Adams and Thomas models satisfactorily fit the data with low RMSE value.
3. Using HCl in a co-flow technique for regenerating LEWATIT shows acceptable desorption in brief time.

Chapter 4:
Continuous Adsorption Using AZLB-Na

4.1 Introduction

Increasing ammonia concentrations in industrial wastewater effluents have become a critical issue resulting from industrial activities due to various harmful effects such as increasing toxicity of aquatic environment and corrosion rate of soil especially ammoina is a main source of the nitrate and nitrate. To reduce ammonia concentrations to more acceptable limits for discharging to the groundwater at 2 mg/L (NH_3−N), adsorption process becomes one of the alternatives options for the treatment of this type of wastewater (Foo & Hameed, 2009). An adsorption process using resins/zeolites has some attractive features such as high treatment loading and removal efficiency, low cost and fast kinetics (Gupta *et al.*, 2015). Also, it is easy to maintain and operate, relatively inexpensive (compared to air stripping), appropriate for a cold environment (unlike biological processes) and high selectivity to the ammonia ions. (Sreejalekshmi *et al*., 2009; Wang *et al.*, 2014). An ammonia removal using resins/zeolites in the adsorption process has been studied by several researchers in past years. For example, Okuhara *et al*. (2007) used diverse types of Na-form zeolites to remove ammonia at low initial concentrations (2-10 ppm). Vassileva & Voikova (2009) investigated the use of natural and NaCl pretreated Bulgarian clinoptilolite for ammonium removal from aqueous solutions with ammonium concentrations ranging from 175 to 250 mg/L using batch studies under different conditions of adsorbent mass, initial ammonium concentration, pH, and temperature. Leyva-Ramos *at el.* (2010) studied ion exchange of ammonium from aqueous solutions using chabazite, considering the effects of surface properties, pH, temperature and zeolite

modifications on exchange capacity. They concluded that pH has an active while temperature has slight effect on exchange capacity of the chabazite. In this work, our expansion on these studies is by using diverse types of the adsorbents (10 resins and 6 zeolites) for removing ammonia concentration as nitrogen at lower concentrations (3.8 – 8 mg/L) real industrial wastewater samples to determine the most effective ones Also, a continuous adsorption process was chosen for removing ammonia of 22.7 mg/L concentration from real industrial wastewater using Ace chromatography column loaded by an AZLB-Na zeolite.

4.2 Real Wastewater

Approximately 40 L of the wastewater was delivered from a Canadian company located in the north. The water was stored in the cold room at 4 ^{o}C and used in laboratory at ambient conditions for subsequent adsorption experiments.

4.3 Adsorbents

Various resins and zeolites were assessed for their ability to remove ammonia from the wastewater as follows. The Na^{+} form cationic exchange resins were Diaion PK216, Diaion PK228, Diaion SK1B, Tulsion T-42 Na, and Tulsion T-52 Na and the H^{+} form cationic exchange resins were Dowex, LEWATIT MonoPlus S108H, Purolite MN500, Purolite C100H, and Purolite C104 Plus while the zeolites were Cliniptilolite NM-Ca, NV-Na, and NV-Na *TM Ammonia Specific and Bowie Chabazite AZLB-Na (see Table 4.1), AZLB-Ca and ZMI. All the zeolites were washed, filtered and oven-dried before use. The type and modification of the

zeolites as well as pH, and temperature effect on their capacity for removal ammonia from wastewater (Jha & Hayashi, 2009; Leyva-Ramos *et al.*, 2010).

Table 4.1: Some physical and chemical specifications of the AZLB-Na.

Form	Granules	Color	Reddish/Tan
Crystal size	< 1.0 micron	Operating pH	3 − 14
Density	1.73 g/cm^3	Operating Temperature	Max. 120 ^oC
Capacity	2.5 Meq/q	Regenerant	NaOH

4.4 Adsorption Analysis

For the adsorption experiments on real wastewater, analysis was conducted using a pH meter (JENCO Electronics LTD, Model 1671) to measure the pH of the wastewater before and after adding AZLB-Na, high-range Hach kits for ammonia (Ammonia HR TNT, Hach Company/Hach Lange GmbH, USA) to mix with ammonia samples using the manufacturer's procedure provided for the kits, and an UV-vis spectrophotometer (HP8452A diode array) to determine the ammonia concentration as nitrogen (NH_3−N).

4.5 Experimental Adsorption Tests

Screening rests were performed as follow: 1.0 gram of each adsorbent was added to 35 mL of the real wastewater in each of the 40-mL amber vials. A 0.1- mL sample of the solution was collected immediately and analyzed for NH_3−N and then the contents were left to stand for 7 hours while being shaken multiple times by hand before a final sample was collected and analyzed NH_3−N. The results in mg/L (NH_3−N) adsorbent were compiled to determine the most efficient adsorbent before proceeding onto more detailed studies of the selected

adsorbents. The adsorption capacity q_t (mg/g) of ammonia at time t can be calculated as follows:

$$q_t = \frac{(C_0 - C_t)\,V}{m} \tag{4.1}$$

where C_o and C_t are the ammonia concentrations (mg/L) (as nitrogen, i.e., NH_3–N) of wastewater at $t = 0$ and some later time t, respectively, m is the mass of the adsorbent (g), q_t is the experimental adsorption capacity at time (mg/g) and V is the volume of the adsorbate (L).

4.6 Relationship Between Isotherms and Breakthrough Curve

Based on constants obtained from Langmuir and Freundlich isotherms in a batch adsorption (From Chapter 2), breakthrough curves in a continuous adsorption can be predicted using the following expressions derived by Chern and Chien (2002):

Langmuir: $$t = t_{0.5} + \frac{\rho q_{max}}{\varepsilon k_L a C_o}\left[\ln 2(C_t/C_o) + \frac{1}{1+k_L C_o}\ln\frac{1}{2(1-(C_t/C_o))}\right] \tag{4.2}$$

Freundlich: $$t = t_{0.5} + \frac{\rho k_f C_o^{n-1}}{\varepsilon k_L a}\left[\int_{0.5}^{1}\frac{1}{(C_t/C_o)-(C_t/C_o)^{1/n}}d(C_t/C_o)\right] \quad \text{for } C_t/C_o \geq 0.5 \tag{4.3}$$

$$t = t_{0.5} + \frac{\rho k_f C_o^{n-1}}{\varepsilon k_L a}\left[\int_{0.5}^{0}\frac{1}{(C_t/C_o)-(C_t/C_o)^{1/n}}d(C_t/C_o)\right] \text{ for } C_t/C_o \leq 0.5 \tag{4.4}$$

where C_t is the NH_3–N concentration (mg/L) in wastewater at time t, $k_L a$ is the volumetric mass transfer coefficient (1/min), $t_{0.5}$ is the time when $C_t/C_o = 0.5$, ρ is the density of the wastewater (mg/cm^3) and ε is the porosity of the column.

By finding a volumetric mass transfer coefficient as Equation 4.5 (Chern & Chien, 2002; Kananpanah *et al.*, 2009), it will be easy to predict a breakthrough curve in a fixed-bed column using Equation 4.2 for Langmuir isotherm and Equations 4.3 & 4.4 for Freundlich isotherm with ascending and descending intervals of C_t/C_o respectively.

$$\left(\frac{d(C_t/C_o)}{dt}\right)_{0.5} = \frac{\varepsilon k_L a}{\rho k_f C_o^{n-1}}\left((C_t/C_o) - (C_t/C_o)^{1/n}\right) \quad (4.5)$$

4.7 Fixed-Bed Column

As shown in Figure A.3, The large column (Ace chromatography column) was made of a 25-mm inner diameter × 600-mm long piece of glass tubing with taped threaded glass ends, and threaded teflon endcaps. Appropriate plastic tubing (1/4'' and 1/8" ID) were connected to an adjustable-headed peristaltic pump (Stunner pumps) with a duct tape to pass wastewater into the column at a rate of the 1-10 pump setting which approximately equals to 0.0057-0.10514 L/min as shown in Figure A.4. AZLB-Na was examined at mass of 38.5 g while the real water was delivered at rate of 0.0385 L/min through the column until the breakthrough of the ammonia was observed. The procedure was as follows: the desirable AZLB-Na mass was weighed and then added into the column with measuring the bed depth to be used in the model. A peristaltic pump was connected to the column by the appropriate tubing as mentioned above to the column top and the speed was adjusted to be at a 4-pump setting to deliver wastewater at rate of 0.0385 L/min. By opening the top valve and running the pump, wastewater was passed into the column to remove the sticky AZLB-Na on the column wall, ensure the whole mass filled the column and adjust height of the water to be two cm above the AZLB-Na resin

and then passing wastewater. The bottom valve was adjusted to make the drained DI water from the column as speed as the entering water to the column. A 1-L beaker was located under the bottom valve to collect the samples until breakthrough was achieved by monitoring the rise in the NH_3–N in the adsorption sample volume and then plotting ratio C_t/C_o vs. time.

4.8 Breakthrough Curve Analysis

4.8.1 Models

The Bohart-Adams and Thomas models were used to describe the behavior of continuous ammonia adsorption in a fixed-bed column using AZLB-Na for comparison with our experimental data (Bohart and Adams, 1920; Thomas, 1944). According to the Bohart-Adams model, the NH_3–N concentration in the discharge from the column is given by the following expression

$$\frac{C_t}{C_o} = \frac{1}{1+exp\left(\frac{-k_{BA}N_oZ}{v}+k_{BA}C_ot\right)} \tag{4.6}$$

$$ln\left(\frac{C_o}{C_t}-1\right) = \frac{-k_{BA}N_oZ}{v} + k_{BA}C_ot \tag{4.7}$$

where k_{AB} is the Bohart-Adams rate constant (L/mg-min), N_o is the saturation concentration (mg/L), v is the linear velocity of wastewater (cm/min) and Z is the bed depth (cm). Based on Equation 4.7, a plot of $ln\left(\frac{C_o}{C_t}-1\right)$ versus t should be linear and k_{BA} and N_o can be determined by applying $slope/C_o$ and $intercept\ v/k_{AB}\,Z$, respectively. The corresponding relations based on the Thomas models are:

$$\frac{C_t}{C_o} = \frac{1}{1+exp\left(\frac{k_{Th}q_{max}m}{Q}-k_{Th}C_ot\right)} \tag{4.8}$$

$$ln\left(\frac{C_o}{C_t}-1\right)=\frac{k_{Th}q_{max}m}{Q}-k_{Th}C_o t \quad (4.9)$$

where k_{Th} is the Thomas rate constant (L/mg.min), q_{max} is the maximum concentration (mg/g) and Q is the volumetric flow rate of wastewater (L/min). Based on Equation 4.9, this model also predicts that a plot of $ln\left(\frac{C_o}{C_t}-1\right)$ versus t should be linear and that the model parameters k_{Th} and q_{max} can be determined from $slope/_{C_o}$ and $intercept\ Q/_{k_{Th}\ m}$, respectively.

4.8.2 Experimental Design

To study the effect of operating variables (mass of AZLB-Na, bed depth and flowrate) on the discharge concentration and breakthrough curves, the following equations were used (Bertagnolli *et al.*, 2011; Sotelo *et al.*, 2013; de Franco *et al.*, 2017):

$$q_b=\frac{C_oQ}{m}\int_0^{t_b}\left(1-\frac{C_b}{C_o}\right)\,dt \quad (4.12)$$

$$q_s=\frac{C_oQ}{m}\int_0^{t_s}\left(1-\frac{C_s}{C_o}\right)\,dt \quad (4.13)$$

where C_b and C_s are the NH_3–N concentrations in wastewater (mg/L) at breakthrough ($0.05C_o$) and saturation ($0.95C_o$), respectively, q_b and q_s are the adsorption capacities at breakthrough and saturation (mg/g), respectively, and t_b and t_s are the times (min) required for breakthrough and saturation, respectively, to be reached. The fractional bed utilization FBU is the ratio between the ammonia capacity at breakthrough to the ammonia capacity at saturation, i.e.,

$$FBU=\frac{q_b}{q_s} \quad (4.14)$$

The adsorption efficiency AE % is the ratio between the mass m_{ads} of adsorbed ammonia to the inlet mass m_{total} of ammonia fed to the column expressed as a percentage (Goshadrou and Moheb, 2011):

$$AE\% = \frac{m_{ads}}{m_{total}} \times 100 \tag{4.15}$$

m_{ads} and m_{total} are calculated from Equations 4.16 & 4.17 as follows:

$$m_{ads} = QC_o \int_0^{t_s} \left(1 - \frac{C_s}{C_o}\right) dt \tag{4.16}$$

$$m_{total} = QC_o t_s \tag{4.17}$$

The mass transfer zone MTZ can be calculated as follows (Vieira *et al.*, 2009, Bertagnolli *et al.*, 2011):

$$MTZ = (1 - \frac{q_b}{q_s})Z \tag{4.18}$$

In adsorption columns tests, data obtained from the laboratory can be used to determine service times for scaling up to the pilot plant. Many mathematical models have been developed but the following one obtained from the linearized Bohart and Adams model has been widely used (Hutchins, 1973) and is applied in this study to calculate the service time t:

$$t = \frac{N_o}{C_o v} Z - \frac{1}{C_o k_{BA}} \ln\left(\frac{C_o}{C_b} - 1\right) \tag{4.19}$$

$$t = aZ - b \tag{4.20}$$

$$a = \frac{N_o}{C_o v} \tag{4.21}$$

$$b = \frac{1}{C_o k_{BA}} \ln\left(\frac{C_o}{C_b} - 1\right) \quad (4.22)$$

where a and b are the slope and intercept of the linearized Bohart-Adam model, respectively.

4.9 Desorption Process

A next step after completing the experiment is regenerating the AZLB-Na resin. A procedure of the regeneration is as follows: AZLB-Na was drained of all wastewater before the solution was introduced. (10:100 w/v) sodium hydroxide was prepared for the AZLB-Na and passed through the column at a 4-pump setting which equals to 0.0385 L/min in the co-flow direction as the same as wastewater. The reasons of the co-flow direction are recommended by the manufacturers for greater percentage in regenerating the AZLB-Na resin and it was unknown whether the peristaltic pump can deliver the solution up. In the elusion plot, the mass desorbed by (10:100 w:v) NaOH can be calculated by multiplying the area under the curve between ammonia concentrations as N and time by volumetric flow rate Q as follows (Sotelo *et al.*, 2013):

$$m_d = Q \int_{t_p}^{t_{el}} C_{el} dt \quad (4.23)$$

where Q is the volumetric flow rate, C_{el} is the ammonia NH_3–N concentration in elution solution, t_{el} is the time for termination of the elution step and t_p is the time to achieve maximum NH_3–N concentration.

The elution efficiency DE % is the ratio between m_d and m_{ads} expressed as a percentage:

$$DE\% = \frac{m_d}{m_{ads}} \times 100 \quad (4.24)$$

Finally, the concentration factor CF is the ratio between the maximum NH_3–N concentration C_p during the desorption step to the NH_3–N concentration in the inlet to the adsorption step (Volesky *et al.*, 2003; Sotelo *et al.*, 2013):

$$CF = \frac{C_p}{C_o} \quad (4.25)$$

Apparent desorption rate coefficient can be calculated as follows:

$$\frac{d(C_{el,t}/C_{el,o})}{dt} = -k'_d C_{el,t} \quad (4.26)$$

The first order rate model for the desorption process is expressed as (Sparks and Jardine, 1981):

$$\ln\left(C_{el,t}/C_{el,o}\right) = -k'_d t \quad (4.27)$$

where $C_{el,o}$ and $C_{el,t}$ are the NH_3–N concentration in the elution solution at initial and time (mg/L) and k'_d is the apparent desorption rate constant (1/min). In plotting $\ln\left(C_{el,t}/C_{el,o}\right)$ vs. t, $k'_d = -slope$.

4.10 Regression

The models were fit to the experimental data by minimizing the root-mean-square error (RMSE) between the measured $(C_t/C_o)_{exp,i}$ and computed $(C_t/C_o)_{mod,i}$ values for each absorbent and the coefficient of determination (R^2)(Barrett, 1974), i.e.,

$$RMSE = \sqrt[2]{\frac{1}{N-2}\sum_{i=1}^{N}\left((C_t/C_o)_{exp,i} - (C_t/C_o)_{mod,i}\right)^2} \quad (4.28)$$

$$R^2 = 1 - \frac{\sum_{i=1}^{N}(C_t/C_o)_{exp,i} - \overline{(C_t/C_o)_{mod,i}}}{\sum_{i=1}^{N}(C_t/C_o)_{exp,i} - (C_t/C_o)_{mod,i}} \quad (4.29)$$

where N is the number of samples collected and $\overline{(C_t/C_o)_{mod,i}}$ is the mean of the computed values.

4.11 Results and Discussion

4.11.1 Screening Tests

As shown in Table 4.2, sixteen ion-exchange adsorbents (10 resins and 6 zeolites) were tested for their efficiency in removing ammonia from the real wastewater by adding one gram of each adsorbent into 35 mL of the real water. The preliminary results showed in the section 2.9.1 of the chapter two. A more detailed study of the three selected adsorbents from a first group (two most effective resins Dowex and Purolite MN500 and most effective zeolite ALZB-Na) was conducted over a five-hour period with samples collected at t = 0, 1, 3 and 5 hr., using 0.5 and 1 g of each adsorbent and. As shown in Figure 4.1, the starting concentration was also plotted as mg/g to keep the plots on a reasonable scale for comparison although no adsorbent was present for the time zero sample. As shown in Figure 4.2, the results demonstrated that adsorption of ammonia by the Dowex resin was the most efficient adsorbent for the ammonia (~ 76 and 89% removal when 0.5 and 1.0 g adsorbent, respectively, are used) compared to Purolite MN500 (~ 35 and 54%, respectively) and ALZB-Na zeolite (~ 38 and 55%, respectively). Each adsorbent reached saturation within an hour when 0.5 g was used and within 3 hours when 1 g adsorbent was present. The effect of the ion-exchange resins on the solution pH was markedly different from that of the zeolite. The final pH at the end of 5 hrs

adsorption decreased from 5.16 to 1.84 and 1.91 when Dowex and the Purolite MN500 resins, respectively, were used, but only to 6.32 when ALZB-Na zeolite was used. The reason is related to compositions of the both resins and zeolites since H^+ is released by the ion exchange reaction, whereas adsorption by zeolite does not.

4.11.2 Fixed-Bed Column

As shown in Figure 4.3 and Table 4.3, models constants were calculated using the intercepts and slope of the fitting models and applying Equations 4.7-4.9. It can be observed that the rate constants of both models are the same and fit the experimental data with low RMSE value as in Table 4.4 represents design values using an AZLB-Na zeolite.

4.11.3 Desorption Process

Elution efficiency effects by many factors; percentage, and flowrate of the regenerate, contact time, surface area, type of the flow (co-current or counter current), and type of the regenerate (basic, acid or salt). An AZLB-Na desorption is usually recommended using (8-10 wt%) NaOH according to the manufacturer's procedure of the AZLB-Na. Comparing to the other work, as shown in the Figures 4.4 & 4.5, approximately 0.0385 L/min flow rate of (10:100 w/v) NaOH was passed to regenerate AZLB-Na. The desorbed mass was calculated was calculated using Equation 4.23. This analysis showed the peak NH_3–N concentration C_p and CF found to be 160.2 mg/L and 7.05 respectively while the desorption efficiency and apparent desorption constant rate was 17.1 % and 0.123± 0.027 (1/min) using linear fitting with $R^2 = 0.91$ respectively.

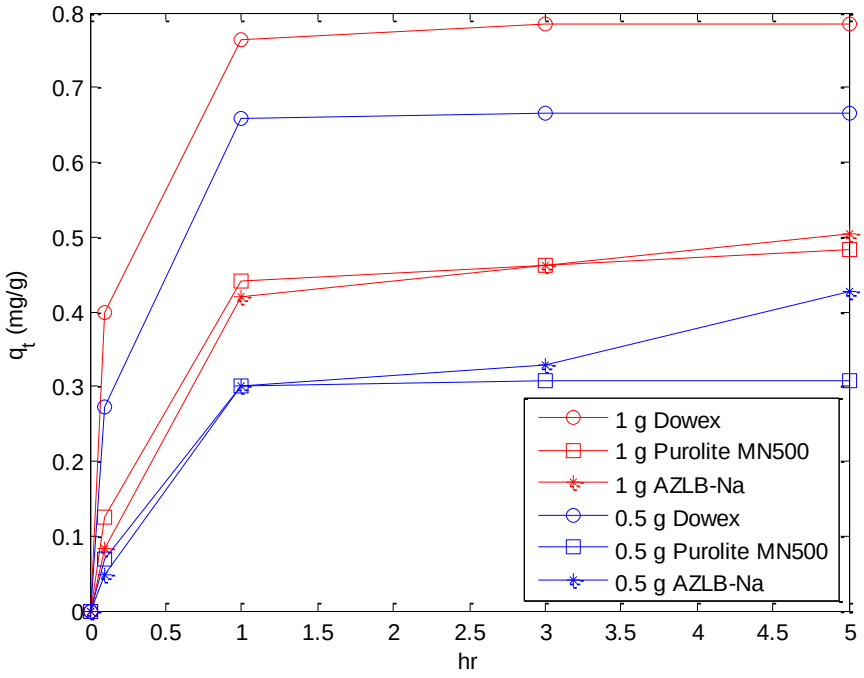

Figure 4.1: Adsorption capacities using 0.5 and 1 g of each adsorbent in real wastewater.

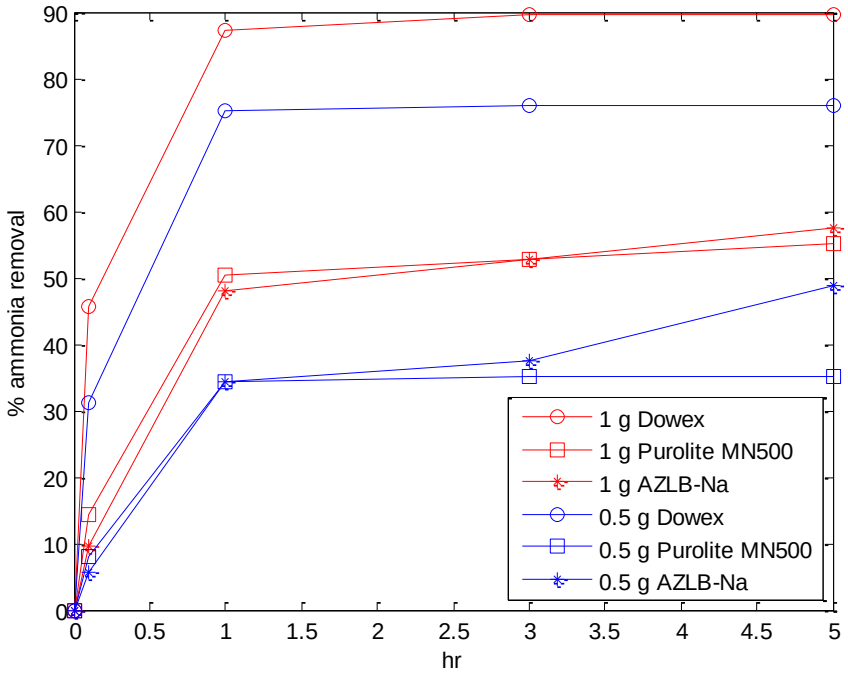

Figure 4.2: Percentage of the ammonia removal of real wastewater using 0.5 & 1 g of each adsorbent.

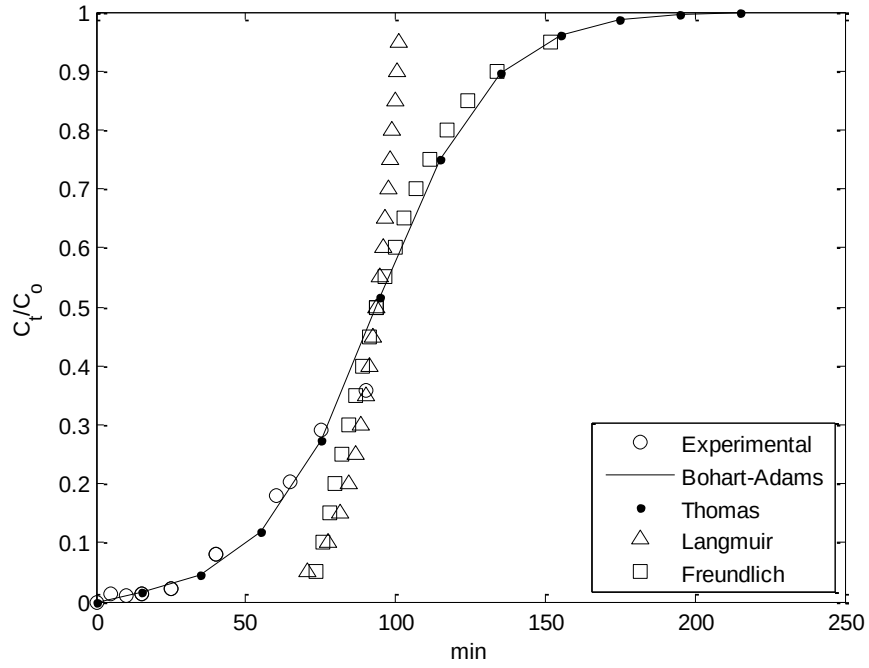

Figure 4.3: Breakthrough curves using a large column.

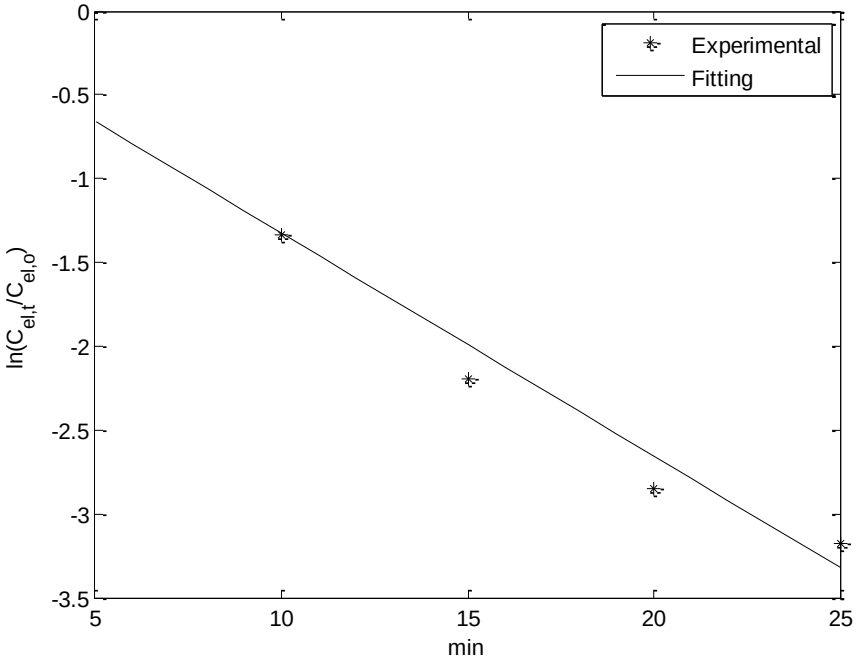

Figure 4.4: Plot of the apparent desorption rate coefficient.

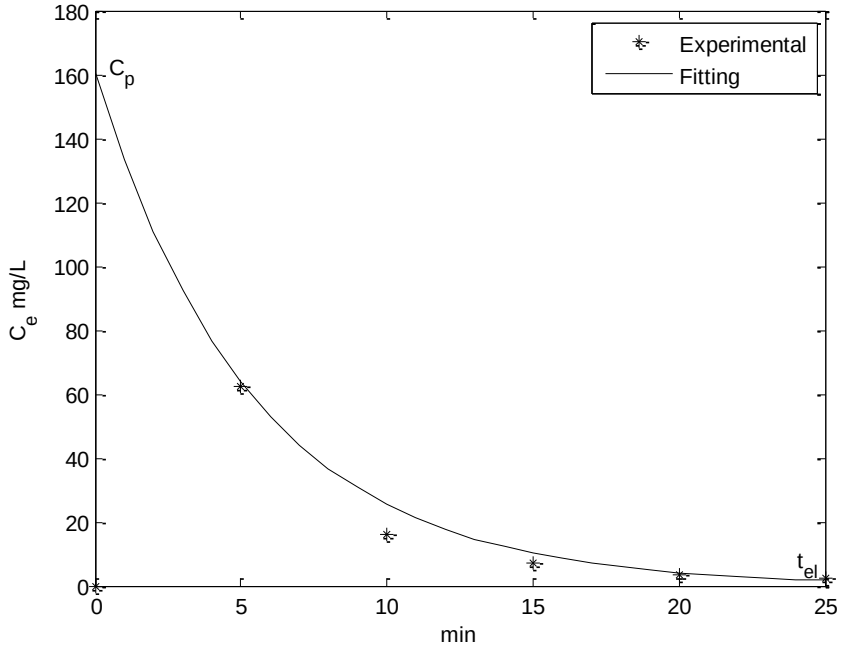

Figure 4.5: Elusion plot of AZLB-Na.

Table 4.2: Ammonia concentration (NH_3–N) using 1 g of each adsorbent and neutral pH.

Adsorbent	mg/L (NH_3–N) at 5 sec	mg/L (NH_3–N) at 7 hr	(%) removal at 5 sec	(%) removal at 7 hr	pH
First group: Initial NH_3–N (mg/L) = 8 mg/L - Initial pH = 5.16 at 22.5 ºC					
Dowex 50Wx8	3	0.4	62.5	95.0	Acidic
Purolite MN500	6.3	3	21.2	62.5	Acidic
Purolite C104Plus	7.9	9.4	1.20	*	Acidic
Purolite C100H	6.3	0.8	21.2	90.0	Acidic
Zeolite NM-Ca	7.1	5	11.2	37.5	Basic
Zeolite NV-Na	6.1	3.2	23.7	60.0	Basic
Second group: Initial NH_3–N (mg/L) = 3.8 mg/L - Initial pH = 5.12 at 22.5 ºC					
Zeolite AZLB-Na	2.5	1.3	34.20	65.78	Basic
Zeolite NV-Na *TM	3.3	3.2	13.15	15.78	Basic
Zeolite AZLB-Ca	2.9	1.9	23.68	50.00	Basic
DIAION PK228	3	1.8	21.05	52.63	Acidic
DIAION SK1B	2.8	1.8	26.31	52.63	Acidic
DIAION PK216	2.7	2.1	28.94	44.73	Acidic
Tulsion T-42 Na N-B1-TX	2.7	2.2	28.94	42.10	Acidic
Tulsion T-52 Na BCN-B1-TX	3.4	1.0	10.50	73.68	Acidic
LEWATIT monoPlus S 108 H	3.2	1.3	15.70	65.78	Acidic
KMI Zeolite	2.9	2.6	23.68	31.75	Basic

Table 4.3: Constants of Thomas and Bohart-Adams models.

Bohart-Adam			Thomas		
k_{BA}, L/mg.min	N_o, mg/L	RMSE	k_{Th}, L/mg.min	q_{max}, mg/g	RMSE
0.0023	1510.2	0.137	0.0023	1788.4	0.137

Table 4.4: Design values of both Thomas and Bohart-Adams models.

$k_L a$ 1/min	t_b min	t_s min	q_b mg/g	q_s mg/g	FBU	AE %	MTZ cm
5.359	36.4	151.8	0.789	2.575	0.234	25.27	6.888

4.12 Conclusions

From this research study, the following conclusions can be made from the experimental- and theoretical results obtained:

1. Depending on screening results, Dowex, and LEWATIT (Acidic resins) and AZLB-Na, and NV-Na (Basic zeolites) are the most efficient.
2. An AZLB-Na zeolite is more effective for the ammonia adsorption using a co-flow technique.

Chapter 5:
CO_2 Emissions Management in a FCC Unit

5.1 Introduction

Petroleum refining processes are one of the major sources of carbon dioxide (CO_2) emissions since approximately 4% of the global CO_2 emissions are produced by refineries amounting to one billion tons of CO_2 per year. Therefore, refineries are a suitable candidate for carbon capture and storage (CCS) due to the large amount of carbon dioxide, especially in the Fluidized Catalytic Cracking (FCC) units which represents approximately 30 – 40% of the total carbon emissions (Stockle & Bullen, 2008; de Mello *et al*., 2009, 2013; van Straelen *et al*., 2010; Miracca *et al*., 2013). CO_2 emitted from refineries can be reduced in several areas such as energy efficiency improvements or by implementing carbon capture and sequestration (Stockle and Bullen, 2008).

In previous work, de Mello *et al.* (2009) compared, based on technical and economic aspects, two schemes: post-combustion and oxy-combustion to capture CO_2 from FCC units and presented cost estimates for each scheme and concluded that the cost of the oxy-combustion is higher than that of post-combustion as well as using CO_2 capture will not change the product profile and affect the conversion of coke deposited. Also, they estimated the flue-gas composition depending on mass/energy balances. Finally, they found that it is technically possible to operate the FCC unit in an oxy-combustion scheme. Fu & Anantharaman (2017) developed models of the oxy-combustion in the regenerator-FCC unit because of a lack of investigation in this field in public literature that were derived from literature work of the post-combustion of the FCC unit. Also, they concluded that it is possible to capture carbon from

emissions of FCC units when working under an oxy-combustion process and CO_2 concentration in the flue gases can reach 95%. Also, their models could be used for further optimization techniques. On the other hand, van Straelen *et al.* (2010) evaluated costs for post-combustion in a complex refinery and concluded that the application of post-combustion is promising for various CO_2 emission sources at refineries. Furthermore, Petrobras used an oxy-combustion scheme in its FCC unit to retrofit carbon capture. Shell also performed a study on CO_2 reduction and the use of oxy-combustion (de Mello *et al.*, 2009). More recently, Escudero *et al.* (2016) concluded that levels of carbon dioxide are always high in refineries since they have a range of final conversion products. Also, they found that it can be economically and technically possible to capture carbon dioxide from an oxy-combustion scheme in the refinery sector. FCC units can be considered as one of the main sources that contribute to the most carbon dioxide emissions in refineries. According to tests under a CO_2 capture project in Brazil, it is technically feasible to retrofit a FCC unit to capture carbon dioxide by an oxy-combustion system since it is found that total refinery emissions decreased by 20% to 30% (Escudero *et al.,* 2016). We expand on these studies by: i) describing the system using the simplified models, especially in oxy-combustion system where no clear published models exist, ii) identifying the side constraints from the dynamic behavior of each stream in the unit and iii) examining the effects of integrating a carbon capture unit within the FCC unit.

5.2 Fluidized Catalytic Cracking (FCC) Unit

5.2.1 FCC Process Description

Converting heavy oil fractions (Gasoil) to valuable products such as gasoline and liquid petroleum gas is a main objective of the FCC unit. As shown in Figure 5.1, a mixture of the fresh hydrocarbon feed and catalyst with 0.1% of the regenerated catalyst is preheated at 204 − 400 ^{o}C to prevent coking and then pumped to the riser bottom to meet the high-temperature regenerated catalyst from the regenerator at 716^{o}C. The heat carried by the regenerated catalyst vaporizes and raises the mixture to the desired cracking reaction temperature at 522^{o}C until separation of the oil vapors from the catalyst at the reactor top. The contact time between the regenerated catalyst and mixture in the reactor is 2-10 seconds. Then, hydrocarbon vapors are treated with steam injection at 522^{o}C to separate them from the catalyst surfaces and then passed through the fractionating column for multiprocessing to yield usable products. Coke forms on the catalysts surfaces due to cracking reactions and causes reduction in its activity. Therefore, the spent catalyst leaves the reactor containing deposited coke and passes to the regenerator where coke contacts and reacts with air or oxygen depending on the combustion system for 10-15 minutes of residence time. Variations of the air or oxygen flow rate are one of the vital tools for controlling the regenerator temperature where the air/oxygen temperature is 370 – 593^{o}C. Finally, the regenerated catalyst enters the bottom of the riser through the side valve, and thus a continuous catalyst circulation loop is completed. A temperature range of the reactor and regenerator is 496 – 565^{o}C and 677 – 732^{o}C respectively while reactions of the reactor and regenerator are endothermic (1.55622×10^{6} kJ/min) and exothermic (8.4999×10^{6} kJ/min) respectively. Heat losses in the reactor and regenerator are 2% and 4% respectively

due to convection and radiation (Gary, Hankwerk, & Kaiser, 2007; Lieberman, 2009). Because of the full post-combustion reactions inside the regenerator, the CO_2 emitted typically represents 10 – 20% of flue gases while in an oxy-combustion, the CO_2 percentage is higher around 90 – 95% because flue gases are not containing nitrogen. Two combustion systems (post- and oxy-combustion) are possible depending on the FCC regenerator design. Differences between the two systems are many, such as the amount and concentration of the carbon dioxide in flue gases, and the operating cost. Also, post-combustion system happens in the presence of air (including nitrogen) while in the oxy-combustion takes place in the presence of pure oxygen diluted with carbon dioxide. Large amounts of nitrogen are produced by post-combustion while in the oxy-combustion it is not the case because of the use of an air separation unit (ASU) to remove nitrogen, but this increases the operating costs (Lecomte *et al.*, 2010). It is important to mention the kinetic reactions of the combustion that take place in the regenerator and give details about concentrations of the reactants/products including carbon dioxide. The reactions are as follows (Bollas *et at.*, 2007):

$$C + \frac{1}{2}O_2 \xrightarrow{K_1} CO \text{ , } r_1 = K_1[C]\,[O_2]$$

$$C + \frac{1}{2}O_2 \xrightarrow{K_2} CO_2 \text{ , } r_2 = K_2[C]\,[O_2]$$

$$CO + \frac{1}{2}O_2 \xrightarrow{K_3} CO_2 \text{ , } r_3 = K_3[O_2^{0.5}]\,[CO]\,[H_2O^{0.5}]$$

$$CO + \frac{1}{2}O_2 \xrightarrow{K_4} CO_2 \text{ , } r_4 = K_4[CO]$$

$$2H + \frac{1}{2}O_2 \xrightarrow{K_5} H_2O \text{ , } r_5 = K_5[H]\,[O_2]$$

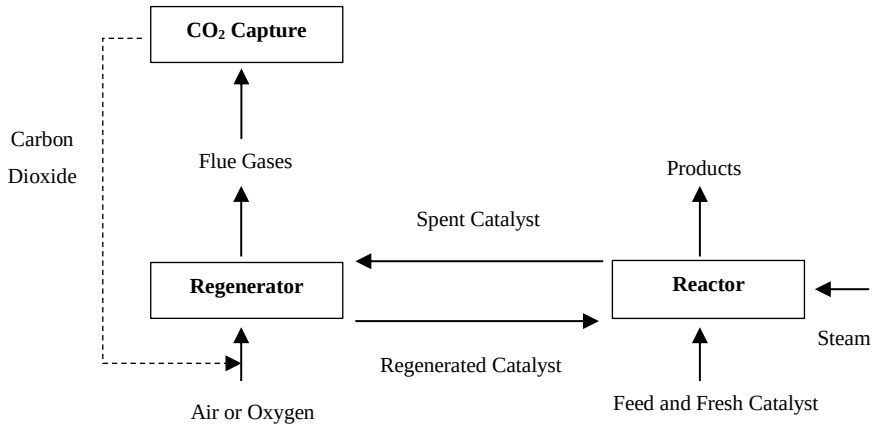

Figure 5.1: A systematic diagram of the FCC unit with the CO_2 capture unit.

5.2.2 Validation of the FCC Simplified Model

Modeling of refining and industrial processes represents the fundamental block to many tasks such as optimization, design, and control. Advantages of simplified models are many such as firstly, giving better predictions and estimations than extended models, especially when the data have a lack of information Secondly, using and developing in many different fields of chemical engineering such as optimization, process control, and design with reducing nonlinearity, complexity and the number of equations (Perregaard 1993; Brendel *et al.*, 2006). Thirdly, reducing computational simulation burdens by gaining insight into the process models (Perregaard, 1993). Finally, they are less expensive in usage and more reliable since they do not contain many unknown variables (Brooks and Tobias, 1996). Due to the difficulties that come with deriving the models, the modelers should use simplified models associated with choosing the reasonable assumptions such as considering some parameters at reasonable values, neglecting some terms in mass/heat balances and/or fixing specific heats if the temperature range is convergent. To obtain accurate results using the simulations, the researchers and engineers must have sufficient wide-range knowledge about the processes with

selecting the appropriate assumptions and have data that describe the best predictions. With information limitations about the process and existing unknown parameters, many processes have complexity and there are difficulties in obtaining accurate mechanisms. The aims of using simplified models focused on acceptable assumptions during formulating models as well as fixing some parameters at appropriate values. Developing mechanistic models represents many challenges since it is costly, difficult and requires sufficient data to predict all unknown variables and parameters of the models (Wang *et al.,* 2007). Results of the simulation models show good agreement comparing with the available data in the literature when using the same operating conditions (Elnashaie, 1994). Using simulations, the solution of the dynamic or steady state problems requires choosing special calculation methods with correct numerical features.

McFarlene *et al.* (1993), Arbel *et al.* (1995) and Bollas *et al.* (2007) presented models of the fluidized catalytic cracking unit in detail including mass/heat balances and kinetic reactions of both reactor and regenerator, control system and optimization. McFarlene *et al.* (1993) presented mechanistic models of both reactor and regenerator, covered most of the dynamic behaviors in the FCC unit including interaction between two processes, on-line optimization and process control and concluded that the FCC process is a highly nonlinear system and has interactions among the variables. Arbel *et al.* (1995) described models of the FCC unit in detail including kinetic rates of CO and CO_2 combustion and their effects on the FCC unit performance. Bollas *et al.* (2007) studied the dynamic behavior of the FCC unit using a dynamic simulator by imposing step changes in some manipulated variables, measuring reactor and regenerator temperatures and regenerator flue gas flowrates in both open- and closed loops

and comparing those to a simulator with the conclusion that the dynamic simulator can serve to develop off-line optimization studies and model-based control. Fahim *et al.,* (2010) studied and described material/heat balances of the FCC unit at steady state. Our model was based on the models presented in literature. Comparing to that of Fahim *et al.* (2010), the model has a static and dynamic behavior. State space analysis is a method used by many researchers to describe dynamic systems of multiple-inputs and multiple-outputs (MIMO) since it is easy and depends on matrix algebra (Coughanower & LeBlanc, 2009) as follows:

$$\begin{bmatrix} \dot{x}_1 \\ \dot{x}_2 \\ \cdots \\ \dot{x}_n \end{bmatrix} = \begin{bmatrix} a_{11} & a_{12} & \cdots & a_{1n} \\ a_{12} & a_{22} & \cdots & a_{2n} \\ \cdots & \cdots & \cdots & \cdots \\ a_{n1} & a_{n2} & \cdots & a_{nn} \end{bmatrix} \begin{bmatrix} x_1 \\ x_2 \\ \cdots \\ x_n \end{bmatrix} + \begin{bmatrix} b_{11} & b_{12} & \cdots & b_{1m} \\ b_{12} & b_{22} & \cdots & b_{2m} \\ \cdots & \cdots & \cdots & \cdots \\ b_{n1} & b_{n2} & \cdots & b_{nm} \end{bmatrix} \begin{bmatrix} u_1 \\ u_2 \\ \cdots \\ u_n \end{bmatrix} \quad (5.1)$$

where x_1, $x_2 \ldots x_n$ are state variables while u_1, $u_2 \ldots u_n$ are influencing ones. In matrix form, Equation 5.1 can be written as:

$$\dot{x} = Ax + Bu \quad (5.2)$$

$$y = Cx \quad (5.3)$$

where y is a vector of the outputs (y_1, $y_2 \ldots y_n$), A, B are matrixes representing coefficients of influencing and output variables respectively and C is an identity matrix. In MIMO systems, this method was used to find dynamic responses and transfer functions between influencing and output variables. On the other hand, it causes the models to lose some accuracy because of converting the system to the linear state.

5.2.3 Simplified FCC Unit Modeling

Because of high economic and environmental importance, modelling and optimization of the FCC unit represent big challenges research because process models should be described in

detail (Bollas *et al.,* 2007). Therefore, mass and heat balances of the FCC process need to be modeled, calculated correctly and employed to study through the process variables (i.e., flow rates and temperatures). Simulation models of any process are derived from mass balance, energy balance and kinetic equations while considering some assumptions to help the researchers reduce and resolve the complexity of models. Therefore, prediction of the changes consequence of the system influencing and/or operating conditions is the aim of dynamic modeling. In modern refineries, FCC units are the principal elements to modify heavy petroleum fractions into more valuable products such as high-octane number gasoline, middle distillates, and light gases. Big challenges occur in studying the operating conditions of FCC units that have large effects on physical properties of the catalyst (Lieberman, 2009). The reasons to study temperature effects on both the reactor and regenerator performance in FCC units are many. Firstly, reactor temperature plays a key role in FCC unit performance since increases in the conversion are achieved by increases in reactor temperature to produce gasoline with high octane number (Ellis *et al.,* 1998). Also, increasing rates and temperatures of the feed, and regenerated catalyst lead to an increase in reactor temperature to crack feedstocks (Lieberman, 2009; Sadeghbeigi, 2012). Secondly, regenerator temperature plays a key role in maintaining the best heat distribution in both reactor and regenerator. Keeping regenerator temperatures within normal ranges is necessary to avoid catalyst deactivation caused by high regenerator temperatures such as severe afterburning. Reducing regenerator temperature can be achieved by decreasing the feed temperature along with increasing the catalyst circulation rate, reducing the air temperature to 150^{o}C or more since the air can cut the regenerator temperature by 75^{o}C. Also, hydrothermal deactivation can be caused by exposing

the catalyst to a high-temperature steam (more than 700^{o}C) since flue gas in the regenerator contains water vapor which is produced from coke combustion (Lieberman, 2009). Finally, temperature is controlled in afterburning by maximizing the feed preheat temperature, maintaining steady spent catalyst rate, and optimizing stripping and flue gas excess oxygen. The afterburning level in the regenerator commonly depends on the operating conditions of the unit and contact between the air and the spent catalyst (Sadeghbeigi, 2012). Mass rate of the air can be used to control the afterburning in the regenerator and to prevent damages in cyclones of the regenerator since it is a customary practice in many FCC units. In addition, feed quality, fresh catalyst rate, and air rate could also affect the regenerator temperature, therefore, heat balances around both reactor and regenerator are important to ensure best system performance by finding optimal operating conditions using optimization techniques. Heat release by coke combustion provides heat to all reactor streams such as raising the feed, and steam temperatures to the reactor temperature, making up heat losses by radiation, conduction, etc., and supplying reaction heat. In regenerator, such as raising coke, and air temperatures to regenerator one, and making up heat losses by radiation, conduction, etc. (Gary, Handwerk, & Kaiser, 2007). To maintain good balancing between reactor and regenerator temperatures, the distribution of combustion heat should vary based on stream needs and design considerations but in general, the heat distribution percentages of the losses, steam, air, reaction, and feed are 2, 8, 20, 30, and 40 respectively (Jones & Pujado, 2006). In the post-combustion system, the reactor (Equations 5.4 & 5.5) and regenerator (Equations 5.6 & 5.7) models were derived with assuming heat losses are equal to 2% of the regenerated catalyst and 4% of the combustion heat for the reactor and regenerator respectively, and

specific heats of the influencing variables were constant (Jones & Pujado, 2006; Sadeghbeigi, 2012) as follows:

$$\int_{T_{ref}}^{T_{feed}} m_{feed}\overline{Cp_{feed}}\,dt + \int_{T_{ref}}^{T_{freshcat}} m_{freshcat}\overline{Cp_{freshcat}}\,dt + \int_{T_{ref}}^{T_{reg}} m_{regcat}\overline{Cp_{regcat}}\,dt$$

$$+ \int_{T_{ref}}^{T_{steam}} m_{steam}\overline{Cp_{steam}}\,dt - \int_{T_{ref}}^{T_{rec}} m_{product}\overline{Cp_{product}}\,dt$$

$$- \int_{T_{ref}}^{T_{rec}} m_{spdcat}\overline{Cp_{spdcat}}\,dt + m_{feed}\Delta H_{rxn} - 0.02\int_{T_{ref}}^{T_{reg}} m_{regcat}\overline{Cp_{regcat}}\,dt$$

$$= \left(M_{spdcat}\overline{Cp_{spdcat}} + M_{products}\overline{Cp_{products}}\right)\frac{dT_{rec}}{dt} \tag{5.4}$$

After integration, Equation 5.4 reduces to:

$$m_{feed}\overline{Cp_{feed}}\left(T_{feed} - T_{ref}\right) + m_{freshcat}\overline{Cp_{freshcat}}\left(T_{freshcat} - T_{ref}\right) +$$

$$m_{regcat}\overline{Cp_{regcat}}\left(T_{reg} - T_{ref}\right) + m_{steam}\overline{Cp_{steam}}\left(T_{steam} - T_{ref}\right) -$$

$$m_{product}\overline{Cp_{product}}\left(T_{rec} - T_{ref}\right) - m_{spdcat}\overline{Cp_{spdcat}}\left(T_{rec} - T_{ref}\right) + m_{feed}\Delta H_{rxn} -$$

$$0.02m_{regcat}\overline{Cp_{regcat}}\left(T_{reg} - T_{ref}\right) = \left(M_{spdcat}\overline{Cp_{spdcat}} + M_{products}\overline{Cp_{products}}\right)\frac{dT_{rec}}{dt} \tag{5.5}$$

where $\overline{C_p}$ is the mean heat capacity (kj/kg.^{o}C), m is the mass flow rate (kg/min) and T is the temperature (^{o}C) . Similarly, we have:

$$\int_{T_{ref}}^{T_{air}} m_{air}\overline{Cp_{air}}\,dt + m_{spdcat}\overline{Cp_{spdcat}}(T_{rec} - T_{ref}) - \int_{T_{ref}}^{T_{reg}} m_{fluegas}\overline{Cp_{fluegas}}\,dt$$

$$- \int_{T_{ref}}^{T_{reg}} m_{regcat}\overline{Cp_{regcat}}\,dt - m_{coke}\Delta H_{combxn} - 0.04\, m_{coke}\Delta H_{combxn}$$

$$= \left(M_{regcat}\overline{Cp_{regcat}} + M_{fluegas}\overline{Cp_{fluegas}}\right)\frac{dT_{reg}}{dt} \tag{5.6}$$

After integration, Equation 5.6 reduces to:

$$m_{air}\overline{Cp_{air}}(T_{air} - T_{ref}) + m_{spdcat}\overline{Cp_{spdcat}}(T_{rec} - T_{ref}) - m_{fluegas}\overline{Cp_{fluegas}}(T_{reg} - T_{ref}) - M_{regcat}\overline{Cp_{regcat}}(T_{reg} - T_{ref}) - m_{coke}\Delta H_{combxn} - 0.04\, m_{coke}\Delta H_{combxn} = \left(M_{regcat}\overline{Cp_{regcat}} + M_{fluegas}\overline{Cp_{fluegas}}\right)\frac{dT_{reg}}{dt} \tag{5.7}$$

While in an oxy-combustion system, two considerations will be applied in the regenerator model: first, oxygen heat equals to the air one while second, an oxygen flowrate equals to the air one of post-combustion as follows:

$$\int_{T_{ref}}^{T_{oxy}} m_{oxy}\overline{Cp_{oxy}}\,dt = \int_{T_{ref}}^{T_{air}} m_{air}\overline{Cp_{air}}\,dt \tag{5.8}$$

$$m_{oxy}\overline{Cp_{oxy}}(T_{oxy} - T_{ref}) = m_{air}\overline{Cp_{air}}(T_{air} - T_{ref}) \tag{5.9}$$

$$m_{oxy} = m_{air} \tag{5.10}$$

Therefore, Equations 5.6 & 5.7 will be as follows:

$$\int_{T_{ref}}^{T_{oxy}} m_{oxy}Cp_{oxy}\ dt + \int_{T_{ref}}^{T_{rec}} m_{spdcat}Cp_{spdcat}\ dt - \int_{T_{ref}}^{T_{reg}} m_{fluegas}Cp_{fluegas}\ dt$$

$$- \int_{T_{ref}}^{T_{reg}} m_{regcat}Cp_{regcat}\ dt - \Delta H_{combxn} - 0.04\, m_{coke}\Delta H_{combxn}$$

$$= \left(M_{regcat}Cp_{regcat} + M_{fluegas}Cp_{fluegas}\right)\frac{dT_{reg}}{dt} \tag{5.11}$$

$$m_{oxy}Cp_{oxy}\left(T_{oxy} - T_{ref}\right) + m_{spdcat}Cp_{spdcat}\left(T_{rec} - T_{ref}\right) - m_{fluegas}Cp_{fluegas}\left(T_{reg} - T_{ref}\right) - m_{regcat}Cp_{regcat}\left(T_{reg} - T_{ref}\right) - \Delta H_{combxn} - 0.04\, m_{coke}\Delta H_{combxn} =$$

$$\left(M_{regcat}Cp_{regcat} + M_{fluegas}Cp_{fluegas}\right)\frac{dT_{reg}}{dt} \tag{5.12}$$

Differences between post- and oxy-combustion models are many: first, specific heat of the air does not equal to that of the oxygen because air contains nitrogen while oxygen is diluted with carbon dioxide, therefore; it will affect the dynamic behavior of the system since total mass and heat balances must be recalculated. Second, carbon dioxide concentrations in flue gases are different because of the use of the air separation unit to remove nitrogen from air. Despite these existing differences, switching between two systems takes 5-15 min, therefore, flexibility in operations and designs gives advantages to modern FCC units (de Mello *et al.*, 2009).

5.2.4 Optimization Technique

Optimization is considered as one of the effective techniques used by researchers and engineers to solve many relevant management problems by finding best solutions such as increasing profits, minimizing time required, and enhancing operating conditions of the process. Basic

optimization problems consist of many simple/complex mathematical expressions depending on the system (Edgar, Himmelblau, & Lasdon, 2001). Using appropriate software, optimization becomes more effective, easy to use with including many quantitative functions and methods and helps researchers to find results faster by leading to more reliable solutions. To achieve the best optimization results, objective functions and constraints must be presented very well by including at least one objective function (cost or profit function, etc.), equality constraints, inequality constraints and/or side constraints. Mathematical programming is widely used and an appropriate technique in refining operations, oil production and refinery energy (Draman *et al.*, 2002; Göthe-Lundgren *et al.*, 2002; Gunnerud & Foss, 2010; Gueddar & Dua, 2012). The optimization framework can be described as follows:

Optimizing objective function: f(x)

Subject to:

- $h(x_i) = 0$ equality constraints,
- $g(x_i) \geq 0$ *in*equality constraints,
- $x_i^L \leq x_i \leq x_i^U$ side constraints.

where x_i is the vector of the n variables, $h(x_i)$ and $g(x_i)$ are the vectors of the equality and inequality equations respectively and x_i^L, and x_i^U are lower and upper limits respectively (Edgar, Himmelblau, & Lasdon, 2001; Venkataraman, 2009).

5.2.5 Relative Gain Array (RGA)

RGA is a square-gains matrix in which summation of all rows/columns must be equal to one and an appropriate method to show interactions tightness for choosing the best pair of the input

and output variables that have the largest gains in the matrix. Mathematically, calculating RGA depends only on gains of the open and closed loops at steady state as follows:

$$\lambda_{ij} = ijth\ element\ of\ k_p \times ijth\ element\ of\ \left[k_p^{-1}\right]^T \quad (5.13)$$

where λ_{ij} are the elements of the gains matrix (dimensionless), $\left[k_p^{-1}\right]^T$ is the transport of the gains matrix inverse (dimensionless) and i, and j are the subscripts refer to rows and columns respectively. By finding λ_{11}, values of the other relative gains can be calculated where $\lambda_{12} = \lambda_{21} = 1 - \lambda_{11}$, and $\lambda_{22} = 1 - \lambda_{21}$. RGA provides useful criteria to measure an interaction as follows: no interaction exists between input variables and output ones ($\lambda_{12} = 0\ or\ 1$), an interaction exists ($0 < \lambda_{11} < 1$), an interaction is very dangerous ($\lambda_{11} < 0$) (Luyben, 1989).

5.3 Carbon Capture Unit

5.3.1 CO_2 Capture Process Description

As shown in Figure 5.3, two main processes are in a carbon capture unit: The first one is an absorber where the flue gas is fed and contacted at the bottom of the absorption column with the mono ethanol amine (MEA) to produce stripped-CO_2 gas exiting at the top of the column while the second one is a stripping column in which CO_2-rich amine is preheated and regenerated at elevated temperature. Lean-CO_2 MEA exiting from top of stripping column is cooled and fed to the absorption column while CO_2 is captured at the top of stripping column for sequestration or used as a side stream product (Wilcox, 2012). After CO_2 separation from the flue gas stream using a solvent, it is compressed and transported to suitable storage depending on the amount of CO_2 (van Staelen *et al.*, 2010).

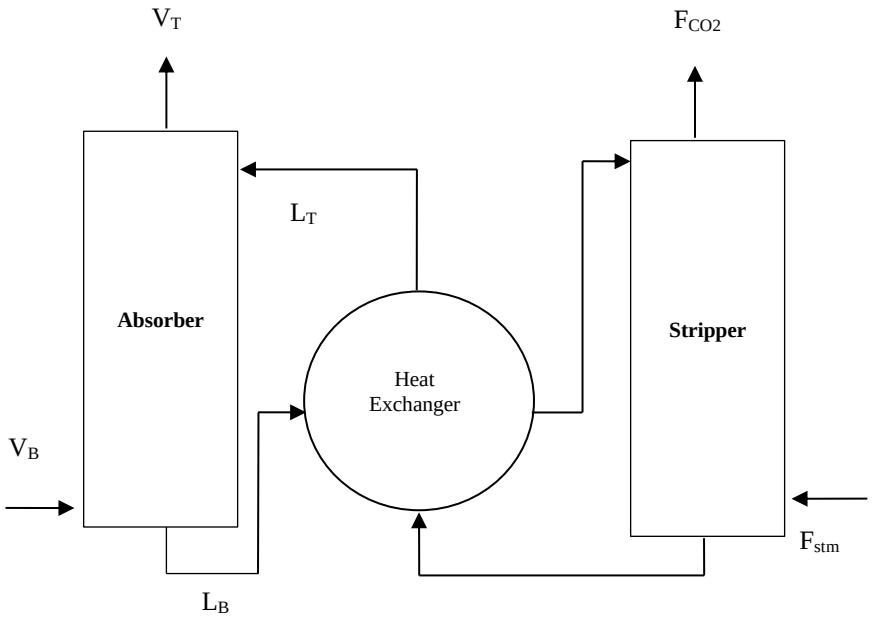

Figure 5.2: A systematic diagram of the CO_2 capture unit.

5.3.2 Simplified CO_2 Modelling

CO_2 emissions still represent a problematic issue, so finding optimal design and operation represent a crucial challenge for capturing CO_2 (Kvamsdal *et al.*, 2009). Carbon capture using an amine absorption unit has many advantages such as availability, a wide usage in industries and relatively inexpensive compared to the membrane separation technique (Meerman *et al.*, 2012; Tarun *et al.*, 2012). One of the goals of using dynamic simulation is for improving the overall design and optimizing the operation. Kvamsdal *et al.* (2009) developed a dynamic model of the absorber to evaluate all operational challenges of the process and concluded that a dynamic-model absorber can be used to study operability in absorber columns. Posch & Haider (2013) described a dynamic simulation of the absorption unit using MEA solution in the absorption process as well inlet temperature of the flue gas, lean solvent of the absorption and flue gas flow as influencing variables in their simulation. Bui *et al.* (2013 & 2014)

examined effects of the variables such as CO_2 lean solvent flow rate, % CO_2 removal, MEA wt %, temperature, and pressure of the stripper and temperature of the inlet lean solvent in the absorber on performances of both absorption and stripping. A simplified model of CO_2 capture consisted of material/energy balances in both absorption/stripping processes since the system is complex and has high interaction in optimal design and operating conditions. Balances of the absorption process are as follows:

Total mass balance: $L_T + V_B = L_B + V_T$ (5.15)

Total heat balance: $L_T H_{LT} + V_B H_{VB} = L_B H_{LB} + V_T H_{VT}$ (5.16)

Component balance of CO_2: $L_T x_{T,CO_2} + V_B y_{B,CO_2} = L_B x_{B,CO_2} + V_T y_{T,CO_2}$ (6.17)

while for stripping process,

Total mass balance: $L_B + F_{stm} = L_T + F_{CO_2}$ (5.18)

Total heat balance: $L_B H_{LB} + F_{stm} H_{stm} = L_T H_{LT} + F_{CO_2} H_{CO_2}$ (5.19)

Component balance of CO_2:

$L_T x_{T,CO_2} + V_B y_{B,CO_2} = L_B x_{B,CO_2} + V_T y_{T,CO_2}$ (5.20)

The degree of capture is one of the criteria used to measure the efficiency of the carbon capture unit which is defined as follows (Dowell & Shah, 2014).

$$Degree\ of\ capture = \frac{CO_2 generated\ by\ a\ refinery - CO_2 emitted}{CO_2 generated\ by\ a\ refinery} \quad (5.21)$$

Or,

$$\text{Degree of capture} = \frac{L T x_{T,CO_2} - V T y_{T,CO_2}}{L T x_{T,CO_2}} \quad (5.22)$$

In optimization techniques, the objective function should be maximizing the % CC using the above equation, while equality constrains are material balance and component balance.

The objective functions that can be used include:

1- Maximizing degree of capture in an absorber.

2- Minimizing MEA in an absorber to minimize the cost.

3- Minimizing temperature in a stripper to minimize the heat exchanger duty.

4- Maximizing temperature in a stripper to maximize captured CO_2.

The constraints can be the mass, component, and heat balances of CO_2 for both absorption and stripping columns. The above criteria could be used to compare between two schemes (post-combustion and oxy-combustion) using their flue gases as a feed to carbon capture unit. Nowadays, much research is presented to run the carbon capture in flexible operations. The main aim is to reduce the net cost of operation by using a renewable energy such as solar energy that is used to substitute for the energy in the reboiler of the stripper (Qadir *et al.*, 2015). Typically, in a fixed operation of the capture plant, all variables (for example flow rates/temperatures of the gas and liquid phases) are considered to be at their nominal values while in a flexible one, some of these can be changed dynamically to run the process by reducing the CO_2 capture level or the rate of spent solvent regeneration (Zaman & Lee, 2015; Zaman *et al.*, 2016). Qadir *et al.* (2015) developed reduced models to examine reboiler duty and auxiliary power requirement in the carbon capture plant. Zaman & Lee (2015) and Zaman *et al.* (2016) presented various modes of the optimization in a flexible operation for post-combustion capture plant to optimize capture level and amount of the spent solvent.

5.4 Results and Discussion

5.4.1 Dynamic Behaviors of the FCC Unit

For the post-combustion system, Figures 5.4 & 5.5 show the dynamic responses of positive- and negative changes in the flow rates to study their effects on the temperatures. Some flow rates have considerable effects while others have sensible ones. Some increases are with positive changes while others decrease since majority of the change nature in these types takes step behavior. The aim of using step changes is to determine the nature of the relationship between flow rates and temperatures and the magnitude of the change; therefore, finding lower/upper limits of the flow rates to not run the FCC unit out of the minimum and maximum temperatures. For the oxy-combustion system, Figures 5.6-5.9 show the dynamic responses of positive- and negative changes in the flow rates to study their effects on the temperatures. Also, CO_2 percentage in our results using a post-combustion system was 19.3 % which is closer to 14.2% (de Mello *et al.*, 2013) and 13.5% (Fu & Anantharaman, 2017) while it was 93.6% using an oxy-combustion system/same heat comparing to 94.3% (de Mello *et al.*, 2013) and 94.1% (Fu & Anantharaman, 2017) as well as it was 93.6% using an oxy-combustion system/same volume comparing to 94.8% (de Mello *et al.*, 2013) and 91.7% (Fu & Anantharaman, 2017). To find the lower/upper limits from the dynamic responses, the following equations were employed for temperature responses which proportional to negative/positive changes in flowrates,

$$LL_i = m_{o,i} + \frac{T_{o,j} - T_{min,j}}{k_{pi,j}} \tag{5.34}$$

$$UL_i = m_{o,i} + \frac{T_{max,j} - T_{o,j}}{k_{pi,j}} \tag{5.35}$$

While for temperature responses which reverse to a negative/positive change in flowrates,

$$LL_i = m_{o,i} + \frac{T_{max,j} - T_{o,j}}{k_{pi,j}} \tag{5.36}$$

$$UL_i = m_{o,i} + \frac{T_{o,j} - T_{min,j}}{k_{pi,j}} \tag{5.37}$$

where $m_{o,i}$ and $T_{o,j}$ are steady states for each flowrate and temperature respectively, $T_{min,j}$ and $T_{max,j}$ are minimum and maximum temperatures for reactor/regenerator respectively, LL_i and UL_i are lower and upper limits of the flowrates respectively.

5.4.2 Optimization Technique of the FCC Unit

Two different reactions take place inside the FCC unit: an endothermic reaction is in the reactor while an exothermic one in the regenerator which directly affect temperatures and other parameters. Therefore, keeping appropriate reactor/regenerator temperatures plays a key role in operating the FCC unit in a satisfactory performance. For the reactor, objective function: minimizing reactor temperature,

$$\text{Min } T_{rec} = T_{ref} + \left[\left(m_{feed}Cp_{feed}T_{feed} + m_{regcat}Cp_{regcat}T_{reg} + m_{feed}\Delta H_{rxn} - 0.02\, m_{regcat}Cp_{regcat}T_{reg}\right)/\left(m_{products}Cp_{products} + m_{fluegases}Cp_{fluegases}\right)\right] \tag{5.38}$$

Equality constraints:

$$m_{feed} + m_{regcat} - m_{products} - m_{spdcat} - m_{steam} = 0 \tag{5.39}$$

Side constraints are in Table 5.1.

For the post-combustion regenerator, objective function: minimizing regenerator temperature,

$$\text{Min } T_{reg} = T_{ref} + \left[\left(m_{air}Cp_{air}\left(T_{air} - T_{ref}\right) + m_{spdcat}Cp_{spdcat}\left(T_{rec} - T_{ref}\right) - m_{coke}\Delta H_{combxn} - 0.04\, m_{coke}\Delta H_{combxn}\right)/\left(m_{fluegases}Cp_{fluegases} + m_{regcat}Cp_{regcat}\right)\right] \quad (5.44)$$

Equality constraints:

$$m_{air} + m_{spdcat} - m_{feed} - m_{regcat} = 0 \quad (5.40)$$

Side constraint are in Table 5.2.

For the oxy-combustion regenerator/same heat, objective function: minimizing regenerator temperature,

$$\text{Min } T_{reg} = T_{ref} + \left[\left(m_{oxy}Cp_{air}\left(T_{air} - T_{ref}\right) + m_{spdcat}Cp_{spdcat}\left(T_{rec} - T_{ref}\right) - m_{coke}\Delta H_{combxn} - 0.04\, m_{coke}\Delta H_{combxn}\right)/\left(m_{fluegas}Cp_{fluegases} + m_{regcat}Cp_{regcat}\right)\right] \quad (5.41)$$

Equality constraints:

$$m_{oxy} + m_{spdcat} - m_{fluegases} - m_{regcat} = 0 \quad (5.42)$$

Side constraints: as in Table 5.2.

For the oxy-combustion regenerator/same volume, objective function: minimizing regenerator temperature,

$$\text{Min } T_{reg} = T_{ref} + \left[\left(m_{oxy}Cp_{air}\left(T_{air} - T_{ref}\right) + m_{spdcat}Cp_{spdcat}\left(T_{rec} - T_{ref}\right) - m_{coke}\Delta H_{combxn} - 0.04\, m_{coke}\Delta H_{combxn}\right)/\left(m_{fluegas}Cp_{fluegases} + m_{regcat}Cp_{regcat}\right)\right] \quad (5.43)$$

Equality constraints:

$$F_{oxy} + F_{spdcat} - F_{fluegases} - F_{regcat} = 0 \quad (5.44)$$

Side constraints: as in Table 5.2.

Tables 5.3 & 5.4 represent optimal values of the post- and oxy-combustion systems respectively.

5.4.3 RGA of the FCC Unit

15 combinations of the RGA were found in the FCC system as shown in Tables 5.5 & 5.6. Only 8 cases were accepted because of their interactions according to their RGA's values. For the post-combustion system, the values are as follows:

$$k_p = \begin{bmatrix} 0.98 & 4.65 & -1.69 & -6.63 & 1.10 & -0.85 \\ 1.65 & 2.95 & -2.84 & -4.22 & -1.23 & -0.87 \end{bmatrix} \times 10^{-2}$$

While for the oxy-combustion system of both constant heat and volume are as follows:

$$k_p = \begin{bmatrix} 1.01 & 4.65 & -1.71 & -6.63 & 1.10 & -0.85 \\ 1.70 & 2.95 & -2.86 & -4.22 & -1.23 & -0.87 \end{bmatrix} \times 10^{-2}$$

It can be observed from RGA results that some flowrates have large effects on reactor/regenerator temperatures such as flowrates of air, regenerated catalyst and spent catalyst.

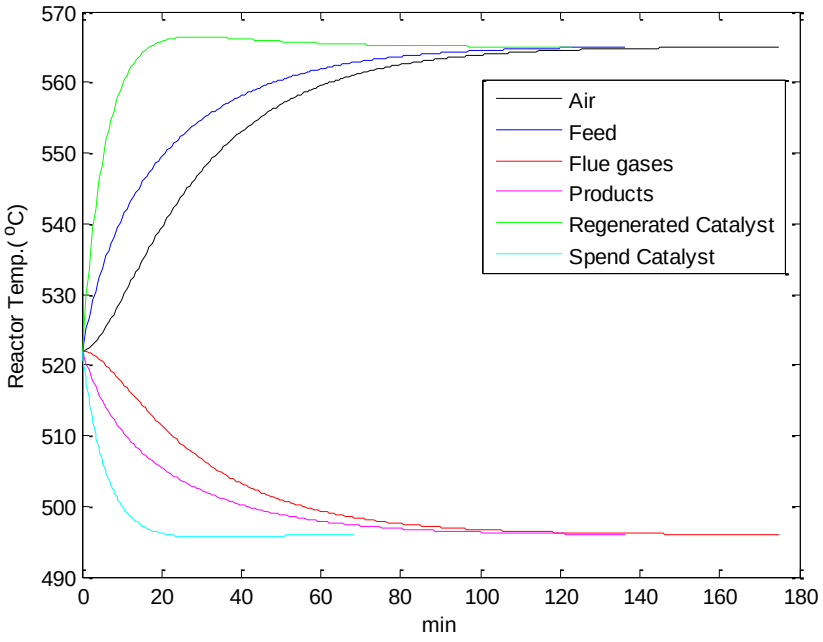

(a)

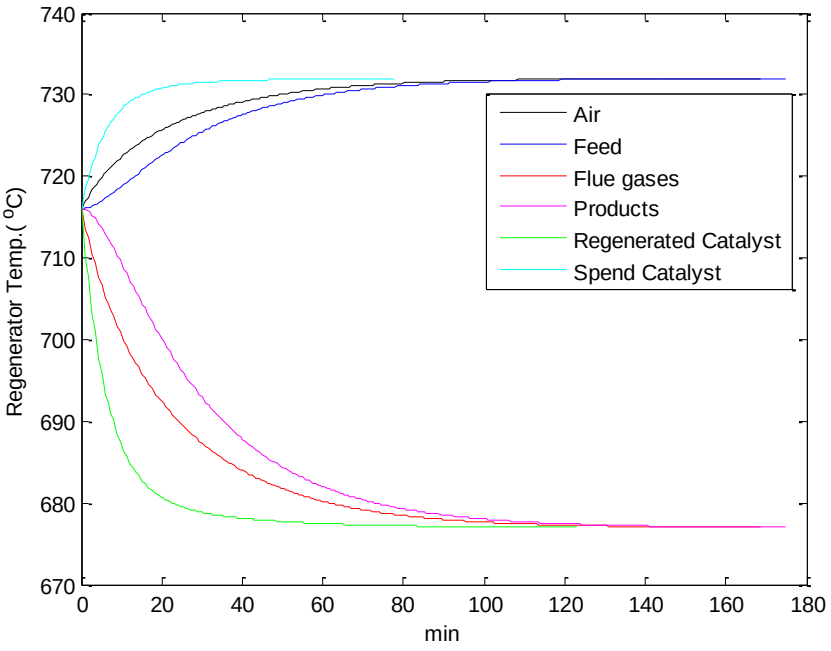

(b)

Figure 5.3: Temperatures responds by a positive change in the post-combustion system for (a) reactor and (b) regenerator.

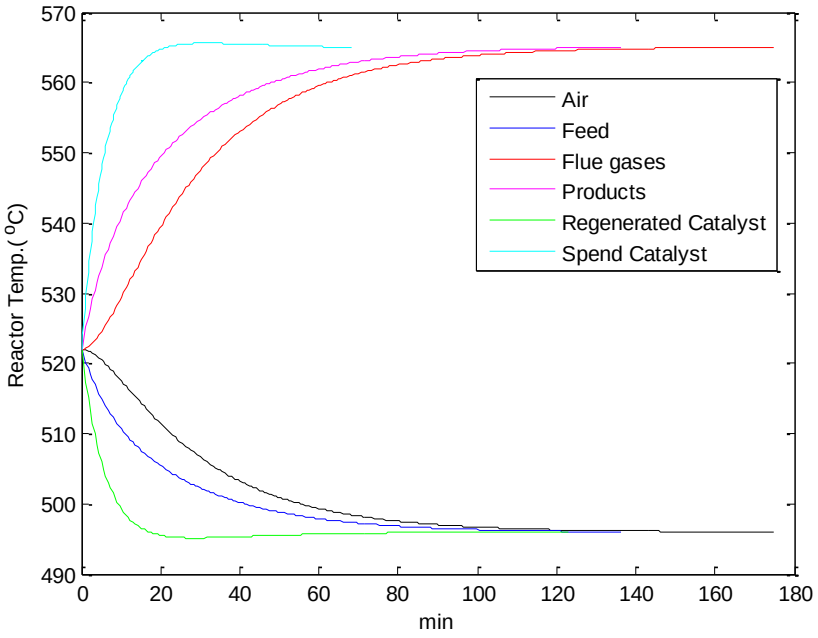

(a)

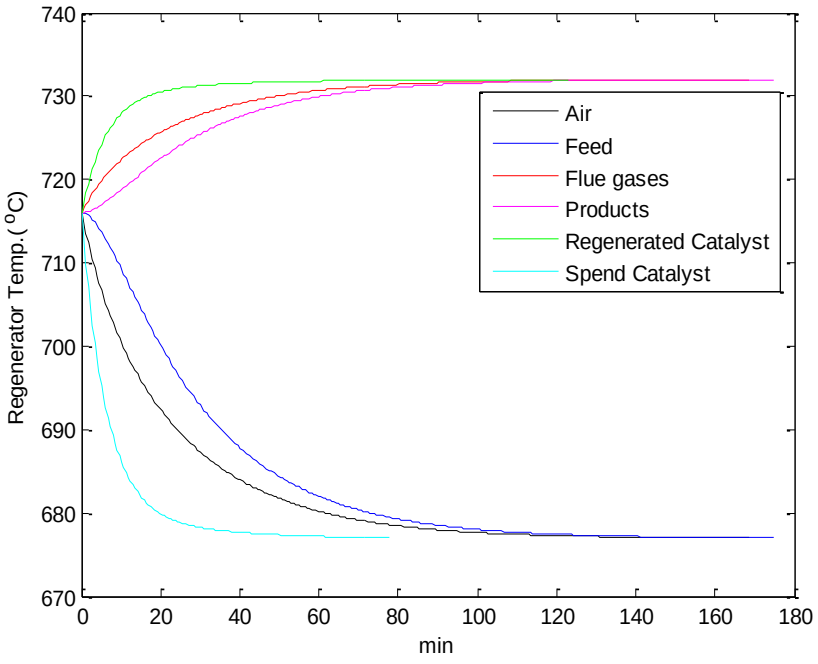

(b)

Figure 5.4: Temperatures responds by a negative change in the post-combustion system for (a) reactor and (b) regenerator.

.

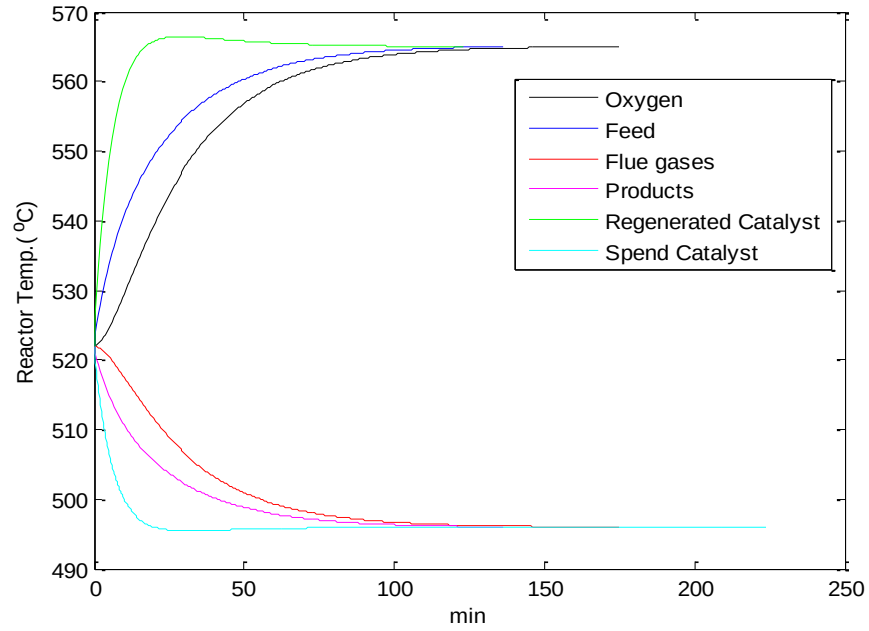

(a)

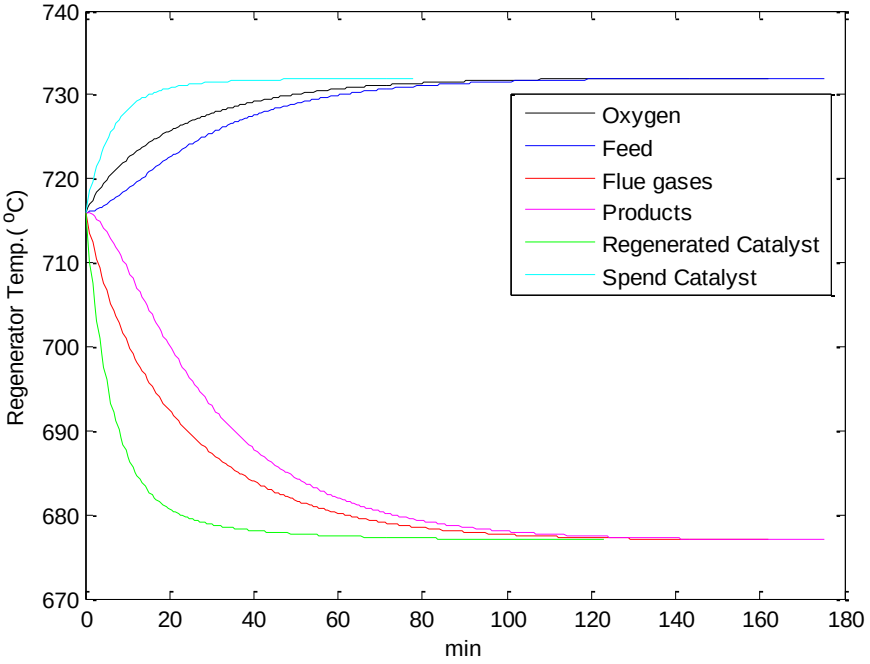

(b)

Figure 5.5: Temperatures responds by a positive change in the oxy-combustion system/same heat for (a) reactor and (b) regenerator.

.

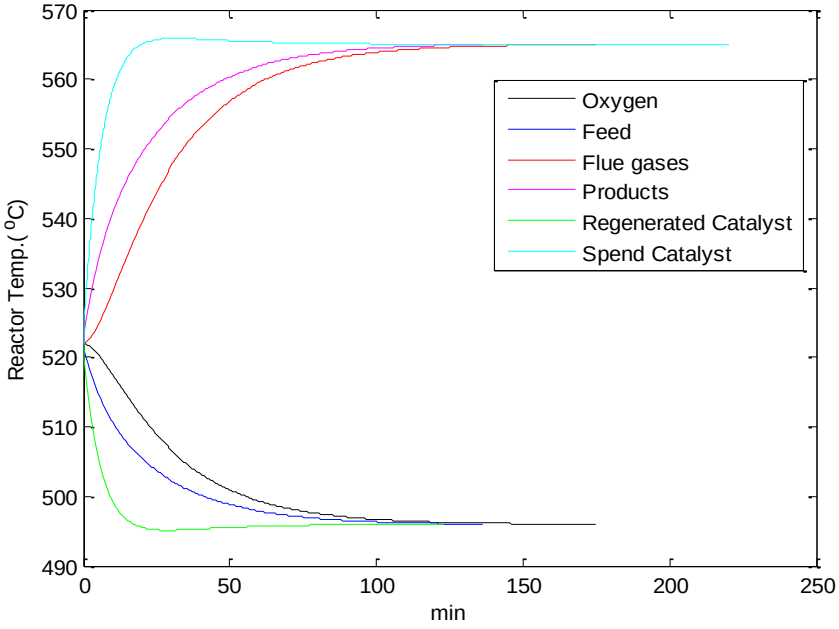

(a)

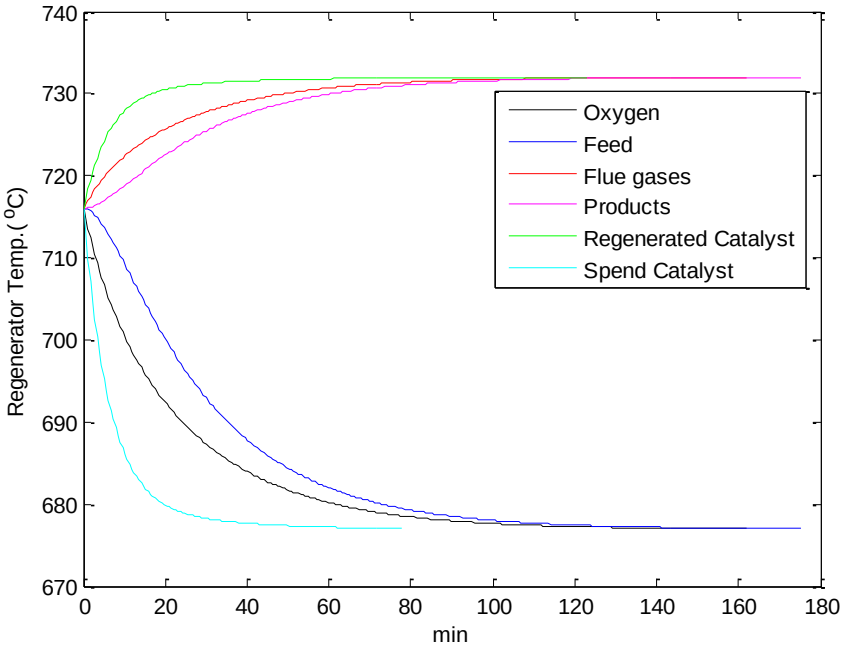

(b)

Figure 5.6: Temperatures responds by a negative change in the oxy-combustion system/same heat for (a) reactor and (b) regenerator.

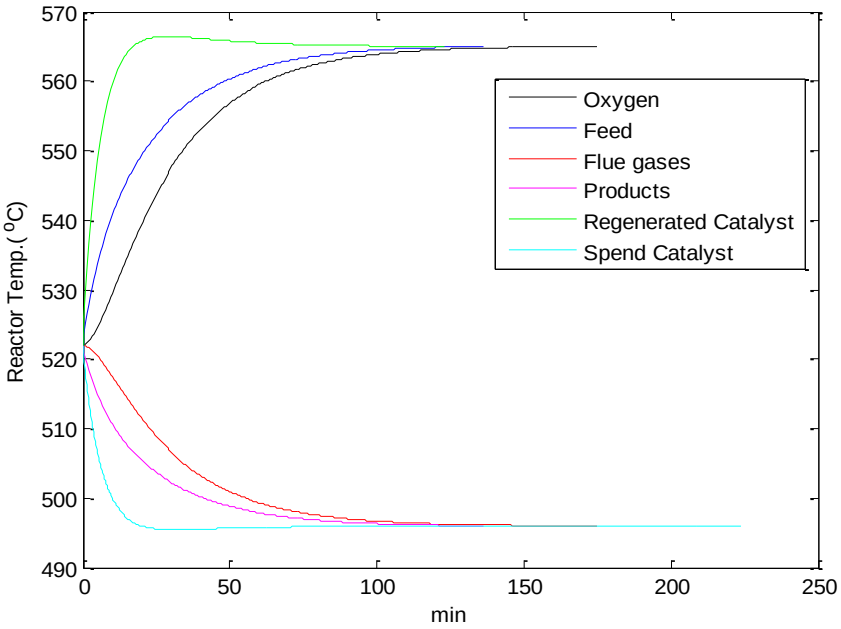

(a)

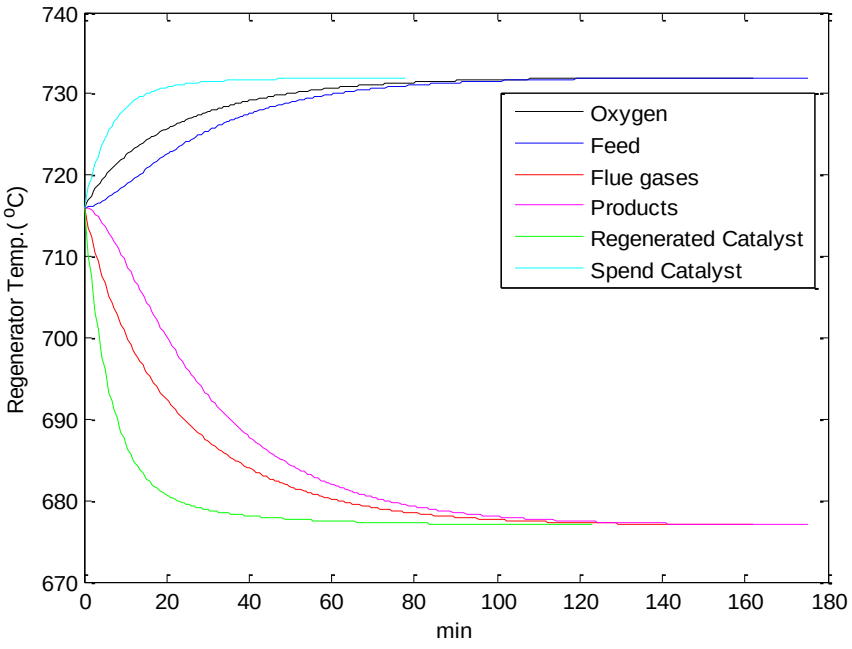

(b)

Figure 5.7: Temperatures responds by a positive change in the oxy-combustion system/same volume for (a) reactor and (b) regenerator.

.

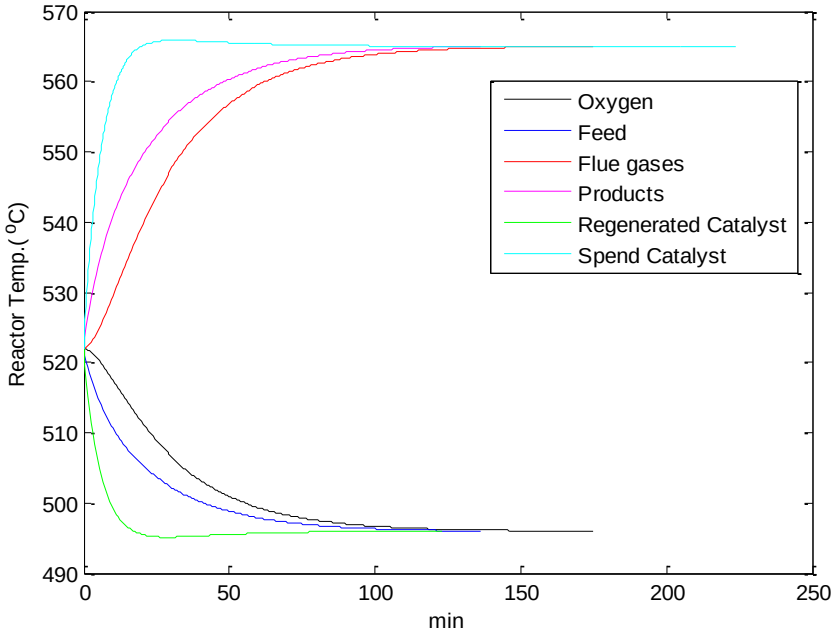

(a)

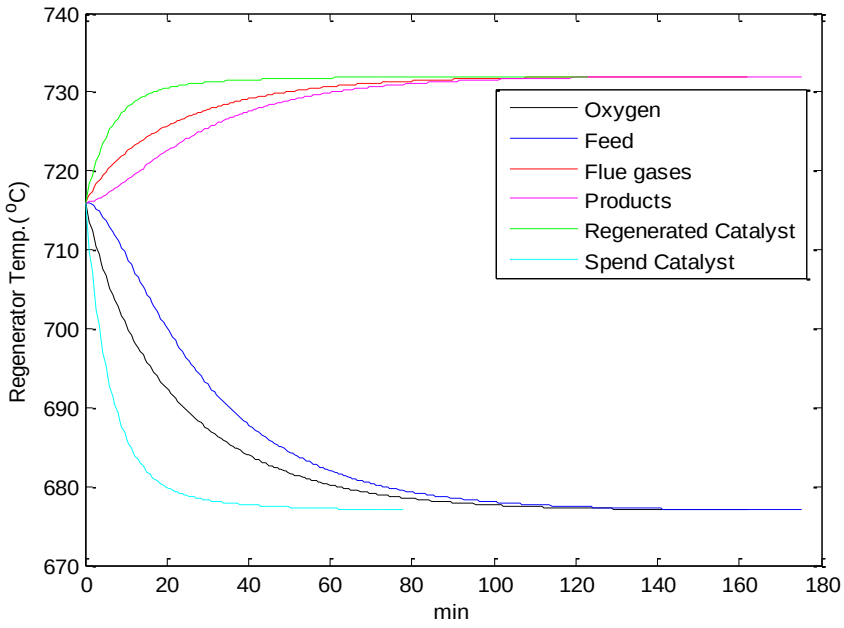

(b)

Figure 5.8: Temperatures responds by a negative change in the oxy-combustion system /same volume for (a) reactor and (b) regenerator.

Table 5.1: Lower/Upper limits of the reactor using post- and oxy-combustion systems.

Limits	Air/Oxygen	Feed	Flue Gases	Products	Regenerated Catalyst	Spent Catalyst
Post-combustion						
Lower	636.83	4,420.6	948.78	4,201.0	20,983.0	18,493.0
Upper	7,667.2	5,905.1	5,029.9	5,241.6	27,233.0	26,597.0
Oxy-combustion / same heat						
Lower	715.92	4,420.6	1,006.4	4,201.0	20,982.0	18,460.0
Upper	7,536.4	5,905.1	5,052.7	5241.6	27,233.0	26,617.0
Oxy-combustion / same volume						
Lower	714.7	4,420.6	969.32	4021.0	20,982.0	18,460.0
Upper	7,538.4	5,905.1	5,017.4	5,241.6	27,233.0	26,617.0

All values are in kg/min.

Table 5.2: Lower/Upper limits of the regenerator using post- and oxy-combustion systems.

Limits	Air/Oxygen	Feed	Flue Gases	Products	Regenerated Catalyst	Spent Catalyst
Post-combustion						
Lower	921.08	3,660.0	2,928.9	4,469.9	22,039.0	19,037.0
Upper	7,667.2	5,905.1	5,029.9	5,241.6	27,233.0	26,597.0
Oxy-combustion / same heat						
Lower	990.83	3,660.0	2969.4	4,469.9	33,039.0	19,037.0
Upper	7,536.4	5,905.1	5,052.7	5,241.6	27,233.0	26,617.0
Oxy-combustion / same volume						
Lower	989.73	3,660.0	2,933.2	4,469.9	22,039.0	19,037.0
Upper	7,538.4	5,905.1	5,017.6	5,241.6	27,233.0	26,617.0

All values are in kg/min.

Table 5.3: Optimal values of the reactor using post- and oxy-combustion systems.

Feed	Products	Regenerated Catalyst	Spent Catalyst	Feed Temperature
Post-combustion				
4420.6	5241.6	20,982	26,597	204
Oxy-combustion / same heat				
4420.6	5241.6	20,982	26,617	204
Oxy-combustion / same volume				
4420.6	5241.6	20,982	26,617	204

Table 5.4: Optimal values of the regenerator using post- and oxy-combustion systems.

Air/ Oxygen	Flue Gases	Regenerated Catalyst	Spent Catalyst	Air/Oxygen Temperature
Post-combustion				
3286	3492.1	23337	23543	450
Oxy-combustion / same heat				
3286	3528	23337	23543	450
Oxy-combustion / same volume				
3280	3492.1	23337	23543	450

All values are in kg/min except temperature is in ^{o}C.

Table 5.5: RGA values using a post-combustion system.

$RGA_1 = \begin{matrix} & m_{air} & m_{rg} \\ \end{matrix}$ $\begin{bmatrix} 0.400 & 0.600 \\ 0.600 & 0.400 \end{bmatrix} \begin{matrix} T_{rec} \\ T_{reg} \end{matrix}$	$RGA_2 = \begin{matrix} & m_{air} & m_{s} \\ \end{matrix}$ $\begin{bmatrix} 0.377 & 0.623 \\ 0.623 & 0.377 \end{bmatrix} \begin{matrix} T_{rec} \\ T_{reg} \end{matrix}$	$RGA_3 = \begin{matrix} & m_{feed} & m_{rg} \\ \end{matrix}$ $\begin{bmatrix} 0.637 & 0.363 \\ 0.363 & 0.637 \end{bmatrix} \begin{matrix} T_{rec} \\ T_{reg} \end{matrix}$
$RGA_4 = \begin{matrix} & m_{feed} & m_{s} \\ \end{matrix}$ $\begin{bmatrix} 0.615 & 0.385 \\ 0.385 & 0.615 \end{bmatrix} \begin{matrix} T_{rec} \\ T_{reg} \end{matrix}$	$RGA_5 = \begin{matrix} & m_{fluegases} & m_{rg} \\ \end{matrix}$ $\begin{bmatrix} 0.400 & 0.600 \\ 0.600 & 0.400 \end{bmatrix} \begin{matrix} T_{rec} \\ T_{reg} \end{matrix}$	$RGA_6 = \begin{matrix} & m_{fluegases} & m_{s} \\ \end{matrix}$ $\begin{bmatrix} 0.377 & 0.623 \\ 0.623 & 0.377 \end{bmatrix} \begin{matrix} T_{rec} \\ T_{reg} \end{matrix}$
$RGA_7 = \begin{matrix} & m_{products} & m_{rg} \\ \end{matrix}$ $\begin{bmatrix} 0.637 & 0.363 \\ 0.363 & 0.637 \end{bmatrix} \begin{matrix} T_{rec} \\ T_{reg} \end{matrix}$	$RGA_8 = \begin{matrix} & m_{products} & m_{s} \\ \end{matrix}$ $\begin{bmatrix} 0.615 & 0.385 \\ 0.385 & 0.615 \end{bmatrix} \begin{matrix} T_{rec} \\ T_{reg} \end{matrix}$	

Table 5.6: RGA values using an oxy-combustion system of both same heat and volume.

$RGA_1 = \begin{matrix} & m_{oxy} & m_{rg} \\ \begin{matrix} T_{rec} \\ T_{reg} \end{matrix} & \begin{bmatrix} 0.400 & 0.600 \\ 0.600 & 0.400 \end{bmatrix} \end{matrix}$	$RGA_2 = \begin{matrix} & m_{oxy} & m_{s} \\ \begin{matrix} T_{rec} \\ T_{reg} \end{matrix} & \begin{bmatrix} 0.378 & 0.622 \\ 0.622 & 0.378 \end{bmatrix} \end{matrix}$	$RGA_3 = \begin{matrix} & m_{feed} & m_{rg} \\ \begin{matrix} T_{rec} \\ T_{reg} \end{matrix} & \begin{bmatrix} 0.637 & 0.363 \\ 0.363 & 0.637 \end{bmatrix} \end{matrix}$
$RGA_4 = \begin{matrix} & m_{feed} & m_{s} \\ \begin{matrix} T_{rec} \\ T_{reg} \end{matrix} & \begin{bmatrix} 0.616 & 0.384 \\ 0.384 & 0.616 \end{bmatrix} \end{matrix}$	$RGA_5 = \begin{matrix} & m_{fluegases} & m_{rg} \\ \begin{matrix} T_{rec} \\ T_{reg} \end{matrix} & \begin{bmatrix} 0.400 & 0.600 \\ 0.600 & 0.400 \end{bmatrix} \end{matrix}$	$RGA_6 = \begin{matrix} & m_{fluegases} & m_{s} \\ \begin{matrix} T_{rec} \\ T_{reg} \end{matrix} & \begin{bmatrix} 0.378 & 0.622 \\ 0.622 & 0.378 \end{bmatrix} \end{matrix}$
$RGA_7 = \begin{matrix} & m_{products} & m_{rg} \\ \begin{matrix} T_{rec} \\ T_{reg} \end{matrix} & \begin{bmatrix} 0.637 & 0.363 \\ 0.363 & 0.637 \end{bmatrix} \end{matrix}$	$RGA_8 = \begin{matrix} & m_{products} & m_{s} \\ \begin{matrix} T_{rec} \\ T_{reg} \end{matrix} & \begin{bmatrix} 0.616 & 0.384 \\ 0.384 & 0.616 \end{bmatrix} \end{matrix}$	

5.5 Conclusions

From the results of this chapter, the following conclusions can be drawn:

1. An oxy-combustion system can be used instead of a post-combustion one since the system showed stability.
2. The oxy-combustion system resulted in reduced CO_2 emissions as is well known.
3. RGA can be used as a criterion to indicate the most effective variable in the FCC units.

Chapter 6:
Conclusions and Recommendations for Future Work

The following conclusions can be drawn from the thesis:

1. According to the capacities and percentages of ammonia removal results, the adsorption kinetics were very fast for the acidic resins while relatively slow for the neutral or basic zeolites.
2. The studied adsorbents have capacities approximately in the range from 0.2 to 0.4 mg/g for target concentrations of 1 mg/L ammonia or less.
3. HCl and NaOH can be used in a desorption process of the LEWATIT and AZLB-Na respectively.
4. An oxy-combustion system is an effective way to reduce carbon dioxide emissions because the process is flexible and stable and CO_2 reduction could be in the range 90-95 %.

The following recommendations can be drawn from the thesis:

1. Examining other types of resins/zeolites for ammonia removal from wastewaters using the same procedure as in this thesis, Also, studying other physical and chemical properties in more detail such as particle size, surface area, porosity, etc. may result in better understanding of the mechanisms and limitations.
2. Studying other isotherms such as Bangham, Elovich, interparticle diffusion, and Tempkin, especially three-parameter isotherms such as Hill, Sips, and Toth, and

kinetics in the batch process to describe behaviors of the adsorbents that were used in this thesis in both cases linear and non-linear.

3. Studying other models such as Clark, Wolboroska and Yoon-Nelson in the continuous process to describe breakthrough analysis in both linear and non-linear.
4. Studying side effects of using adsorbents by trying various parameters for regenerating resins and zeolites such as different flowrates, concentration, flow directions, regenerants (NaCl or H_2SO_4) for resins and regenerant (NaCl) for zeolites. Also, finding appropriate treatments of the wastewater pH after adding adsorbents since resins make pH acidic while zeolites make it basic.
5. Using Multi-objective optimization in implementing carbon capture in FCC units, for example, objective functions can be maximizing conversion and minimizing coke.

Bibliography

Abdolali A., Ngo H. H., Guo W., Zhou J. L., Zhang J., Liang S., Chang S. W., Nguyen D. D., Liu Y. (2017). Application of a breakthrough biosorbent for removing heavy metals from synthetic and real wastewaters in a lab-scale continuous fixed-bed column. *Bioresource Technology*, *229*, 78-87.

Abrams, I. M., & Millar, J. R. (1997). A history of the origin and development of macroporous ion-exchange resins. *Reactive and Functional Polymers*, *35*(1-2), 7-22.

Addington, L., Fitz, C., Lunsford, K., Lyddon, L., & Siwek, M. (2011, September). Sour water: where it comes from and how to handle it. In *GPA Europe Annual Conference, Praga* (pp. 21-23).

Alchin, D. (1998). Ion exchange resins. *Chemical Processes in New Zealand. New Zealand Institute of Chemistry Education, pp XIII-D-1–XIII-D-7*.

Alwan, G. M., Mehdi, F. A., Arazak, A. A. & Manual N. (2010). Operation and Ph Control of A Wastewater Treatment Unit Using Labview. *Engineering and Technology Journal*, *28*(17), 5524-5546.

Alwan, G. M., & Mehdi, F. A. (2010). Study the Stability of a Wastewater Treatment Unit using LABVIEW. *Tikrit Journal of Engineering Sciences*, *17*(4), 21-31.

Ames Jr, L. L. (1960). The cation sieve properties of clinoptilolite. *American Mineralogist: Journal of Earth and Planetary Materials*, *45*(5-6), 689-700.

Arbel, A., Huang, Z., Rinard, I. H., Shinnar, R., & Sapre, A. V. (1995). Dynamic and control of fluidized catalytic crackers. 1. Modeling of the current generation of FCC's. *Industrial & engineering chemistry research*, *34*(4), 1228-1243.

Barrett, J. P. (1974). The coefficient of determination—some limitations. *The American Statistician*, *28*(1), 19-20.

Bashir, M. J., Aziz, H. A., Yusoff, M. S., & Adlan, M. N. (2010). Application of response surface methodology (RSM) for optimization of ammoniacal nitrogen removal from semi-aerobic landfill leachate using ion exchange resin. *Desalination*, *254*(1-3), 154-161.

Batley, G. E., & Simpson, S. L. (2009). Development of guidelines for ammonia in estuarine and marine water systems. *Marine Pollution Bulletin*, *58*(10), 1472-1476.

Bertagnolli, C., Kleinübing, S. J. and Da Silva, M. G. C. (2011). Preparation and characterization of a Brazilian bentonite clay for removal of copper in porous beds. *Applied Clay Science*, *53*(1), 73-79.

Bohart, G. S. and Adams, E. Q. (1920). Some aspects of the behavior of charcoal with respect to chlorine. *Journal of the American Chemical Society*, *42*(3), 523-544.

Bollas, G. M., Vasalos, I. A., Lappas, A. A., Iatridis, D. K., Voutetakis, S. S., & Papadopoulou, S. A. (2007). Integrated FCC riser—regenerator dynamics studied in a fluid catalytic cracking pilot plant. *Chemical Engineering Science*, *62*(7), 1887-1904.

Brendel, M., Bonvin, D., & Marquardt, W. (2006). Incremental identification of kinetic models for homogeneous reaction systems. *Chemical engineering science*, *61*(16), 5404-5420.

Brooks, R. J., & Tobias, A. M. (1996). Choosing the best model: Level of detail, complexity, and model performance. *Mathematical and computer modelling*, *24*(4), 1-14.

Bui, M., Gunawan, I., Verheyen, V., Artanto, Y., Meuleman, E., & Feron, P. (2013). Dynamic modeling and validation of post-combustion CO_2 capture plants in Australian coal-fired power stations. *Energy Procedia*, *37*, 2694–2702.

Bui, M., Gunawan, I., Verheyen, V., Feron, P., Meuleman, E., & Adeloju, S. (2014). Dynamic modelling and optimisation of flexible operation in post-combustion CO_2 capture plants-A review. *Computers and Chemical Engineering*, *61*, 245–265.

Cabrera-Lafaurie, W. A., Román, F. R. and Hernández-Maldonado, A. J. (2014). Removal of salicylic acid and carbamazepine from aqueous solution with Y-zeolites modified with extraframework transition metal and surfactant cations: equilibrium and fixed-bed adsorption. *Journal of Environmental Chemical Engineering*, *2*(2), 899-906.

Chern, J. M. and Chien, Y. W. (2002). Adsorption of nitrophenol onto activated carbon: isotherms and breakthrough curves. *Water Research*, *36*(3), 647-655.

Colvin, R. J., Rozich, A. F., Hough, B. J., & Gaudy Jr, A. F. (1991). Use of respirometry to evaluate the biodegradability of emulsified specialty chemcial products. In *Proceedings of the Industrial Waste Conference, Purdue University (USA)*.

Cooney, E. L., Booker, N. A., Shallcross, D. C., & Stevens, G. W. (1999). Ammonia removal from wastewaters using natural Australian zeolite. I. Characterization of the zeolite. *Separation Science and Technology*, *34*(12), 2307-2327.

Coughanowr, D. R., & LeBlanc, S. E. (2009). *Process systems analysis and control* (3rd Edition, p.477-489). McGraw-Hill company, New York, USA.

de Franco, M. A. E., de Carvalho, C. B., Bonetto, M. M., de Pelegrini S., R. and Féris, L. A. (2017). Removal of amoxicillin from water by adsorption onto activated carbon in batch process and fixed bed column: Kinetics, isotherms, experimental design and breakthrough curves modelling. *Journal of Cleaner Production*, *161*, 947-956.

de Mello, L. F., Gobbo, R., Moure, G. T., & Miracca, I. (2013). Oxy-combustion technology development for Fluid Catalytic Crackers (FCC)–large pilot scale demonstration. *Energy procedia*, *37*, 7815-7824.

de Mello, L. F., Pimenta, R. D., Moure, G. T., Pravia, O. R., Gearhart, L., Milios, P. B., & Melien, T. (2009). A technical and economical evaluation of CO_2 capture from FCC units. *Energy Procedia*, *1*(1), 117-124.

DOE, U. (2003). Water Use in Industries of the Future: Petroleum Refining. *US Department of Energy*.

Dowell, N. M., & Shah, N. (2014). Optimisation of post-combustion CO_2 capture for flexible operation. *Energy Procedia*, *63*, 1525-1535.

Draman, M., Altinel, I. K., Bajgoric, N., Ünal, A. T., & Birgören, B. (2002). A clone-based graphical modeler and mathematical model generator for optimal production planning in process industries. *European Journal of Operational Research*, *137*(3), 483-496.

Edgar F., Himmelblau, D., & Lasdon, L. (2001). *Optimization of chemical processes* (2nd Edition, p.14-18). McGraw-Hill Book company, New York, USA.

Ellis, R. C., Li, X., & Riggs, J. B. (1998). Modeling and optimization of a model IV fluidized catalytic cracking unit. AIChE Journal, 44(9), 2068-2079.

Elnashaie, S. S. (1994). *Modelling, simulation and optimization of industrial fixed bed catalytic reactors* (Vol. 7). CRC Press.

EPA (2013). Aquatic life Ambient Water Quality Criteria for Ammonia – Freshwater, EPA-822-R-13-001, U.S. Environmental Protection Agency.

Escudero, A. I., Espatolero, S., & Romeo, L. M. (2016). Oxy-combustion power plant integration in an oil refinery to reduce CO_2 emissions. *International Journal of Greenhouse Gas Control*, *45*, 118-129.

Fahim, M. A., Al-Sahhaf, T. A., & Elkilani, A. (2009). *Fundamentals of petroleum refining* (1st Edition, p.199-235). Elsevier, Oxford, UK.

Foo, K. Y. and Hameed, B. H. (2009). An overview of landfill leachate treatment via activated carbon adsorption process. *Journal of hazardous materials*, *171*(1), 54-60.

Freundlich H.M.F., (1906). Uber die adsorption in losungen, Zeitschrift für Physikalische Chemie (Leipzig) 57A.

Fu, C., & Anantharaman, R. (2017). Modelling of the oxy-combustion fluid catalytic cracking units. In *Computer Aided Chemical Engineering* (Vol. 40, pp. 331-336). Elsevier.

Gary, J. H., Handwerk, G. E., & Kaiser, M. J. (2007). *Petroleum refining: Technology and economics* (5th Edition, p.121-147). CRC press, Taylor & Francis Group, USA.

Goshadrou, A. and Moheb, A. (2011). Continuous fixed bed adsorption of CI Acid Blue 92 by exfoliated graphite: An experimental and modeling study. *Desalination*, *269*(1-3), 170-176.

Göthe-Lundgren, M., Lundgren, J. T., & Persson, J. A. (2002). An optimization model for refinery production scheduling. *International Journal of Production Economics*, *78*(3), 255-270.

Guaya, D., Valderrama, C., Farran, A., Armijos, C., & Cortina, J. L. (2015). Simultaneous phosphate and ammonium removal from aqueous solution by a hydrated aluminum oxide modified natural zeolite. *Chemical Engineering Journal*, *271*, 204-213.

Gueddar, T., & Dua, V. (2012). Novel model reduction techniques for refinery-wide energy optimisation. *Applied energy*, *89*(1), 117-126.

Gunnerud, V., & Foss, B. (2010). Oil production optimization—A piecewise linear model, solved with two decomposition strategies. *Computers & Chemical Engineering*, *34*(11), 1803-1812.

Gupta, V. K., Sadegh, H., Yari, M., Shahryari Ghoshekandi, R., Maazinejad, B., & Chahardori, M. (2015). Removal of ammonium ions from wastewater A short review in development of efficient methods. *Global Journal of Environmental Science and Management*, *1*(2), 149–158.

Hedström, A. (2001). Ion exchange of ammonium in zeolites: a literature review. *Journal of environmental engineering*, *127*(8), 673-681.

Ho, Y. S., & McKay, G. (1999). Pseudo-second order model for sorption processes. *Process biochemistry*, *34*(5), 451-465.

Huang, H., Xiao, X., Yan, B., & Yang, L. (2010). Ammonium removal from aqueous solutions by using natural Chinese (Chende) zeolite as adsorbent. *Journal of Hazardous materials*, *175*(1), 247-252.

Huang, J., Kankanamge, N. R., Chow, C., Welsh, D. T., Li, T., & Teasdale, P. R. (2017). Removing ammonium from water and wastewater using cost-effective adsorbents: A review. *Journal of Environmental Sciences*.

Huo, H., Lin, H., Dong, Y., Cheng, H., Wang, H., & Cao, L. (2012). Ammonia-nitrogen and phosphates sorption from simulated reclaimed waters by modified clinoptilolite. *Journal of hazardous materials*, *229*, 292-297.

Hutchins, R. A. (1973). New method simplifies design of activated carbon systems. *Chem. Eng.*, *80*, 133-138.

Jermakka, J., Wendling, L., Sholberg, E., Heinonen, H., Merta, E., Laine-Ylijoki, J., Kaartinen, T., & Mroueh, U.-M. (2015). Nitrogen compounds at mines and quarries. Sources, behaviour and removal from mine and quarry waters. Literature study. VTT Technology, VTT, Espoo.

Jha, V. K., & Hayashi, S. (2009). Modification on natural clinoptilolite zeolite for its NH_4^+ retention capacity. *Journal of Hazardous Materials*, *169*(1-3), 29-35.

Jones, D. S., & Pujadó, P. P. (Eds.). (2006). *Handbook of petroleum processing* (1st Edition, p.239-279). Springer, Dordrecht, The Netherlands.

Jorgensen, T. C., and Weatherley, L. R. (2003). Ammonia removal from wastewater by ion exchange in the presence of organic contaminants. *Water Research*, *37*(8), 1723–1728.

Jorgensen, T. C., and Weatherley, L. R. (2006). Continuous removal of ammonium ion by ion exchange in the presence of organic compounds in packed columns. *Journal of Chemical Technology and Biotechnology*, *81*(7), 1151-1158.

Kananpanah, S., Dizadji, N., Abolghasemi, H. and Salamatinia, B. (2009). Developing a new model to predict mass transfer coefficient of salicylic acid adsorption onto IRA-93: Experimental and modeling. *Korean journal of chemical engineering*, *26*(5), 1208-1212.

Karadag, D., Tok, S., Akgul, E., Turan, M., Ozturk, M., & Demir, A. (2008). Ammonium removal from sanitary landfill leachate using natural Gördes clinoptilolite. *Journal of Hazardous Materials*, *153*(1-2), 60-66.

Kvamsdal, H. M., Jakobsen, J. P., & Hoff, K. A. (2009). Dynamic modeling and simulation of a CO_2 absorber column for post-combustion CO_2 capture. *Chemical Engineering and Processing: Process Intensification*, *48*(1), 135–144.

Lahav, O., & Green, M. (1998). Ammonium removal using ion exchange and biological regeneration. *Water Research*, *32*(7), 2019-2028.

Lagergren, S. (1898). Zur theorie der sogenannten adsorption geloster stoffe. *Kungliga svenska vetenskapsakademiens. Handlingar*, *24*, 1-39.

Langmuir, I. (1918). The adsorption of gases on plane surfaces of glass, mica and platinum. *Journal of the American Chemical society*, *40*(9), 1361-1403.

Langwaldt, J. (2008). Ammonium removal from water by eight natural zeolites: A comparative study. *Separation Science and Technology*, *43*(8), 2166-2182.

Largitte, L., & Pasquier, R. (2016). A review of the kinetics adsorption models and their application to the adsorption of lead by an activated carbon. *Chemical Engineering Research and Design*, *109*, 495-504.

Lecomte, Fabrice Broutin, Paul Lebas, Etienne. (2010). CO_2 Capture - *Technologies to Reduce Greenhouse Gas Emissions. Editions Technip*.

Levenberg, K. (1944). A method for the solution of certain non-linear problems in least squares. *Quarterly of applied mathematics*, *2*(2), 164-168.

Leyva-Ramos, R., Monsivais-Rocha, J. E., Aragon-Piña, A., Berber-Mendoza, M. S., Guerrero-Coronado, R. M., Alonso-Davila, P., & Mendoza-Barron, J. (2010). Removal of ammonium from aqueous solution by ion exchange on natural and modified chabazite. *Journal of environmental management*, *91*(12), 2662-2668.

Lieberman, N. P. (2009). *Troubleshooting process operations* (4^{th} Edition, p.161-186). PennWell, Oklahoma, USA.

Lin, L., Lei, Z., Wang, L., Liu, X., Zhang, Y., Wan, C., ... & Tay, J. H. (2013). Adsorption mechanisms of high-levels of ammonium onto natural and NaCl-modified zeolites. *Separation and purification technology*, *103*, 15-20.

Lin, X., Huang, Q., Qi, G., Shi, S., Xiong, L., Huang, C., Li H. and Chen, X. (2017). Estimation of fixed-bed column parameters and mathematical modeling of breakthrough behaviors for adsorption of levulinic acid from aqueous solution using SY-01 resin. *Separation and Purification Technology*, *174*, 222-231.

Luus, R., & Woo, S. S. (2001). Optimization of a model IV fluidized catalytic cracking unit. *The Canadian Journal of Chemical Engineering*, *79*(4), 542-547.

Luyben, W. L. (1989). *Process modeling, simulation and control for chemical engineers* (2nd Edition, p.575-579). McGraw-Hill Higher Education, New York, USA.

Maji, S. K., Pal, A., Pal, T. and Adak, A. (2007). Modeling and fixed bed column adsorption of As (III) on laterite soil. *Separation and Purification Technology*, *56*(3), 284-290.

Malovanyy, A., Sakalova, H., Yatchyshyn, Y., Plaza, E., & Malovanyy, M. (2013). Concentration of ammonium from municipal wastewater using ion exchange process. *Desalination*, *329*, 93-102.

Marañón, E., Ulmanu, M., Fernandez, Y., Anger, I., & Castrillón, L. (2006). Removal of ammonium from aqueous solutions with volcanic tuff. *Journal of Hazardous Materials*, *137*(3), 1402-1409.

Marquardt, D. W. (1963). An algorithm for least-squares estimation of nonlinear parameters. *Journal of the society for Industrial and Applied Mathematics*, *11*(2), 431-441.

McFarlane, R. C., Reineman, R. C., Bartee, J. F., & Georgakis, C. (1993). Dynamic simulator for a Model IV fluid catalytic cracking unit. Computers and Chemical Engineering, 17(3), 275–300.

McFarlane, R. C., Reineman, R. C., Bartee, J. F., & Georgakis, C. (1993). Dynamic simulator for a model IV fluid catalytic cracking unit. *Computers & chemical engineering*, *17*(3), 275-300.

Meerman, J. C., Hamborg, E. S., Van Keulen, T., Ramírez, A., Turkenburg, W. C., & Faaij, A. P. C. (2012). Techno-economic assessment of CO_2 capture at steam methane reforming facilities using commercially available technology. *International journal of greenhouse gas control*, *9*, 160-171.

Miracca, I., Crombie, M., Forsyth, J., Lowe, C., Moure, G. T., Iyer, M., & Bohm, M. (2013). The CO_2 Capture Project Status and Prospects of the Capture Program. *Energy Procedia*, *37*, 7825-7831.

Muhamad, H., Doan, H. and Lohi, A. (2010). Batch and continuous fixed-bed column biosorption of Cd^{2+} and Cu^{2+}. *Chemical Engineering Journal*, *158*(3), 369-377.

Perregaard, J. (1993). Model simplification and reduction for simulation and optimization of chemical processes. *Computers & Chemical Engineering*, *17*(5-6), 465–483.

Posch, S., & Haider, M. (2013). Dynamic modeling of CO_2 absorption from coal-fired power plants into an aqueous monoethanolamine solution. *Chemical Engineering Research and Design*, *91*(6), 977–987.

Qadir, A., Sharma, M., Parvareh, F., Khalilpour, R., & Abbas, A. (2015). Flexible dynamic operation of solar-integrated power plant with solvent based post-combustion carbon capture (PCC) process. *Energy Conversion and Management*, *97*, 7-19.

Sadaf, S., & Bhatti, H. N. (2014). Batch and fixed bed column studies for the removal of Indosol Yellow BG dye by peanut husk. *Journal of the Taiwan Institute of Chemical Engineers*, *45*(2), 541-553.

Sadeghbeigi, R. (2012). *Fluid catalytic cracking handbook: An expert guide to the practical operation, design, and optimization of FCC units* (3rd Edition, p.125-167). Elsevier, Oxford, UK.

Sica, M., Duta, A., Teodosiu, C., & Draghici, C. (2014). Thermodynamic and kinetic study on ammonium removal from a synthetic water solution using ion exchange resin. *Clean Technologies and Environmental Policy*, *16*(2), 351-359.

Sotelo, J. L., Rodríguez, A., Álvarez, S. and García, J. (2012). Removal of caffeine and diclofenac on activated carbon in fixed bed column. *Chemical Engineering Research and Design*, *90*(7), 967-974.

Sotelo, J. L., Ovejero, G., Rodríguez, A., Álvarez, S. and García, J. (2013). Analysis and modeling of fixed bed column operations on flumequine removal onto activated carbon: pH influence and desorption studies. *Chemical engineering journal*, *228*, 102-113.

Sparks, D. L., & Jardine, P. M. (1981). Thermodynamics of Potassium Exchange in Soil Using a Kinetics Approach 1. *Soil Science Society of America Journal*, *45*(6), 1094-1099.

Sreejalekshmi, K. G., Krishnan, K. A., & Anirudhan, T. S. (2009). Adsorption of Pb (II) and Pb (II)-citric acid on sawdust activated carbon: Kinetic and equilibrium isotherm studies. *Journal of Hazardous Materials*, *161*(2), 1506-1513.

Stockle, M., & Bullen, T. (2008). Integrate refinery carbon dioxide reduction plans plant-wide: Carbon capture and reduction schemes or combination of various processes have economic value and depend on many factors. Hydrocarbon processing, 87(11), 106-111.

Tarun, C. B., Croiset, E., Douglas, P. L., Gupta, M., & Chowdhury, M. H. (2007). Techno-economic study of CO_2 capture from natural gas based hydrogen plants. *International Journal of Greenhouse Gas Control*, *1*(1), 55-61.

Thomas, H. C. (1944). Heterogeneous ion exchange in a flowing system. *Journal of the American Chemical Society*, *66*(10), 1664-1666.

Tyagi, R. D., Tran, F. T., & Chowdhury, A. K. M. M. (1993). Biodegradation of petroleum refinery wastewater in a modified rotating biological contactor with polyurethane foam attached to the disks. *Water research*, *27*(1), 91-99.

van Straelen, J., Geuzebroek, F., Goodchild, N., Protopapas, G., & Mahony, L. (2010). CO_2 capture for refineries, a practical approach. *International Journal of Greenhouse Gas Control*, *4*(2), 316-320.

Vassileva, P., & Voikova, D. (2009). Investigation on natural and pretreated Bulgarian clinoptilolite for ammonium ions removal from aqueous solutions. *Journal of hazardous materials*, *170*(2), 948-953.

Venkataraman, P. (2009). *Applied optimization with MATLAB programming* (1st Edition, p.1-23). John Wiley & Sons, New York, USA.

Vieira, M. G. A., Gimenes, M. L. and Da Silva, M. G. C. (2009). Modelling of the process of adsorption of nickel in bentonite clay. *Chem Eng Trans*, *17*, 421-426.

Vocciante, M., Alessandra De Folly, D., Finocchi, A., Tagliabue, M., Bellettato, M., Ferrucci, A., Reverberi, A. & Ferro, S. (2018). Adsorption of Ammonium on Clinoptilolite in Presence of Competing Cations: Investigation on Groundwater Remediation. *Journal of Cleaner Production*.

Volesky, B., Weber, J. and Park, J. M. (2003). Continuous-flow metal biosorption in a regenerable Sargassum column. *Water Research*, *37*(2), 297-306.

Wang, F. Y., Zhu, Z. H., Massarotto, P., & Rudolph, V. (2007). A simplified dynamic model for accelerated methane residual recovery from coals. *Chemical engineering science*, *62*(12), 3268-3275

Wang, S., & Peng, Y. (2010). Natural zeolites as effective adsorbents in water and wastewater treatment. *Chemical Engineering Journal*, *156*(1), 11-24.

Wang, X., Lü, S., Gao, C., Xu, X., Zhang, X., Bai, X., Liu, M., & Wu, L. (2014). Highly efficient adsorption of ammonium onto palygorskite nanocomposite and evaluation of its recovery as a multifunctional slow-release fertilizer. *Chemical Engineering Journal*, *252*, 404-414.

Wang, Y., Kmiya, Y., & Okuhara, T. (2007). Removal of low-concentration ammonia in water by ion-exchange using Na-mordenite. *Water research*, *41*(2), 269-276.

Wang, Y., Liu, S., Xu, Z., Han, T., Chuan, S., & Zhu, T. (2006). Ammonia removal from leachate solution using natural Chinese clinoptilolite. *Journal of Hazardous Materials*, *136*(3), 735-740.

Weatherley, L. R., & Miladinovic, N. D. (2004). Comparison of the ion exchange uptake of ammonium ion onto New Zealand clinoptilolite and mordenite. *Water Research*, *38*(20), 4305-4312.

Weber, T. W., & Chakravorti, R. K. (1974). Pore and solid diffusion models for fixed-bed adsorbers. *AIChE Journal*, *20*(2), 228-238.

Widiastuti, N., Wu, H., Ang, H. M., & Zhang, D. (2011). Removal of ammonium from greywater using natural zeolite. *Desalination*, *277*(1), 15-23.

Yan, L., Wang, Y., Li, J., Ma, H., Liu, H., Li, T., & Zhang, Y. (2014). Comparative study of different electrochemical methods for petroleum refinery wastewater treatment. *Desalination, 341*, 87-93.

Zaman, M., Jang, H., Rizwan, M., & Lee, J. H. (2016). Optimal design for flexible operation of the post-combustion CO_2 capture plant with uncertain economic factors. *Computers and Chemical Engineering*, *84*, 199–207.

Zaman, M., & Lee, J. H. (2015). Optimization of the various modes of flexible operation for post-combustion CO_2 capture plant. *Computers and Chemical Engineering*, *75*, 14–27.

Zhang, M., Zhang, H., Xu, D., Han, L., Niu, D., Tian, B., Zhang, J., Zhang, L. & Wu, W. (2011). Removal of ammonium from aqueous solutions using zeolite synthesized from fly ash by a fusion method. *Desalination*, *271*(1), 111-121.

Appendix A:
Adsorption Process and Photolysis of Ammonia

First Group

Dowex

Purolite MN500

Purolite C104Plus

Purolite C100H

Zeolite NM-Ca

Zeolite NV-Na

Second Group

Zeolite AZLB-Na

Zeolite NV-Na *TM
Ammonia Specific

Zeolite AZLB-Ca

DIAION PK228

DIAION SK1B

DIAION PK216

Tulsion T-42 Na N-B1-TX

Tulsion T-52 Na BCN-B1-TX

LEWATIT monoPlus S 108 H

KMI Zeolite

Figure A.1: Adsorbents (Resins/Zeolites).

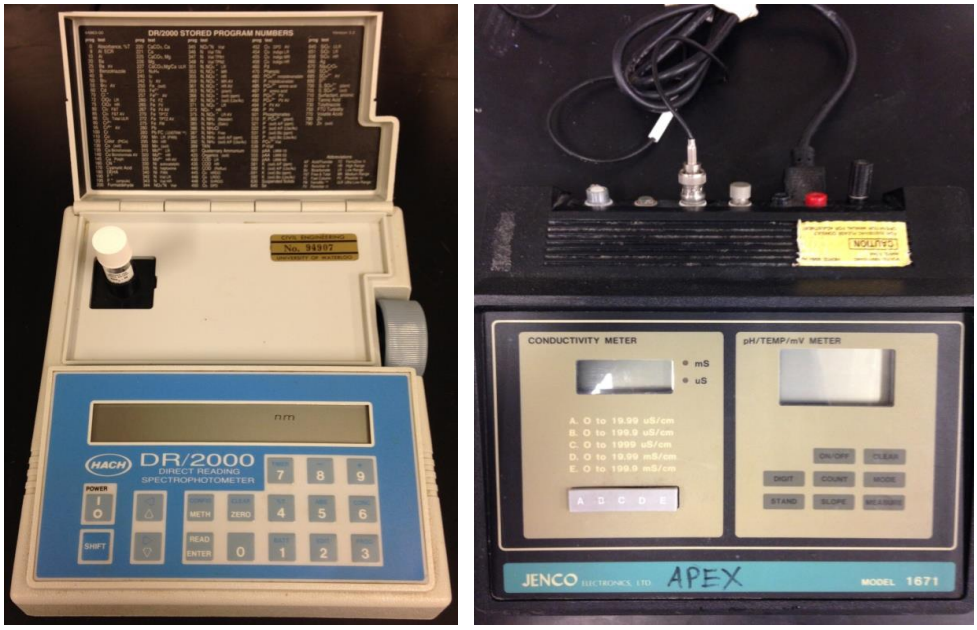

Figure A.2: (Left) Spectrophotometer & (Right) pH meter.

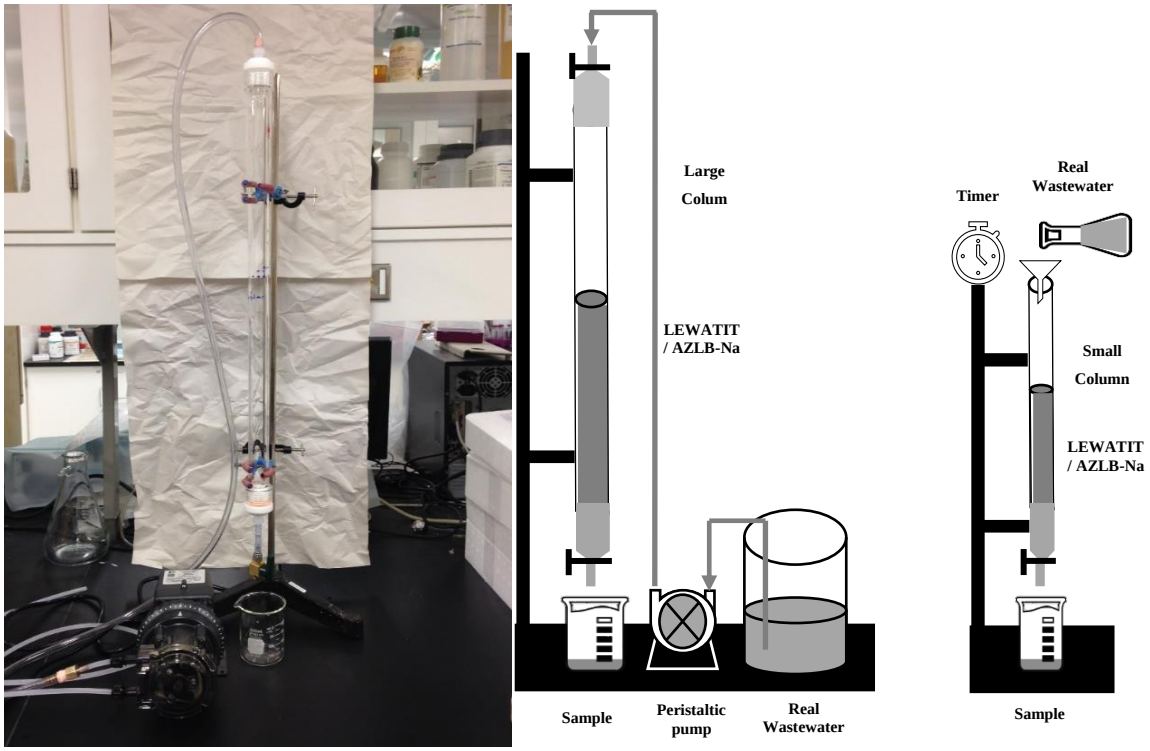

Figure A.3: (Left) Ace column, (Middle) A systematic diagram of the flow process using the Ace column and (Right) A systematic diagram of the flow process using the mini-column.

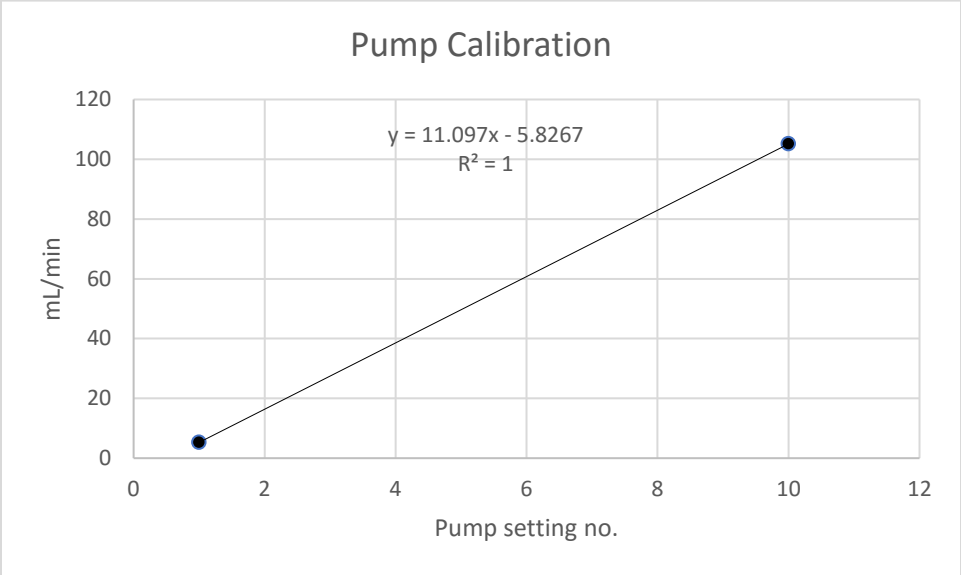

Figure A.4: A calibration of the peristaltic pump.

Table A.1: Some specifications of the adsorbents (resins/zeolites).

No.	Trade Name	Chemical Name	Type	pH
First Group				
1	Dowex™ 50Wx8 50-100 Mesh	Sulfonated polymer of styrene, ethylstyrene and divnylbenzene in the hydrogen form	Resin	Acidic
2	Purolite MN500	Polystyrene sulfonic acid	Resin	Acidic
3	Purolite C104Plus	Polyacrylic acid	Resin	Acidic
4	Purolite C100H	Polystyrene sulfonic acid	Resin	Acidic
5	NM-Ca 14×40 Mesh	Potassium Aluminosilicate	Zeolite	Basic
6	NV-Na 14×40 Mesh	Potassium Aluminosilicate	Zeolite	Basic
Second Group				
7	AZLB-Na 14×50 Mesh	Anhydrous Sodium Aluminosilicate	Zeolite	Basic
8	NV-Na *TM 14×40 Mesh	Hydrous Sodium Aluminosilicate	Zeolite	Basic
9	AZLB-Ca 14×50 Mesh	Hydrous Calcium Sodium Aluminosilicate	Zeolite	Basic
10	DIAION PK228	Benzene, diethenyl-, polymer with ethenylbenzene and ethenylethylbenzene sulfonated, sodium salts	Resin	Acidic
11	DIAION SK1B	Benzene, diethenyl-, polymer with ethenylbenzene and ethenylethylbenzene sulfonated, sodium salts	Resin	Acidic
12	DIAION PK216	Benzene, diethenyl-, polymer with ethenylbenzene and ethenylethylbenzene sulfonated, sodium salts	Resin	Acidic
13	Tulsion T-42 Na N-B1-TX	Styrene-divinylbemzene copolymer with sulpheric acid group in the sodium form	Resin	Acidic
14	Tulsion T-52 Na BCN-B1-TX	Sulfonated copolymer of styrene and dininylbenzene in the sodium form	Resin	Acidic
15	LEWATIT monoPlus S 108 H	Benzene, diethenyl-, polymer with ethenylbenzene and ethenylethylbenzene sulfonated	Resin	Acidic
16	KMI Zeolite 12×20	Potassium Sodium Magnesium Calcium Aluminosilicate mineral	Zeolite	Basic

Table A.2: Adsorption data of the selected adsorbents using synthetic waster.

Time	Capacity, mg/g	% removal	pH
Dowex			
0	1.220	0	7.00
0.1	0.445	64.28	3.27
5	0.007	99.37	2.98
10	0	100	2.95
20	0	100	2.95
30	0	100	2.95
60	0	100	2.95
120	0	100	2.95
180	0	100	2.95
AZLB-NA			
0	1.220	0	7.00
0.1	0.703	43.6	7.43
5	0.140	88.72	8.07
10	0.078	93.73	8.14
20	0.062	94.99	8.24
30	0.054	95.61	8.25
60	0.031	97.49	8.26
120	0.023	98.12	8.26
180	0.023	98.12	8.26
LEWATIT			
0	1.220	0	7.00
0.1	0.594	52.37	3.69
5	0.046	96.24	3.17
10	0	100	3.17
20	0	100	3.17
30	0	100	3.17
60	0	100	3.17
120	0	100	3.17
180	0	100	3.17
NV-NA			
0	1.220	0	7.00
0.1	0.672	46.11	7.22
5	0.461	63.03	7.45
10	0.117	90.6	7.59
20	0.046	96.24	7.71
30	0.023	98.12	7.80
60	0.015	98.75	7.96
120	0	100	7.96
180	0	100	7.96

Table A.3: Cont'd Table A-2.

Time, min	Capacity, mg/g	% removal	pH
PK216			
0	1.219	0	7.00
0.1	0.711	42.98	6.45
5	0.547	56.14	6.39
10	0.406	67.42	6.36
20	0.359	71.18	6.31
30	0.273	78.07	6.25
60	0.023	98.12	6.11
120	0.007	99.37	6.04
180	0	100	6.04
SKIB			
0	1.220	0	7.00
0.1	0.742	40.47	6.42
5	0.555	55.51	6.32
10	0.430	65.53	6.24
20	0.258	79.32	6.21
30	0.195	84.33	6.21
60	0.132	89.35	6.06
120	0.062	94.99	6.06
180	0.031	97.49	6.06

Table A.4: Adsorption data of the selected adsorbents using real waster.

Time	Capacity	% removal	pH
Dowex			
0	2.721	0	7.68
2.5	0.143	94.71	2.01
5	0.139	94.86	1.97
10	0.139	94.86	1.97
20	0.139	94.86	1.97
30	0.139	94.86	1.97
60	0.139	94.86	1.97
120	0.139	94.86	1.97
180	0.139	94.86	1.97
AZLB-NA			
0	2.721	0	7.68
5	0.411	84.88	7.93
10	0.287	89.43	7.97
20	0.215	92.07	8.02
30	0.187	93.10	8.03
60	0.135	95.01	8.03
120	0.107	96.04	8.03
180	0.107	96.04	8.03
LEWATIT			
0	2.721	0	7.68
2.5	0.387	85.76	2.16
5	0.287	89.43	2.13
10	0.179	93.39	2.04
20	0.179	93.39	1.99
30	0.179	93.39	1.99
60	0.179	93.39	1.99
120	0.179	93.39	1.99
180	0.179	93.39	1.99
NV-NA			
0	2.721	0	7.68
5	0.599	77.97	7.87
10	0.463	82.97	7.92
20	0.367	86.49	7.94
30	0.291	89.28	7.95
60	0.219	91.92	7.97
120	0.159	94.13	7.98
180	0.135	95.01	7.98

Table A.5: Cont'd Table A-4.

Time, min	Capacity, mg/g	% removal	pH
PK216			
0	2.721	0	7.68
5	0.447	83.55	6.60
10	0.311	88.55	7.00
20	0.247	90.9	7.01
30	0.243	91.04	7.06
60	0.243	91.04	7.11
120	0.243	91.04	7.15
180	0.255	90.6	7.21
SKIB			
0	2.721	0	7.68
5	0.399	85.32	6.69
10	0.295	89.13	6.94
20	0.255	90.6	7.05
30	0.251	90.75	7.05
60	0.247	90.9	7.07
120	0.247	90.9	7.10
180	0.247	90.9	7.15

Appendix B:

CO_2 Emissions Management in a FCC Unit

Table B.1: FCC unit data.

Influencing variables at steady state	Mass flow rates (kg/min)	Specific heat (kJ/kg.^{o}C)	Temperature (^{o}C)
Feed	4,980.0	3.266	312
Fresh catalyst	233.37	1.193	312
Products	4,849.5	3.639	522
Regenerated catalyst	23,337.0	1.193	720
Spent catalyst	23,543.0	1.197	522
Coke	206.0	1.670	522
Steam	75.599	1.97	522
Post-combustion			
Air	3,286.0	1.015	450
Flue gases	3,492.1	1.093	720
Oxy-combustion/same heat			
Oxygen	3,321.9	1.046	450
Flue gases	3,528.0	1.026	720
Oxy-combustion/same volume			
Oxygen	3280.0	1.046	450
Flue gases	3,492.1	1.102	720

Table B.2: Matrices A & B.

$a_{11} = \frac{\partial f_1}{\partial T_{rec}} = \frac{-F_{product}Cp_{product} - F_{spdcat}Cp_{spdcat}}{M_{spdcat}Cp_{spdcat} + M_{product}Cp_{product}}$	$a_{12} = \frac{\partial f_1}{\partial T_{reg}} = \frac{F_{regcat}Cp_{regcat}}{M_{spdcat}Cp_{spdcat} + M_{product}Cp_{product}}$
$a_{21} = \frac{\partial f_2}{\partial T_{rec}} = \frac{F_{spdcat}Cp_{spdcat}}{M_{regcat}Cp_{spdcat} + M_{fluegas}Cp_{fluegas}}$	$a_{22} = \frac{\partial f_2}{\partial T_{reg}} = \frac{-F_{spdcat}Cp_{spdcat} - F_{feed}Cp_{feed}}{M_{regcat}Cp_{spdcat} + M_{fluegas}Cp_{fluegas}}$
$b_{11} = \frac{\partial f_1}{\partial F_{air}} = \frac{0}{M_{spdcat}Cp_{spdcat} + M_{product}Cp_{product}}$	$b_{21} = \frac{\partial f_2}{\partial F_{air}} = \frac{Cp_{air}T_{air}}{M_{regcat}Cp_{regcat} + M_{fluegas}Cp_{fluegas}}$
$b_{12} = \frac{\partial f_1}{\partial F_{feed}} = \frac{Cp_{feed}T_{feed} + \Delta H_{Rxn}}{M_{spdcat}Cp_{spdcat} + M_{product}Cp_{product}}$	$b_{22} = \frac{\partial f_2}{\partial F_{feed}} = \frac{0}{M_{regcat}Cp_{regcat} + M_{fluegas}Cp_{fluegas}}$
$b_{13} = \frac{\partial f_1}{\partial F_{fluegas}} = \frac{Cp_{fluegas}T_{fluegas}}{M_{spdcat}Cp_{spdcat} + M_{product}Cp_{product}}$	$b_{23} = \frac{\partial f_2}{\partial F_{fluegas}} = \frac{-Cp_{fluegas}T_{reg}}{M_{regcat}Cp_{regcat} + M_{fluegasg}Cp_{fluegas}}$
$b_{14} = \frac{\partial f_1}{\partial F_{product}} = \frac{-Cp_{product}T_{rec}}{M_{spdcat}Cp_{spdcat} + M_{product}Cp_{product}}$	$b_{24} = \frac{\partial f_2}{\partial F_{product}} = \frac{0}{M_{regcat}Cp_{regcat} + M_{fluegasg}Cp_{fluegas}}$
$b_{15} = \frac{\partial f_1}{\partial F_{regcat}} = \frac{Cp_{regcat}T_{reg}}{M_{spdcat}Cp_{spdcat} + M_{product}Cp_{product}}$	$b_{25} = \frac{\partial f_2}{\partial F_{regcat}} = \frac{-Cp_{regcat}T_{regcat}}{M_{regcat}Cp_{regcat} + M_{fluegasg}Cp_{fluegas}}$
$b_{16} = \frac{\partial f_1}{\partial F_{spdcat}} = \frac{-Cp_{spdcat}T_{rec}}{M_{spdcat}Cp_{spdcat} + M_{product}Cp_{product}}$	$b_{26} = \frac{\partial f_2}{\partial F_{spdcat}} = \frac{Cp_{spdcat}T_{rec}}{M_{regcat}Cp_{regcat} + M_{fluegasg}Cp_{fluegas}}$
$b_{17} = \frac{\partial f_1}{\partial T_{air}} = \frac{0}{M_{spdcat}Cp_{spdcat} + M_{product}Cp_{product}}$	$b_{27} = \frac{\partial f_2}{\partial T_{air}} = \frac{Cp_{air}F_{air}}{M_{regcat}Cp_{regcat} + M_{fluegasg}Cp_{fluegas}}$
$b_{18} = \frac{\partial f_1}{\partial T_{feed}} = \frac{f_{feed}Cp_{feed}}{M_{spdcat}Cp_{spdcat} + M_{product}Cp_{product}}$	$b_{28} = \frac{\partial f_2}{\partial T_{feed}} = \frac{0}{M_{regcat}Cp_{regcat} + M_{fluegasg}Cp_{fluegas}}$